#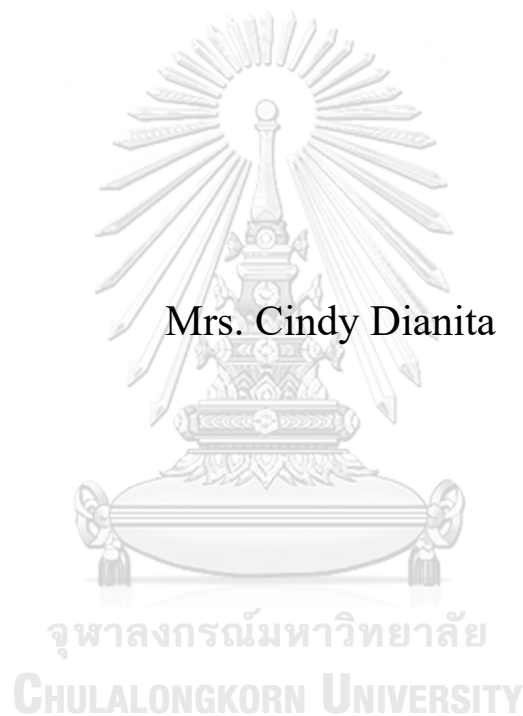 APPLICATION OF CORE ANNULAR FLOW FOR OIL TRANSPORTATION IN DIFFERENT PIPE CONFIGURATIONS USING COMPUTATIONAL FLUID DYNAMICS

Mrs. Cindy Dianita

A Dissertation Submitted in Partial Fulfillment of the Requirements
for the Degree of Doctor of Philosophy in Petrochemistry and Polymer
Science
Field of Study of Petrochemistry and Polymer Science
FACULTY OF SCIENCE
Chulalongkorn University
Academic Year 2022

การประยุกต์การไหลแบบแกนในวงนอกสาหรับการขนส่งน้ามันในรูปแบบท่อต่างๆ ด้วยพลศาสตร์ ของไหลเชิงคานวณ

นางซินดี้ เดียนิตา

Thesis Title	APPLICATION OF CORE ANNULAR FLOW FOR OIL TRANSPORTATION IN DIFFERENT PIPE CONFIGURATIONS USING COMPUTATIONAL FLUID DYNAMICS
By	Mrs. Cindy Dianita
Field of Study	Petrochemistry and Polymer Science
Thesis Advisor	Associate Professor DR. BENJAPON CHALERMSINSUWAN
Thesis Co Advisor	DR. Ratchanon Piemjaiswang

Accepted by the FACULTY OF SCIENCE, Chulalongkorn University in Partial Fulfillment of the Requirement for the Doctor of Philosophy

------------------------------ Dean of the FACULTY OF SCIENCE
(Professor DR. POLKIT SANGVANICH)

DISSERTATION COMMITTEE

------------------------------ Chairman
(Assistant Professor Sasithorn Sunphorka)

------------------------------ Thesis Advisor
(Associate Professor DR. BENJAPON CHALERMSINSUWAN)

------------------------------ Thesis Co-Advisor
(DR. Ratchanon Piemjaiswang)

------------------------------ Examiner
(Professor DR. PORNPOTE PIUMSOMBOON)

------------------------------ Examiner
(Assistant Professor DR. DUANGAMOL TUNGASMITA)

------------------------------ Examiner
(Assistant Professor DR. TEERAWAT SEMA)

ชินดี้ เดียนิตา : การประยุกต์การไหลแบบแกนในวงนอกสำหรับการขนส่งน้ำมันในรูปแบบท่อต่างๆ ด้วย พลศาสตร์ ของไหลเชิงคานวณ. (APPLICATION OF CORE ANNULAR FLOW FOR OIL TRANSPORTATION IN DIFFERENT PIPE CONFIGURATIONS USING COMPUTATIONAL FLUID DYNAMICS) อ.ที่ปรึกษาหลัก : เบญจพล เฉลิมสินสุวรรณ, อ.ที่ปรึกษาร่วม : รัชชานนท์ เปี่ยมใจสว่าง

การประยุกต์ใช้การไหลแบบแกนในวงนอก (Core Annular Flow, CAF) เป็นวิธีที่น่าสนใจในการ ขนส่งน้ำมันหนักผ่านท่อเนื่องจากสามารถลดพลังงานและค่าใช้จ่ายในการดำเนินการ การศึกษานี้ ได้สร้างแบบจำลองพลศาสตร์ ของไหลเชิงคำนวณสามมิติ (Computational Fluid Dynamics, CFD) เพื่อทำนายการไหลแบบแกนในวงนอก ของน้ำมัน-น้ำในท่อแนวนอนแบบมีท่อเชื่อมรูปตัว T และ Y ที่มีสมบัติของน้ำมันหนัก สองแบบแบ่งเป็น น้ำมันมีสมบัติเป็น ของไหลนิวโตเนียนและน้ำมันมีสมบัติเป็นของไหลนอนนิวโตเนียนแบบของไหล Carreau การออกแบบการทดลองทาง สถิติ 2k factorial ถูกนำมาใช้เพื่อศึกษาผลกระทบของรูปทรงท่อต่อประสิทธิภาพการไหล แปดกรณีศึกษาถูกดำเนินการ ด้วยเส้นผ่านศูนย์กลางแบบต่าง ๆ และมุมของท่อเชื่อมแบบต่าง ๆ การออกแบบที่มีประสิทธิภาพสูงที่สุด คือ มีปริมาณน้ำมันสูง และมีค่าเฉลี่ยของการเปลี่ยนแปลงความดันและความเบี่ยงเบนมาตรฐานของความดันต่ำ ผลการจำลองแสดงให้เห็นว่า พบการ ไหลแบบแกนในวงนอกที่เสถียรในพื้นที่ก่อนท่อเชื่อมแต่เมื่อผ่านท่อเชื่อมจะเกิดความปั่นป่วนขึ้นในกระบวนการ การฟื้นคืน ความเสถียรของการไหลแบบแกนในวงนอกหลังจากผ่านท่อเชื่อมรูปตัว T โดยไม่ขัดขวางการไหลในกระบวนการได้ถูกเสนอ โดยเฉพาะสำหรับ T50-50 (ท่อเชื่อมรูปตัว T ที่มีเส้นผ่านศูนย์กลางของท่อเข้าและท่อออกเท่ากับ 50 มิลลิเมตร) ซึ่งเป็น กรณีที่เหมาะสมที่สุดในการออกแบบท่อสำหรับการไหลน้ำ-น้ำมันที่เป็นของไหลนอนนิวโตเนียนแบบของไหล Carreau การใส่น้ำเพิ่มเติมเข้าไปในท่อที่จุดเชื่อมท่อเพื่อช่วยการฟื้นคืนโครงสร้างการไหลแบบแกนในวงนอกซึ่งจะช่วยลดการเกิดตะกรัน ในระบบ การออกแบบที่เสนอนั้นแสดงให้เห็นความเสถียรของการไหลแบบแกนในวงนอกที่ดีขึ้นสำหรับพื้นที่หลังท่อเชื่อม จนถึงทางออก การประเมินพลังงานได้ถูกดำเนินการและประมาณการว่า การไหลแบบแกนในวงนอกภายใต้ท่อแบบ T50-50 สามารถลดความดันลดในระบบได้มากกว่า 90% เมื่อเทียบกับการขนส่งที่ไม่มีการไหลแบบแกนในวงนอก นอกจากนี้ ยัง สามารถประหยัดค่าไฟฟ้าในการดำเนินการได้มากกว่า 80% เมื่อเทียบกับการขนส่งน้ำมันแบบสถานะเดียว การจำลองท่อที่ ขยายขนาดขึ้นยังได้ถูกดำเนินการโดยมีขนาดที่ใหญ่ขึ้น 10 เท่า ผลที่ได้พบว่า ผลลัพธ์ของการไหลตามแนวแกนด้านนอกที่ เสถียรยิ่งขึ้นถูกพบเมื่อใช้ท่อขนาดใหญ่

สาขาวิชา	ปิโตรเคมีและวิทยาศาสตร์พอลิเมอร์	ลายมือชื่อนิสิต ....
ปีการศึกษา	2565	ลายมือชื่อ อ.ที่ปรึกษาหลัก ....
		ลายมือชื่อ อ.ที่ปรึกษาร่วม ....

6371036323 : MAJOR PETROCHEMISTRY AND POLYMER SCIENCE

KEYWORD: CFD, Core Annular Flow, Heavy Crude Oil Transportation, T-pipes, Y-pipes, Energy Saving

Cindy Dianita : APPLICATION OF CORE ANNULAR FLOW FOR OIL TRANSPORTATION IN DIFFERENT PIPE CONFIGURATIONS USING COMPUTATIONAL FLUID DYNAMICS. Advisor: Assoc. Prof. DR. BENJAPON CHALERMSINSUWAN Co-advisor: DR. Ratchanon Piemjaiswang

The application of Core Annular Flow (CAF) has become an interesting solution in transporting heavy oil through pipeline because of its energy reduction and cost efficiency. Current study conducted a 3D computational fluid dynamic (CFD) to simulate CAF of oil-water in horizontal T- and Y-pipe junctions with two types of oil characteristic i.e., oil as Newtonian fluid and oil as non-Newtonian Carreau Fluid. The 2^k factorial statistical experimental design was applied to investigate the effect of geometry on the flow performance. Eight cases were run with different diameter combinations and junction angle. The most attractive design was measured by the high value of oil holdup with small average values of pressure gradient and pressure standard deviation. The simulation result showed the stable CAF along the upstream region but then broke up when passing the intersection. A strategy to recover the stability of CAF after passing the intersection area of a T-pipe without interrupting the flow process was also proposed specifically for T50-50 (T-pipe with inlet and outlet diameter of 50 mm) as the most desired design for water-oil as non-Newtonian Carreau Fluid case. An additional water insertion was introduced at the intersection point to support the recovery of CAF structure by suppressing fouling. The proposed design showed significant improvement of CAF consistency for downstream region until pipe outlets. Energy evaluation was also has been conducted and it was estimated that CAF in T50-50 was able to reduce the pressure drop to more than 90% compared to transportation without lubrication. In addition, the cost of power consumption can be saved to more than 80% than single phase oil transportation. A scaled-up pipe size simulation was also completed to 10 times bigger dimension. More consistence result of lubricated flow was shown by bigger dimension pipe.

Field of Study:	Petrochemistry and Polymer Science	Student's Signature ....
Academic Year:	2022	Advisor's Signature ....
		Co-advisor's Signature ....

ACKNOWLEDGEMENTS

TABLE OF CONTENTS

Page

LIST OF TABLES

Page

LIST OF FIGURES

Page

CHAPTER I BACKGROUND

1.1 Introduction

In recent years, there has been a growing interest in utilizing the Core Annular Flow (CAF) method for the transportation of heavy oils. This is due to the fact that significant reserves of heavy and extremely heavy oils are now available in various regions across the globe, while the reserves of lighter oils have been gradually decreasing (Crivelaro et al., 2009; Santos et al., 2014). According to the report, the rising demand for energy necessitates the diversification of supply, and as a result, extra heavy oil is anticipated to make up 7% of the liquid hydrocarbon supply by 2030 (Paszkiewicz, 2012). Abundant reserves of heavy crude oil are found in several countries, such as Canada, Colombia, the United States, Mexico, Chad, Brazil, Venezuela, Russia, Saudi Arabia, Iraq, Indonesia, China, Ecuador, Kuwait, and Angola. Petroleum refiners are attracted to heavy oils due to their comparatively lower price in comparison to conventional oils (light oil), which allows them achieving profitable margins.

Heavy viscous oil is characterized by a high viscosity, which inhibits its flow, while light oil is distinguished by a low viscosity, which enables it to flow with freely. Heavy and extra-heavy crude oils are characterized by a significant proportion of high molecular weight hydrocarbons, encompassing saturates, resins, aromatics, and asphaltenes, as reported in various studies (Anto et al., 2020; Martínez-Palou et al., 2010; Montes et al., 2019; Souas et al., 2020; Taborda et al., 2016). Heavy crude oils exhibit a viscosity range of 100 to 10,000 cp. On the other

hand, extra-heavy oils are characterized by viscosities higher than 10,000 cp (Marappa Gounder, 2019). Because of the high value of viscosity, it becomes a challenge to transport heavy oils effectively and affordably.

Pipelines represent the prevailing method employed in the transportation of crude oil or refined petroleum products within the oil industry. These items are considered to be reliable, environmentally friendly, and economically viable. Pipelines are recognized as a dependable means of transportation for traversing vast distances that may span across urban centers, regions, and even international borders. Although pipeline technologies are well established, the typical pipeline technologies are largely created for light and medium oil crudes. Enhancement of transportation techniques is required for the transportation of heavy and extra-heavy crude oils to improve oil flowability within pipelines.

Three commonly proposed strategies for enhancing the transportation of heavy and extra-heavy oils through pipelines are viscosity reduction, friction reduction, and in situ upgrading to produce synthetic crudes with lower viscosity. This statement is supported by various researchers, including (Hart, 2014; Martínez-Palou et al., 2010; Saniere et al., 2004; Santos et al., 2014).

The implementation of the CAF technique is an appropriate way to mitigate pipeline frictional losses associated with the transportation of viscous crude oils. The implementation of CAF has shown to be an advantageous technological solution for pipelines that transport oils with high viscosity. The transportation of the denser fluid, which is oil, occurs within the core area of the pipe, while being enveloped by a thin film of water formed in the annulus. The decrease of friction is attributed to

the creation of a thin water layer water that serves as a lubricant between the oil and the inner surface of the pipe. Several experiments have demonstrated that in order to generate a CAF structure, the core fluid should possess a higher viscosity than the annulus fluid. Additionally, it is essential to maintain a lower input proportion of the thinner fluid to prevent the core fluid from coming into contact with the pipe inner wall (Antonio C. Bannwart, 2001).

The CAF method was introduced in a patent in the United States by Isaacs and Speed in 1904 for transferring high viscosity fluids using lubrication method (Bensakhria et al., 2004). The greatest significant commercial use of lubricated flow for transporting heavy crude oil was documented in the 1970s with a 6 inch of pipe diameter and 30 km of pipeline length , for the Shell company in California, that transported 24000 barrels per day of heavy oil (Santos et al., 2014). The other case was an oil pipeline located in Indonesia (with 20 inch of pipe diameter and 238 km of length) that transported 40,000 gallons of 70% oil/water emulsion (Simpson, 1963). Additional cases include the 35 km of lubricated pipelines in Lake Maracaibo-Venezuela and Syncrude's Canada Ltd's self-lubricated pipelines (Salager et al., 2001).

There are several theoretical and experimental investigations on CAF reported in some publications, including (Andrade et al., 2013; Babakhani Dehkordi et al., 2018; Balakhrisna et al., 2010; Brauner, 1991; Colombo et al., 2015; Sumana Ghosh et al., 2011; Goldstein et al., 2017; Grassi et al., 2008; Hwang et al., 1997; Jiang et al., 2018; Joseph et al., 1997; Oliemans et al., 1987; Shi et al., 2017; Sotgia et al., 2008; Strazza et al., 2011; Wu et al., 2020). The majority of these studies were conducted for straight pipes with horizontal or vertical orientation, sudden

expansion or contraction (including variations on these designs), horizontal and slightly inclined pipes, and return bending.

Despite its wide application in petroleum industry, limited studies has been conducted on liquid-liquid CAF across T-junction and Y-junction, especially for high viscosity oil-water flow. The use of pipe junctions is a common and reasonably priced option for combining or dividing fluid streams in a pipe network. Previous study stated there still remain unresolved questions regarding how CAFs behavior at pipe fittings and junctions that require further investigation (S. Ghosh et al., 2009). Only a work from (Andrade et al., 2013) focused on the CAF model and simulation of heavy oil-water in a T-shaped pipe. The simulation predicted the annular flow pattern of heavy oil-water in the horizontal pipe and T-shaped pipe accurately. Despite the presence of CAF in both pipe shapes, the CAF pattern in the T-shaped pipe or T-junction was not as consistent as it was in the horizontal pipe.

The CAF technique and a computational tool (CFD) were used in this study to conduct a numerical assessment of heavy oil-water flow through T and Y-shaped junction pipe configurations. By adjusting the pipe diameter and junction angle, eight simulation scenarios were conducted. For the purpose of examining how pipe geometry affects the transportation of heavy oil through T- and Y-shaped junction pipes, the approach of 2^k factorial statistical experimental design was used. Current study was also expected to propose a strategy to recover the stability of CAF particularly after crossing the intersection region of the T-pipe without interrupting or stopping the flow process. A scaled-up pipe simulation was also conducted to predict the adaptability of the design to commercial implementation. An analysis of energy savings was included to illustrate the quantitative evaluation in the attainable

energy savings provided by the CAF method. The workflow of this study is summarized by chart as illustrated by Fig. 1. In this work, the system was assuming as an isothermal condition.

1.2 Objectives

1. To develop computational fluid dynamics model and investigate the occurrence of Core Annular Flow (CAF) for oil pipeline transportation in horizontal T and Y- junctions.

2. To propose strategy for bringing back the CAF for oil pipeline transportation in horizontal T-junction or Y-junction

3. To conduct qualitative and quantitative evaluations in the attainable energy saving of the CAF for oil pipeline transportation in horizontal T-junction or Y-junction.

1.3 Scope of Study

1. Conducting CFD simulation to investigate the occurrence of Core Annular Flow (CAF) for heavy oil-water system in horizontal T and Y- pipe junctions with different combination of the pipe diameters.

2. Conducting CFD simulation to investigate the deformation of CAF due to oil fouling and solutions to bring back the CAF pattern after breaking during the process of oil transportation.

3. Evaluating of the energy savings on pumping viscous oil using the CAF technique.
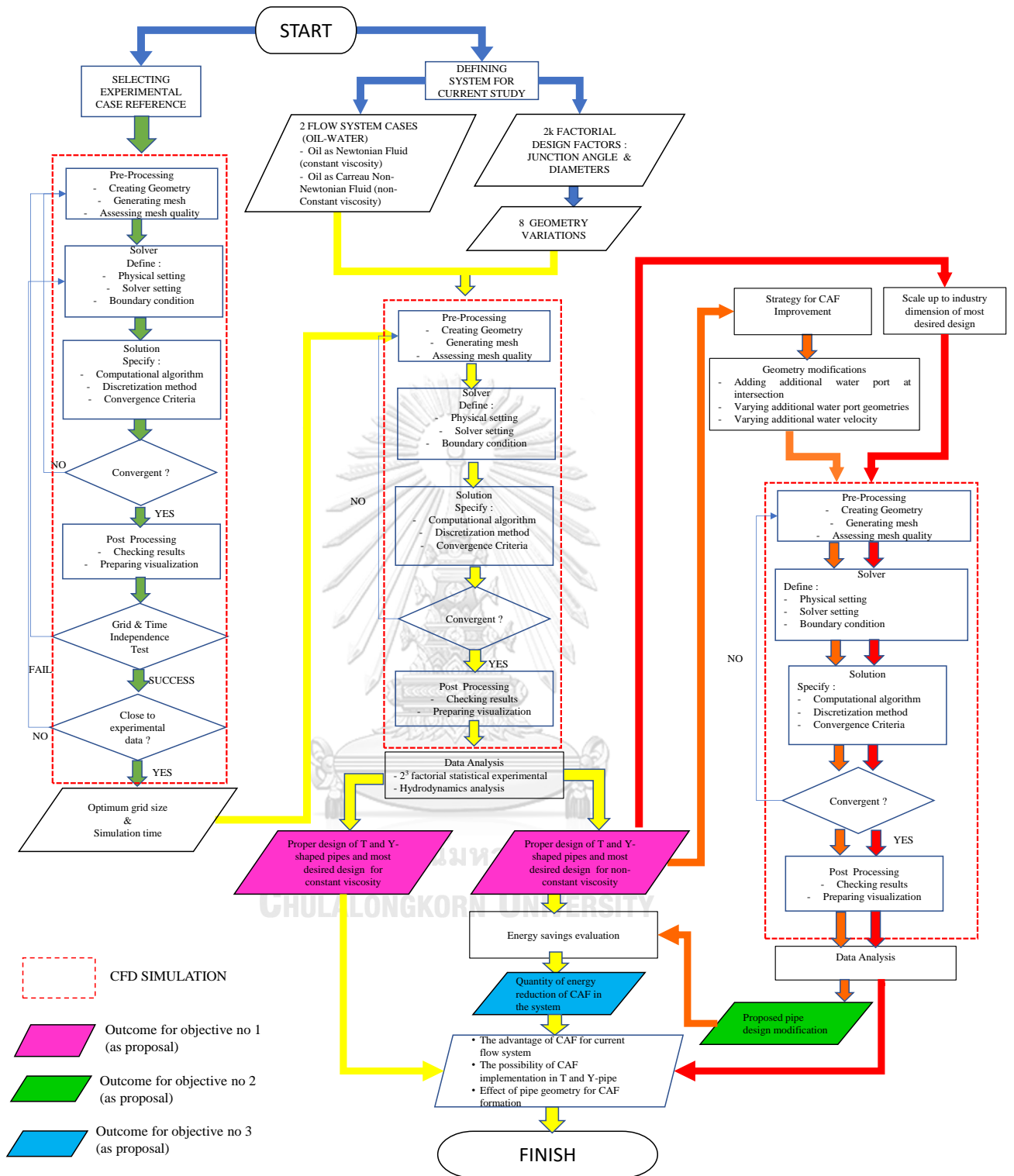
Fig. 1– Flowchart of current work

CHAPTER II THEORY AND LITERATURE REVIEW

2.1 Newton's Law of Viscosity

Newton's law of viscosity states that the shear stress between adjacent fluid layers is proportional to the negative value of the velocity gradient between the two layers. The greater the shear rate or viscosity of a fluid, the greater the resulting shear stress. It is denoted mathematically by the following

$$\tau_{y,x} = -\mu \frac{du_x}{dy} \tag{2.1}$$

where τ =*shear stress*, μ = viscosity, and $\frac{du_x}{dy}$ = *shear rate*. The negative sign indicates that shear stress is applied from high to low velocity areas.

2.2 Non-Newtonian Fluid

A fluid that is not Newtonian may have a viscosity that changes with movement. The viscosity of non-Newtonian fluids changes with the shear rate. There is a structure for the molecular chain in most non-Newtonian fluids. The molecules in some of these fluids have a tendency to orient themselves in planes of maximum tension, which leads to a decrease in viscosity as the velocity gradient rises. These fluids are referred to as "shear-thinning" fluids or pseudo-plastics. The fluid "thins" as the shear rate rises. In some cases, the viscosity will rise in tandem with the velocity gradient. The fluid is referred to as "shear-thickening" or dilatant. Shear-thinning occurs in many biological fluids, including blood and polymer solutions, while shear thickening occurs in suspensions (paints).

In Fig. 2, for non-Newtonian fluids it is indicated by a curved line which indicates that there is a force from the fluid. Heavy oil as a flowing fluid in this study is included in the time-independent category which exhibits pseudoplastic behaviour or also known as shear thinning. Shear thinning behaviour shows a decrease in viscosity with increasing shear rate (γ) (Chhabra et al., 2008).
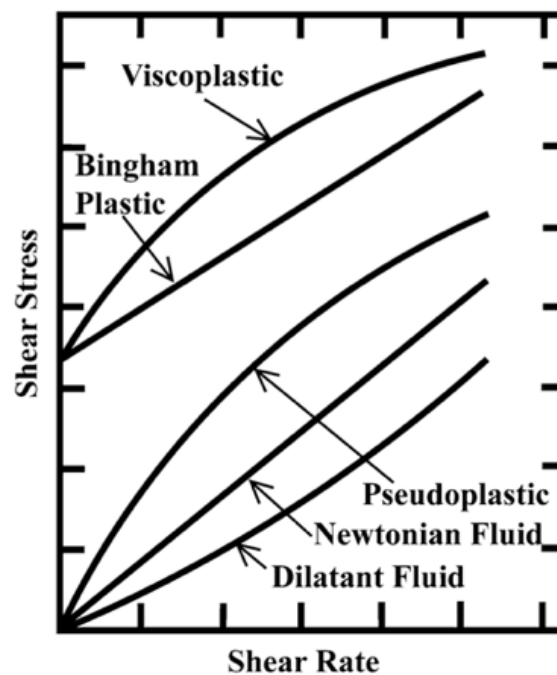
Fig. 2 – Newtonian and non-Newtonian fluid rheology
Source: (Chhabra et al., 2008)

2.3 Heavy Oil

The API scale (an index based on the relative density of the oil) is used by the American Petroleum Institute as the standard for classifying oils, and it is the basis for the definition of heavy oils that is most frequently employed. There is no established standard for the API degree range used to characterize and categorize oils. For instance, heavy oil is defined by the World Petroleum Conference as having an API degree of less than 22.3. According to the American Petroleum Institute, heavy oil is

characterized as having an API index of 20 degrees or less. However, the National Petroleum Agency of Brazil defines 4 oil classifications with API index of heavy oil from 10 degree to 22 degree and extra heavy oil equal to or less than 10 degrees. Heavy oils have a high specific gravity, increased viscosity, low H/C ratio, high levels of asphaltene, resin, heavy metals, sulphur, and nitrogen, and are frequently black in colour (Santos et al., 2014).

The biodegradation process, which breaks down light and medium hydrocarbons on a geological time scale by microorganisms, is primarily responsible for the unique properties of heavy oils. As a result, the reserves are abundant in polyaromatic compounds, resins, and asphaltenes. In addition to biodegradation, heavy oil generation can also occur as a consequence of processes like water washing and phase fracturing, which depend on the loss of a sizable portion of the original mass, and the physical rather than biological removal of light petroleum fractions (Santos et al., 2014).

2.4   Core Annular Flow (CAF) Technology for Oil Transportation

Water-lubricated transportation of heavy viscous oil or usually called as Core Annular Flow (CAF) method is marked with water migration on the pipe wall as high shear region to lubricate the oil flow. With this condition, the lubricated flows require pressures comparable to pumping water alone at the same throughput, regardless of the oil's viscosity since the water's wall shear stresses balance the pumping pressures. As a result, savings of the order of the oil to water viscosity ratio can be achieved.

CAF, both in horizontal and vertical pipes, can be categorized into two patterns i.e., WCAF (wavy Core Annular Flow) and perfectly centered core flows (PCAF).

However, PCAF are rarely stable (Joseph et al., 1997). Waves typically are visible on the surface of the oil core, and they appear to be required for both centering the core when the densities are equal and for levitating the core off the wall when the densities are different.

According to most experiments, the following requirements must be met for the core-annular flow pattern to exist in a pipe:

(a) the core phase must be significantly thicker than the annulus;

(b) The thinner fluid's input fraction needs to be such that it keeps the thicker fluid's core phase continuous and from touching the pipe wall at the same time.

The phenomenon of concentric CAF (CCAF), as shown by Fig. 3(a), of oil-water can be established with a small amount of water. In this condition, it is reported that the pressure gradient is almost independent of the oil viscosity and only slightly higher than for flow of water alone at the mixture flow rate (J. Sun et al., 2022). However, the configuration of CCAF may not be realizable in practical applications due to the density difference between the oil and the lubricating aqueous phase. The oil core is prone to migrate partially or completely to the upper (lower) part of the pipe, which results in an eccentric CAF (ECAF) as illustrated by Fig. 3(b). When the pressure gradient over the pipe is large enough, a balance develops between the buoyancy force and the hydrodynamics force on the core that makes eccentric core-annular flow possible. With decreasing pressure gradient or increasing buoyancy force the eccentricity of the core increases.

In normal CAF operations, a CAF might not be sustainable due to fouling even after a CAF is initiated. The fouling may become so extensive that the entire core sticks at the upper section with a rapid and sharp increase in the pressure drop as a result of

some oil droplets breaking off from the core and impinging on the pipe wall (Strazza et al., 2012). As this occurrence persists, a layer of oil builds up at the wall. Even if the oil deposit on the wall is not particularly thick, the constriction causes the flow to speed up, increasing the likelihood of severe water formation in oil emulsions with a high apparent viscosity.

(a)   (b)
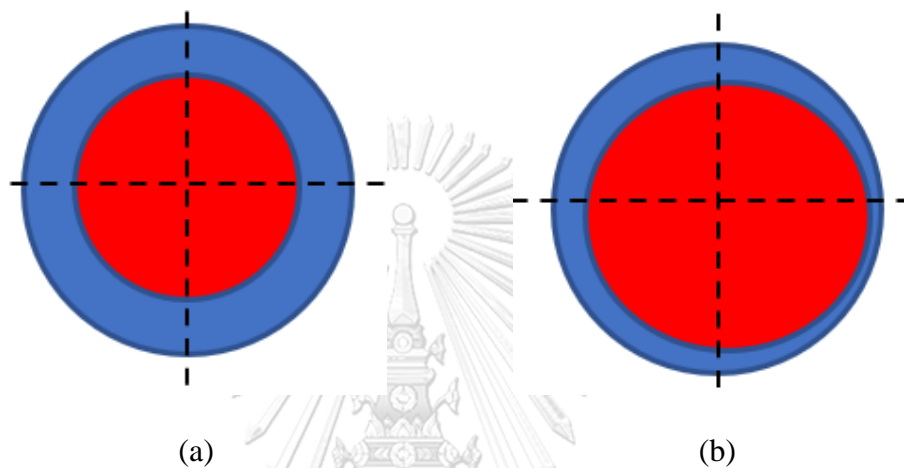
Fig. 3 – Cross sectional illustration of (a) CCAF and (b) ECAF (blue : water, red : oil)

2.5   Flow in T and Y-Junction

The main purposes of T and Y junctions in pipe networks are to spread (diverge) the flow from the main pipe to multiple branching pipes and to gather (converge) the flows from several branching pipes to the main pipe. The way the flow behaves at the junction also varies depending on the input and outflow directions.

When calculating the pressure loss of fluid transported through T and Y-junction, there are 2 types of loss i.e., major loss and minor loss. Major loss, also called frictional loss, is solely dependent on the pipe's material and smoothness. Minor loss is defined as loss due to the change in fluid momentum mainly because of the presence of pipe components with sudden changes in pipe. Li et al. (2013)

identified that occurred pressure reduction of T and Y-junction due to minor loss was as the result of confluence loss and curved loss. The confluence loss is brought on by the fluctuation in cross section area, whereas the curved loss is caused by the change in flow direction.

2.6   Computational Fluid Dynamics (CFD)

Computational fluid dynamics or CFD is a system analysis that involves fluid flow, heat transfer, and related phenomena such as chemical reactions through computer-based simulations. CFD is related to the fluid dynamics equation, namely the Navier-Stokes equation. The basis of this equation lies in the assumption that fluid particles are deformed by shear stress. The CFD approach uses the second law of motion and conservation including the conservation of momentum, mass, and energy (Jamshed, 2015).

In programming, there are several discretization methods, including the Finite Difference Method (FDM) and the Finite Volume Method (FVM). The FDM method is the simplest method obtained from the derivative concept which produces a slope. The first derivative method is also called the forward difference method. The slope for the velocity u in the function can be obtained by Eq. 2.2. The subscripts i and $i+1$ are points for calculating the value of u, and ∂x indicates the grid distance.

$$\frac{\partial u}{\partial x} = \frac{u_{i+1} - u_i}{\Delta x} \tag{2.2}$$

ANSYS Fluent uses the FVM method because it is more complex than the FDM method. FVM can be used for all types of grids. In addition, FVM can also be used in cases involving discontinuities in the flow which cannot be calculated using

the FDM method. In FVM, the term "volume" refers to the fluid dynamics equation in which the domain is discretized using volume control to take discrete points on the mesh (Jamshed, 2015).

In the FVM method, the terms in the conservation equation are converted into face flux and evaluated on finite volume faces because the flux entering a certain volume is identical to the flux leaving the adjacent volume. This makes FVM the preferred method in CFD because it is very conservative. In the finite volume discretization process, the Gauss theorem is applied to change the internal volume from convection and diffusion to surface integral which is taken from the basic equation. The conservation equation for the general scalar ϕ variable in FVM under steady state conditions is as follows (Moukalled et al., 2016).

$$\nabla \cdot (\rho v \phi) = \nabla \cdot \left(\Gamma^{\phi} \nabla \phi \right) + Q^{\phi} \tag{2.3}$$

With the first term ($\nabla \cdot (\rho v \phi)$) indicating the convection term, the second term ($\nabla \cdot \left(\Gamma^{\phi} \nabla \phi \right)$) indicating the diffusion term, and the third term (Q^{ϕ}) indicating the source term.

A. **Pressure Velocity Coupling**

The ANSYS Fluent software provides four types of pressure-velocity coupling algorithms, including: SIMPLE, SIMPLEC, PISO, and Fractional Step (FSM). Steady-state calculations generally use SIMPLE or SIMPLEC, while PISO is recommended for transient calculations. However, PISO can also be used for steady-state and transient calculations on highly skewed meshes. Meanwhile, fractional step (FSM) is considered less stable than PISO. In steady state conditions, PISO with neighbour correction provides benefits not much different from SIMPLE or SIMPLEC with optimal under-relaxation factors. In addition, PISO with skewness

correction is also recommended for steady state and transient conditions in meshes with high levels of distortion. An under-relaxation factor value of 1.0 or close to 1.0 is recommended when using the neighbour correction at PISO. If the case only uses PISO skewness correction, then the under-relaxation factor setting must be 1.0 (e.g., 0.3 for pressure and 0.7 for momentum) (ANSYS, 2018).

B. Second-Order Upwind Scheme

In computational fluid dynamics, the upwind scheme is one of the discretization methods for numerically solving hyperbolic partial differential equations. When flow is parallel to the mesh, for example laminar flow in a rectangular channel modelled by a rectangular or hexahedral mesh, a first-order upwind scheme can be used. For flows that are never parallel to the mesh, such as in triangular and tetrahedral meshes, the results will be more accurate if a second-order upwind scheme is used. Also, the second-order upwind scheme is suitable for quad/hex meshes especially for complex flows. In general, the first-order upwind scheme will produce better convergence than the second-order upwind scheme, but the results obtained are less accurate, especially in the tri/tetra mesh (ANSYS, 2018).

C. Meshing

Meshing is the geometric space of an object broken down into thousands of shapes to define the object's physical form. The mesh can be generated in the form of structured mesh (Fig. 4(a)) and unstructured mesh (Fig. 4(b)) in 3 dimensions consisting of tetrahedral, hexahedral, prism, pyramid, and polyhedral (Fig. 5). Structured meshes are known as meshes with implicit connectivity that facilitate easy identification of elements and nodes. On the other hand, unstructured meshes are meshes with general connectivity whose structure is random. Thus, it needs to

define and store the element connections. In general, unstructured meshes provide more practical mesh adaptivity (refinement/de-refinement based on an initial solution) and a better fit to complex domains, whereas structured meshes often offer simplicity and easy data access.

The choice of which mesh type to use will depend on the application. When choosing mesh type, it needs to consider the setup time, computational expense, and numerical diffusion. The use of structured (consisting of quadrilateral or hexahedral elements) for complex geometries can be incredibly time-consuming. Therefore, setup time for complex geometries is the key rationale for using unstructured meshes employing triangular or tetrahedral cells. In summary, the following practices are generally advised (ANSYS, 2018):

- For simple geometries, use quadrilateral/hexahedral meshes.

- For moderately complex geometries, use unstructured quadrilateral/hexahedral meshes.

- For relatively complex geometries, use triangular/tetrahedral meshes with prism layers.

- For extremely complex geometries, use pure triangular/tetrahedral meshes.

The other mesh type is polyhedral meshes. Polyhedral meshing is starting to be widely applied in ANSYS Fluent solver because of its several advantages. The main advantage of the polyhedral mesh is that each element has many neighbouring elements resulting in a much better gradient approximation. In addition, polyhedral have a lower sensitivity to stretching compared to tetrahedral (Ibraheem, 2021).

(a)   (b)
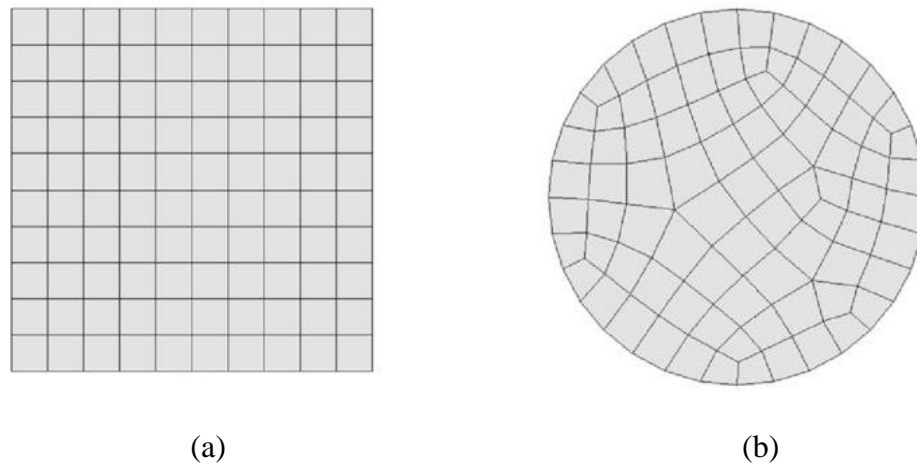
Fig. 4 – Two-dimensional (a) structured and (b) unstructured quadrilateral meshes
Source: (Woodbury et al., 2011)
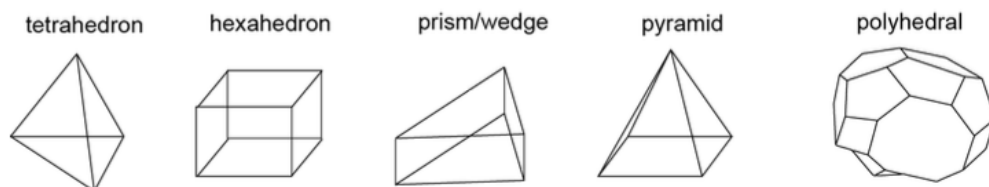
Fig. 5– Types of mesh elements
Source: (Lintermann, 2021)

2.7 2^k Factorial Experimental Design

In some experiments, it is important to examine the combined effect of the factors on a response. In this such condition, factorial designs are frequently used. In the early stages of experimental study, when numerous aspects are expected to be studied, the 2^k design is especially helpful (Montgomery, 2012). It offers the fewest runs necessary for the study of k factors in a complete factorial design. Consequently, factor screening experiments frequently adopt these designs. The first design in the 2^k series has just two factors, like A and B, running at two different levels. This design is called a 2^2 factorial design. The terms "low" and "high" are

arbitrary designations for the levels of the factors. To determine which variables are likely to be important in experiments involving 2^k designs, it is always essential to examine the magnitude and direction of the factor effects. This interpretation can typically be confirmed with the help of the analysis of variance (ANOVA). Because the ANOVA does not provide this information on its own, it should always be taken into account alongside the effect magnitude and direction.

2.8   Energy Reduction of CAF

The hydraulic power (ψ) or energy imparted on the fluid being pumped, can be calculated by Eq. 2.4 (Coelho et al., 2020).

$$\psi = Q.\rho.g.H \tag{2.4}$$

where Q is the volumetric flow rate of the fluid (m^3/s), ρ is the density of the fluid (kg/m^3), g is the acceleration of gravity (9.81 m/s^2) and H is the head produced by the pump (m).

The liquid horsepower (LHP) depends on the volumetric flow rate (Q, m^3/s) and differential pressure across the pump (ΔP, Pa) as formulized as Eq. 2.5.

$$LHP = Q.\rho.g.H \tag{2.5}$$

By considering the pressure gauge upstream the pump negligible, Eq. 2.5 turns into Eq. 2.6 :

$$\psi = Q.P \tag{2.6}$$

The volumetric flow rate of flow through a circular tube can be obtained using Eq. 2.7 (Bird et al., 2002).

$$Q = \frac{\dot{m}}{\rho} = \frac{\pi.(P_{in} - P_{out}).R^4}{8.\mu.L} \tag{2.7}$$

where P_{in} is input pressure, P_{out} is output pressure, R is radius of the pipe, μ is viscosity of fluid, and L is the length of pipe.

The energy savings associated with pumping viscous oil using the core annular flow technique were calculated by comparing the total hydraulic power needed to pump a specific amount of oil using the conventional single-phase oil flow (ψ_s) to the power needed to pump the same amount of oil using two-phase oil-water fluid flow (ψ_B) (Coelho et al., 2020). This parameter is defined as power consumption reduction factor and calculated as:

$$f_\psi = \frac{\psi_s}{\psi_B} = \frac{\psi_s}{\psi_w + \psi_o} \tag{2.8}$$

Consequently, the energy efficiency of the two-fluid flow process increases with the level of this power consumption reduction factor. The two-phase system is energetically preferable to the single-phase oil system, as reflected by the power reduction factors greater than 1. The indirect calculation of the power reduction factor is defined by Eq. 2.9 and depends on the pressure gradient measured in two referred pressure taps (inlet and outlet).

$$f_{\Delta P} = \frac{\Delta P_s}{\Delta P_B} \tag{2.9}$$

To evaluate the lubrication efficiency, the pressure drop reduction ΔP^* (%), calculated according to the following equation (Peysson et al., 2007):

$$\Delta P^* = \frac{\left(\frac{\Delta P}{L}\right)_S - \left(\frac{\Delta P}{L}\right)_B}{\left(\frac{\Delta P}{L}\right)_S} \; x \; 100 \qquad (2.10)$$

2.9 Previous Studies of CAF

Arney et al. (1993) carried out experiments on high viscous oil-water in a horizontal pipe. With superficial velocities varying between 0.14 and 1.16 m/s for oil and 0.06-0.65 m/s for water, waxy crude oil (with viscosities between 200 and 900 Pa s) and fuel oil (with a viscosity of 2.7 Pa s) were employed. A pipe with an internal diameter of 15.9 mm and a length of 6.35 m was used to transport the very viscous oil and water mixture. This work concluded that at low water flow rate, the risk of oil contact at the wall increased, which must be avoided. At higher water flow rates perfect Core Annular Flow (PCAF), wavy Core Annular Flow (WCAF), and oil slug in water were detected. In addition, water holdup was measured by means of a removable section, which included two pairs ball valves. Water holdup was always larger than input water fraction, meaning that oil tended to move with higher velocity. They developed a semi-empirical correlation based on large database (Arney et al., 1993). A formula was derived which was the modification of Oliemans (1987) correlation.

Baanwart (2001) studied modelling aspect of core-annular flow in both horizontal and vertical tubes, and developed correlations for volume fraction and pressure drop for this flow regime. To ensure the possibility of forming core-annular flow regime, they emphasized that two immiscible liquids must have very different viscosity and relatively small density difference. Furthermore, interfacial tension

played an important role in favouring annular configuration. The proposed correlations were compared with data source in the literature survey, showing satisfactory results.

Grassi et al. (2008) set out tests using horizontal pipes filled with paraffin oil and water and inclined at angles of 10° and 15°. No significant variations were found when comparing the flow patterns as a result of changing the inclination angle.

Experimental research was done by Sotgia et al. (2008) on seven distinct horizontal pipes with diameters ranging from 21 to 40 mm. When the water superficial velocity was steadily lowered while the oil superficial velocity was held constant, it was noted that the fluctuation of diameter would have an impact on the flow regime. It was discovered that the momentum carried by annular flow depends on the fluid's physical characteristics but is unaffected by the pipe's diameter.

In order to examine the impact of operating conditions and the curvature radius of the U bend on the hydrodynamics and fouling properties of CAF, Ghosh et al. (2011) conducted a CFD analysis of lubricating oil-water. In their work, it was discussed about the effects of flow direction, input water fraction, and curvature radius to fouling problem. As the result, the upflow direction of CAF was preferred over horizontal flow and downflow to minimize the fouling effect at bend area. In addition, the fouling problem was found to be significantly reduced with the higher water fraction to 0.55. For water fraction higher than 0.55, the chance of fouling was observed to be constant. Another result was also reported that an increase in radius of curvature did not change the tendency of fouling remarkably until a specific value of

the radius. When the radius of curvature was above this value, the fouling tendency increased sharply.

Andrade et al. **(**2013**)** used CFD simulation to study the oil-water CAF via horizontal pipe and T-joint. The CAF stability of the horizontal pipe and T-joint pipe differed as a result. Along the horizontal pipe, CAF was more consistently identified, but as the oil phase entered the T-connection, the pattern of annular flow changed to stratified flow with continuous pressure loss.

Babakhani Dehkordi et al. (2018) carried out CFD study and experimental validation on CAF of viscous oil-water flowing in horizontal pipe with undergoing sudden expansion, this work used three horizontal pipes with different diameter configurations **(**21–30 mm, 30–40 mm, and 30–50 mm**)** represented by twelve cases of simulation runs**.** It was observed more eccentric oil core flow phenomenon for the configuration of sudden expansion**.** Additionally, thicker core flow had been numerically shown to be distant from a singularity, especially for configurations with pipes between 30 and 50 mm.

Jiang et al. (2018 used CFD modeling to study the CAF phenomena of non-Newtonian oil-water systems in return bends. For various oil qualities, bend geometries, and flow directions, their studies observed the pressure profile, volume percentage, velocity, and wall shear stress**.** They concluded that the total pressure gradient and the fouling angle were affected by the geometry parameters**.** Thus, 16–20 and 0**.**67–0**.**75 were proposed as the range of curvature ration and inlet diameter ratio, respectively, for maintaining the stability of CAF**.**

Experimental works concerning on the CAF through straight pipes observed the evolution of CAF by adjusting the range of oil and water superficial velocity to certain values (Jiang et al., 2021; Joseph et al., 1997; Sotgia et al., 2008). These studies also created a flow pattern map to specify the flow regime's border areas and forecast how the flow pattern would change based on the surface velocities of water and oil. In an experimental analysis of flow regimes and pressure drop reduction in oil-water mixtures in horizontal pipes, Sotgia et al. (2008) found that by accommodating the oil superficial velocities to be higher than its critical value, the flow transformed to the core annular and wavy annular patterns were observed for a wide range of water superficial velocities. Additionally, a study by Coelho et al. (2020) showed that more water must be used in order to maintain the CAF structure flowing via hydraulic fittings. For flows with very significant oil cuts (over 70%), it was not practical. In order to ensure the high efficiency of oil-water CAF in a horizontal pipe with a 90o elbow, Jing et al. (2021) similarly came to the conclusion that the water input fraction should be kept at the critical threshold and the oil flow rate should be controlled to the highest possible level.

The experimental work conducted by Coelho et al. (2020) concerned mainly on the energy savings of CAF on heavy oil transportation in the presence of hydraulic fittings. This study calculated the energy savings by comparing the pump power reduction factor, pressure gradient reduction factor, and pump energy usage for two conditions of transporting the same amount of oil: traditional single-phase oil and two-phase oil-water fluid flow (CAF). The experimental studies revealed that oil fouling zones formed near the hydraulic fittings. The overall energy savings from the CAF method were 2.2, which meant that the same quantity of oil could be transported for

half the cost. This observation also revealed that the risk of oil fouling was greater when the input oil cuts exceeded 50% and did not result in a compensatory energy savings.

Jing et al. (2021) conducted simulation work for finding the hydrodynamics conditions under which CAF becomes unstable and the oil waves touch the pipe wall. Simulations were carried out for the horizontal pipe with two diameters (10.5 and 21 mm) and oil to water viscosity ratio of 1040 (but also a variation of this was considered). This work was capable for simulating the growth of waves at the oil-water interface until they touched the pipe wall, which is a necessary condition for the onset of fouling. For each value of the pressure drop or mixture velocity, there was a critical value of the water cut below which the oil reaches the pipe wall. This critical value of the water cut was lower for the larger pipe than the smaller pipe (for a viscosity ratio of 1040). The simulation result of this work indicated that the contact of oil to pipe wall occurred when the mixture velocity was very low. The lower limit of mixture velocity for larger pipe diameter was computed to be higher (1.1 m/s) than the smaller pipe diameter (0.3 m/s).

CHAPTER III CFD MODEL AND THE OCCURRENCE OF CAF FOR OIL PIPELINE TRANSPORTATION IN HORIZONTAL T AND Y-JUNCTIONS

3.1   Introduction

In this study, the modeling and experimental results (Babakhani Dehkordi et al., 2018) and (Babakhani, 2017) were adopted as the main reference case, mainly for the pipe with diameter combination of 21–30 mm. These studies were performed to better understand the hydrodynamic behavior of horizontal pipes with sudden expansion filled with highly viscous oil and water. The fluid moved from upstream or smaller diameter zone to a downstream or bigger diameter zone. Fig. 6 depicts the physical model of a horizontal pipe with sudden expansion.

Several CFD simulation runs on very viscous oil-water flows have been carried out by means of ANSYS FLUENT. Concerning CAF, CFD simulations have been conducted with VOF (Volume of Fluid) model for 8 different pipe designs of horizontal T and Y-shaped pipes have been completed and part of this chapter has been published (Dianita et al., 2021, 2022). The CFD simulation works started with re-simulation work with case reported by (Babakhani Dehkordi et al., 2018) as the reference, followed with grid and time independence study. The simulation for CAF through different dimension of T and Y- pipes divided into 2 different oil properties and viscosity model. The first work adopted the rheological properties of oil as used by (Babakhani Dehkordi et al., 2018) with assumption of constant viscosity of oil.

The second work was carried out by applying unprocessed crude oil as examined by (Montes et al., 2018) and using Carreau viscosity model.

3.2 CFD Simulation Setup

3.2.1 Numerical Multiphase Model

Volume of Fluid (VOF)

The VOF method, which is a kind of Eulerian method, has been widely used in predicting various two-phase fluid flows and is adopted in this analysis. The VOF formulation relies on the fact that two or more fluids do not interpenetrate each other. For each phase considered in the model a variable is introduced as the volume fraction of the phase in the computational unit. In each of the control volumes, all phases' volume fraction sum up to unity. In the CAF flow pattern, the two-phases are immiscible and separated by an interface having a length scale comparable to the pipe diameter (especially for the oil core, but also for the larger oil drops). Such interface is continuously varying in terms of shape and extension, due to the constant evolution of the flow structures. Thus, VOF model is considered as the most suitable model for CAF case. The VOF method is relatively reliable and versatile, and has been embedded into commercial codes. This model has been shown to provide satisfactory calculations for oil-water flow with medium viscosity ratio (Shi et al., 2017). For this study, VOF model was selected for this study and simulations were conducted on 3D domains using the VOF model.

Mathematical Equations

A single set of conservation equations is shared by the two phases, according to the VOF model. The partial differential equations for mass and momentum

equations are discretized and solved across the domain under the assumption that

there is no mass transfer between phases for incompressible flow:

Mass equation:

$$\frac{\partial(\rho)}{\partial t} + \nabla.(\rho u) = 0 \qquad (3.1)$$

Momentum Equation:

$$\frac{\partial(\rho u)}{\partial t} + \nabla.(\rho u.u) = -\nabla P + \nabla.[\mu(\nabla u + \nabla u^T)] + \rho g + F \qquad (3.2)$$

where

F	:	External body force per volume ($kg\ m^{-2}\ s^{-2}$)
u	:	Average velocity ($m\ s^{-1}$)
ε	:	Turbulent dissipation rate ($m^2\ s^{-3}$)
u^T	:	Average turbulence velocity ($m\ s^{-1}$)

The volume fraction of each fluid or phase in the computational cell is able

to be tracked using the VOF formulation. The volume fractions of all phases are

estimated as a unity in each cell or can be written as Eq. 3.3 where α_o and α_w

represent volume fraction of oil and water, respectively.

$$\alpha_o + \alpha_w = 1 \qquad (3.3)$$

Thus, the density (ρ) and viscosity (μ) of the system can be formulated as Eq.

3.4 and Eq. 3.5 respectively.

Mixture density and viscosity:

$$\rho = \rho_o \alpha_o + (1 - \alpha_o)\rho_w \qquad (3.4)$$

$$\mu = \mu_o \alpha_o + (1 - \alpha_o)\mu_w \qquad (3.5)$$

Interface Tracking

In the CAF system of this study, the interface cells are indicated by the value of oil fraction α_o is between 0 and 1. There are two schemes are usually suggested for reconstruction of sharp contours in order to properly capture the interface i.e., Geo-Reconstruct scheme and CICSAM (Compressive Interface Capturing Scheme for Arbitrary Meshes) scheme. Even though CICSAM scheme is recommended for flows with high viscosity fluid but a work by Shi et al. (2021) and Babakhani (2017) showed a smooth interface for oil-water CAF system when applying this scheme. On the other hand, these works successfully captured the wavy interface after applying Geo-Reconstruct scheme. This wavy interface was also observed in the experimental results. Thus, current simulation work adopted this scheme for appropriately capturing the phenomenon in the interface.

Surface Tension

Surface tension, which reduces the area at the interface between two different fluids, is a significant factor in the minimizing of free energy. The CSF model's validity has been demonstrated by its ability to deliver precise surface force fluid flow without modeling limitations on the number, technical difficulty, or dynamic evolution of fluid interfaces with surface tension, as well as by eliminating the need for interface reconstruction and optimizing surface tension calculation (Brackbill et al., 1992). The well-known Laplace-Young equation is valid when there is a constant surface tension along the interface, and the source term is defined as:

$$F = \sigma \kappa \frac{\rho \nabla \alpha_o}{0.5(\rho_o + \rho_w)} \qquad (3.6)$$

where,

σ	:	Surface tension coefficient (N m^{-1})
κ	:	Interface curvature (m-1)
ε	:	Turbulent dissipation rate (m^2 s^{-3})

with gradient volume fraction:

$$n = \nabla \alpha_o \tag{3.7}$$

$$\kappa = \nabla.\hat{n} \tag{3.8}$$

where,

$$\hat{n} = \frac{n}{|n|} \tag{3.9}$$

$\hat{n}$ is unit surface normal vector (m^{-1}) and n is normal vector of surface (m^{-1})

The estimation of the impact of wall adhesion on fluid interfaces associated with this surface model can be determined by evaluating the equilibrium contact angle (θ_w) between the fluid and the wall.

The condition of dynamic boundary is calculated as below:

$$\hat{n} = \hat{n}_w \cos \theta_w + \hat{t}_w \sin \theta_w \tag{3.10}$$

where $\hat{t}_w$ is unit vector tangential to the pipe wall (m^{-1}).

Realizable k–ε (RKE) Model

The employed model to capture turbulence condition in this study was the realizable k-epsilon (RKE) model. The realizable model was introduced as an alternative to the conventional model, which addresses the limitations by including a new eddy-viscosity formula involving the viscosity variable (C_μ) and dissipation (ε) model equation based on the dynamic equation of the mean square vorticity fluctuation (Shih et al., 1995).

Babakhani's (2017) research intended to compare the experimentally measured two-phase pressure drop with the pressure drop that was estimated using the RKE and SST k-ω turbulence models. Because of this, the RKE turbulence showed enhanced predicting capacities. Additionally, RKE provides more precise calculation, especially for flows including rotation, boundary layers, separation, and recirculation. For flows that experience rotation, boundary layer, separation, and recirculation, the RKE model performs better. Following is a model of the RKE transport equations:

Turbulent kinetic energy:

$$\frac{\partial}{\partial t}(\rho k) + \frac{\partial}{\partial x_j}(\rho k u_j)$$

$$= \frac{\partial}{\partial x_j}\left[\left(\mu + \frac{\mu_t}{\sigma_k}\right)\frac{\partial_k}{\partial x_j}\right] + G_k + G_b - \rho\varepsilon - Y_M + S_k$$

(3.11)

Turbulent dissipation rate:

$$\frac{\partial}{\partial t}(\rho\varepsilon) + \frac{\partial}{\partial x_j}(\rho\varepsilon u_j)$$

$$= \frac{\partial}{\partial x_j}\left[\left(\mu + \frac{\mu_t}{\sigma_\varepsilon}\right)\frac{\partial_\varepsilon}{\partial x_j}\right] + \rho C_1 S_\varepsilon - \rho C_2\frac{\varepsilon^2}{k + \sqrt{v\varepsilon}}$$

$$+ C_{1\varepsilon}\frac{\varepsilon}{k}C_{3\varepsilon}G_b + S_\varepsilon$$

(3.12)

where:

$$C_1 = max\left[0.43, \frac{\eta}{\eta + 5}\right], \eta = S\frac{k}{\varepsilon}, S = \sqrt{2S_{ij}S_{ij}}$$

Eddy viscosity:

$$\mu_t = \rho C_\mu \frac{k^2}{\varepsilon}$$

(3. 13)

where,

k	:	Kinetic energy in turbulance ($m^2\ s^{-2}$)
σ_k	:	Turbulent Prandtl number for dissipation rate ($-$)
u_j	:	Radial average velocity ($m\ s^{-1}$)
x_j	:	Location at radial direction (m)
μ_t	:	Turbulent viscosity (Pa s)
G_k	:	Kinetic energy of turbulence that generated as a result of the mean velocity gradients ($kg\ m^{-1}\ s^{-3}$)
G_b	:	Kinetic energy of turbulence that generated as a result of the buoyancy ($kg\ m^{-1}\ s^{-3}$)
Y_M	:	Compressible turbulence's changing dilatation's contribution ($kg\ m^{-1}\ s^{-3}$)
S_ε	:	Source term specified by user ($kg\ m^{-1}\ s^{-4}$)
S_k	:	Source term specified by user ($kg\ m^{-1}\ s^{-3}$)
S_{ij}	:	Model coefficient (in associated to mean velocities) ($m\ s^{-1}$)
C_1	:	Coefficient (depending on the mean velocities and turbulence field) ($-$)
C_2	:	Model constant ($-$)
$C_{1\varepsilon}$	:	Model constant ($-$)
$C_{3\varepsilon}$	:	Model constant ($-$)
C_μ	:	Turbulence viscosity computation coefficient ($-$)
η	:	Model coefficient (m)
v	:	Kinematic viscosity ($m^2\ s{-1}$)

3.2.2 Initial and Boundary Conditions

According to (Babakhani Dehkordi et al., 2018), pressure gradient overprediction was prevented by using the water initialization approach. Water

was pumped into the annulus at a constant, uniform velocity while oil was launched into the core area. Both fluids flowed at the inlet surface at a steady, uniform velocity and filled the same proportion of the pipe's radius. In order to verify that water adhered to the pipe's inner wall and prevent oil fouling, the angle of wall contact was confirmed at 20°. In order to prevent a negative pressure outcome, the pipe outlet was set to atmospheric or zero-gauge pressure at the wall boundary conditions. Table 1 gives an overview of the simulation's parameters.

3.2.3 Computational Domain

Three-dimensional transient simulations were used in this research because They may depict the main flow parameters in the pipe and are more accurate than two-dimensional simulations. To solve generic scalar transport problems, the finite volume technique was used. To improve the precision and convergence of the VOF solution, the PRESTO and PISO algorithms were utilized. These methods were used to resolve the pressure velocity coupling and continuity equation.

The time step was set to 1×10^{-4}s and the modelling was aimed for 4s of simulation time. To achieve the best result while minimizing the amount of mesh elements, the computational domain was generated using hexahedral elements. The computational cells were designed yo be denser for area near pipe wall to increase the precision of flow field computation in the border regions.

The assumption of numerical convergence was made when the momentum, turbulence, and volume fraction equations' residuals were less than 1×10^{-3}. GAMBIT 2.4.6 was used to create the computational domain, which was then exported to the CFD simulation application ANSYS FLUENT. Eight four-core

processors (each thread contains two four-core, 2.93 GHz Intel ® core TM i7 processors, and eight gigabytes of RAM) were used to execute each simulation. Each scenario requires around one week to compute.

3.2.4 Selected Response Variables

This work used 2^k factorial experimental design to evaluate the impact of design parameters (factors) on a response. Thus, the response parameters for monitoring the heavy oil-water flow were the value of pressure gradient (calculated as an average value), the value of pressure deviation, and the total value of resulted oil hold up (calculated as the average value). These parameters were obtained as a single final value from inlet to outlet. The difference in pressure between the inlet and outlet position with respect to the length of a pipe segment is known as a pressure gradient. The pressure value data was collected at various pipe length points for inlet and outlet (2 output branches).

The average of pressure gradient average was calculated by averaging the pressure drop per length for the upstream and downstream sections. The length of upstream region was 500 mm from the first injection point, and the length of downstream was 800 mm long from the junction coordinate. The average of the upstream and downstream pressure gradients was used to determine the overall value of pressure gradient for various pipe configurations.

The pressure in the system should be consistent for the best conditions. The fluids cannot, however, flow without changing the pressure level. The degree of variance or dispersion in a group of pressure measurements was therefore measured using standard deviation. Three pressure standard deviation values were derived using

the pressure values at each zone to depict the pressure values at an intake area and two outflow areas. By averaging the final pressure standard deviation for each geometry alteration, the three pressure standard deviation numbers were derived.

Furthermore, for economic reasons, the highest possible amount of oil (oil holdup) is required to be accomplished when delivering crude oil. Previous studies used hold-up ratios and pressure gradients as flow efficiency factors to calculate idealized CAF and CAF pattern stability. (A. C. Bannwart et al., 2004; Churchill, 1988; Rodriguez et al., 2006). The volumetric portion of oil that is present at the time was called the oil holdup parameter. The volume percentage of in-situ oil from the intake to both sides of the outflow zone was averaged to get the final oil holdup. Reduced average pressure gradient and standard variation of pressure with high final value of oil hold up suggest a more effective heavy oil-water transportation system within the pipe.

Additionally, the contour of each pipe configuration defined the expected flow regime inside the pipe, ensuring the presence of CAF and studying The findings of response variables were linked to the contour of each geometry in order to better analyze flow performance and to detect the existence of CAF throughout the whole geometry.

Regarding the simulation work for assessing the CAF recovery strategy, the required data were oil holdup, oil volume fraction contour, and pressure contour. These results were extracted to further evaluation if the flow improvement could be achieved and to compare the flow performance with the initial design.

Table 1 — Simulation parameters used in this work

Parameter		Input
Model	Solver	Volume of Fluid (VOF)
		Phase interaction (Surface tension coefficient = 0.02 N/m)
		Multiphase (Primary = water; Second = oil)
	Viscous	RKE (constant oil viscosity)
		Carreau Model
Material	Water	$\rho = 999$ kg/m^3
		$\mu = 0.001$ Pa.s
	Oil (constant viscosity)	$\rho = 890$ kg/m3 (medium oil)
		$\mu = 0.838$ Pa.s
	Oil (Carreau fluid)	$\rho_o = 976$ kg/m^3 (heavy oil)
		$\lambda = 0.07$/s
		$N = 0.61$
		$\mu_{0,\dot{\gamma}} = 170.811$ Pa.s
		$\mu_{\infty,\dot{\gamma}} = 17.414$ Pa.s
Boundary Conditions	Water velocity inlet	4.355 m/s
	Oil velocity inlet	6.349 m/s
	Outlet	1.01325 x 10^5 Pa
	Wall	No slip condition
Controls	Solution	Pressure = Presto
		Pressure-Velocity Coupling = PISO
		Volume fraction = Geo-reconstruct
		Turbulent kinetic energy = Second order upwind
		Momentum = Second order upwind
		Transient formulation = Second order
		Turbulent dissipation rate = Second order upwind
	Initialize	Oil volume fraction = 0
	Residual	Absolute criteria
		Continuity = 0.001
		X velocity = 0.001
		Y velocity = 0.001
		Z velocity = 0.001

As one of the simulation works was to scale up the pipe dimension to industrial size, it was also important to select the oil volume fraction as well as the pressure and velocity data for assessing if the scale up result was in line with smaller pipe dimension flow parameters.

For energy evaluation, the oil volume fraction contour was also important for qualitatively predicting the possible energy savings that could be obtained. For quantitative evaluation, the pressure variable was the important response for further calculation of potential energy reduction.

3.3   Re-simulation of The Referenced Work

As stated in the Section 3.1, this work referred to the previous CFD simulation work (Babakhani Dehkordi et al., 2018) that had been validated to experimental work (Babakhani, 2017) with pipe geometry as illustrated by Fig. 6. The pipe consists of two main regions i.e., upstream (0.5 m of length) and downstream sections (0.8 m of length) separated by intersection point. The total length of the pipe was 1.3 m and this length value was selected to reduce the computational time but at the same time was able to facilitate the flow development.

As the initial step, the re-simulation work was completed for the same flow condition and geometry as the referenced work. Once the result of the re-simulation work was similar or close to the experimental works and fulfilled the mesh and grid independence study, this work continued with the modified pipe geometries.
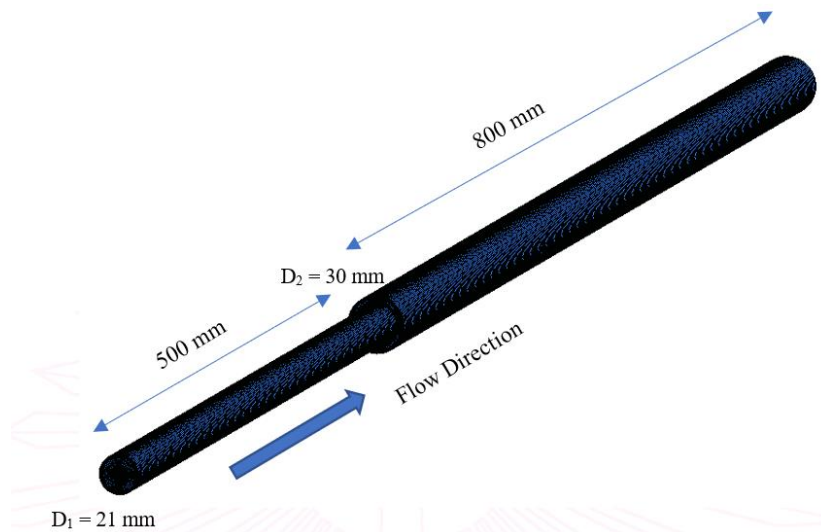
Fig. 6 —The illustration of a horizontal straight pipe with configuration of sudden expansion for re-simulation work (Babakhani Dehkordi et al., 2018)

A grid independence test is performed in every CFD simulation to determine the ideal mesh quantity that has the fewest grids without drastically affecting the numerical outcomes. Using four distinct computational cells—54,254, 182,347, 328,700, and 509,212—to simulate the reference scenario, a grid independence test was carried out in this study (Fig. 7). The numerical results that would be assessed were pressure drop per unit length, pressure distribution, and velocity profile.

3.3.1   Grid Independence Study

The numerical results for pressure gradients for four distinct computational cells are displayed in Table 2. The results showed that the variations in pressure gradient values were quite minor, both upstream and downstream, starting with 328,700 cells. The run with quantity of 509,212 cells caused a 1% change in the upstream pressure gradient as compared to the result with 328,700 cells. When the

cells were changed from 328,700 to 509,212, and this resulted in a 3% increase in the downstream pressure gradient.

Radial Mesh

54,254 cells   182,347 cells   328,700 cells   509,212 cells

Axial Mesh

54,254 cells   182,347 cells

328,700 cells   509,212 cells
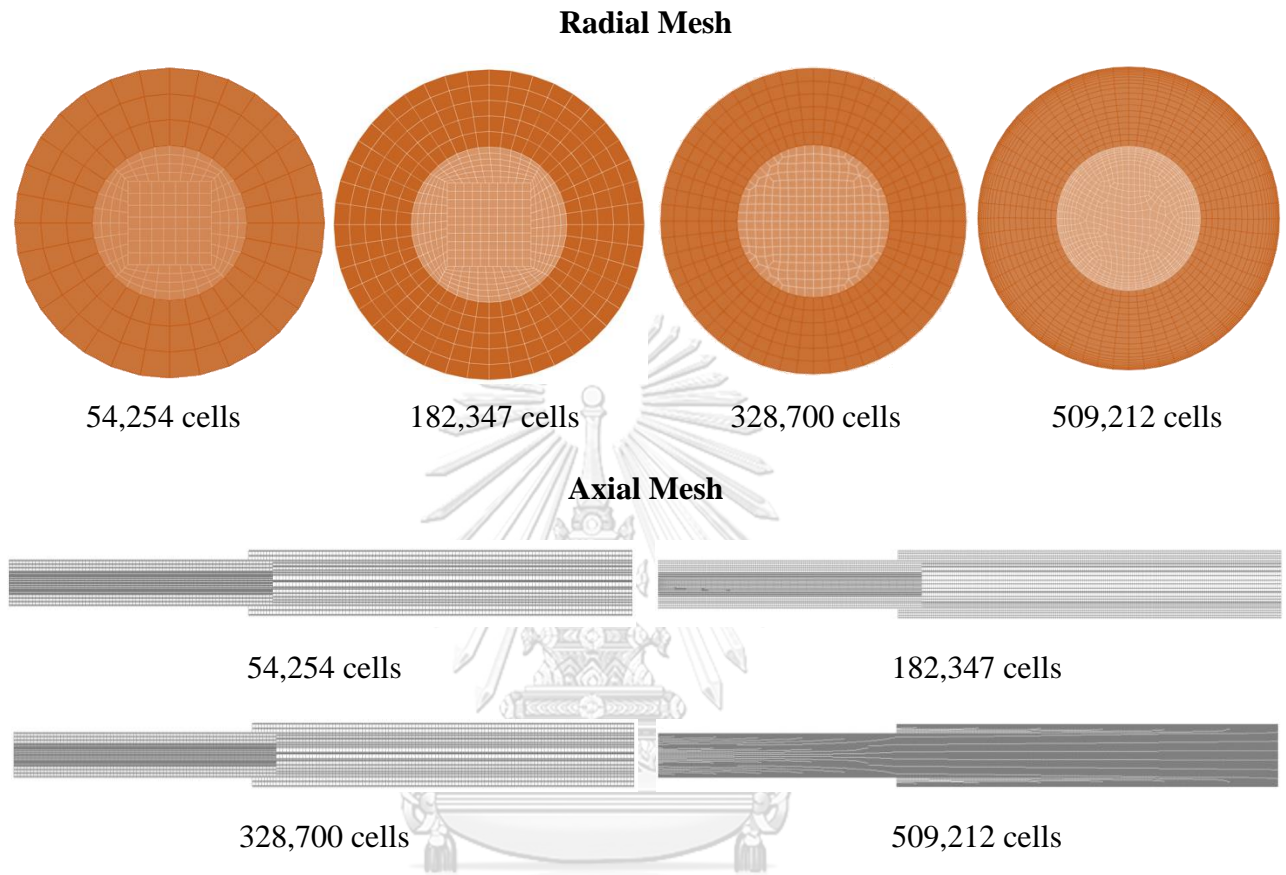
Fig. 7 — Schematic of meshed geometry of the horizontal case with (a) 54,254 cells, (b) 182,347 cells, (c) 328,700 cells, and (d) 509,212 cells

The distribution of resulted pressure along the pipe is depicted in Fig. 8. The top three computational cells consistently displayed nearly identical projected pressure levels since entering the inlet until reaching the outlet of the pipe. A comparable finding that obtained for the velocity profile at various values of Z (from 0.5 m to 1 m) is summarized in Fig. 9. When the value of Z = 1.25 m, a slightly different result is obtained. The distribution of resulted pressure for Z = 1.25 m reveals that there are 2 variants of the mesh number (328,700 and 509,212) still

exhibit a considerably identical line for the resulted pressure distribution. The singularity length is 0.5 m and the maximum axial distance from the singularity is 1.25 m, measured from inlet. A denser mesh is generally preferred because it can provide a better capture of flow conditions. Mesh with higher density number, must involve more computational resources and time. The mesh with a moderate number of cells was chosen since there was little difference in the computational results between the moderate and coarse meshes (Zhao et al., 2019). In this current case, the mesh of 328,700 cells was chosen as the final computational mesh in the next simulation works.

Table 2 – Upstream and downstream pressure gradients for re-simulation case using different computational cells

Mesh number	Pressure at inlet (kPa)		Pressure at outlet (kPa)		Pressure reduction (kPa)		Pressure gradient (kPa/m)		Relative Error to experiment (%)	
	I	II	I	II	I	II	I	II	I	II
54,254	104.182	104.167	99.748	101.328	4.431	2.840	8.870	3.55	5%	131%
182,347	102.371	102.879	97.587	101.328	4.778	1.552	9.561	1.942	3%	26%
328,700	102.161	102.663	97.458	101.328	4.702	1.341	9.390	1.671	1%	9%
509,212	101.951	102.703	97.201	101.328	4.751	1.381	9.501	1.722	2%	12%

* I : upstream, II : downstream
 Pressure gradient results from experiments : 9.29 kPa/m (for upstream), 1.54 kPa/m (for downstream) (the applied experimental condition is listed in Table 3)

The initialization setup for the water, initial oil and water superficial velocities , fluid characteristics (oil and water) as shown in Fig. 6 were all properly executed in this grid independence investigation. These conditions were taken from

Babakhani's experimental work. (Babakhani, 2017). In this flow system, oil occupied the core region with core diameter of 10.5 mm.

Table 3 ─ Summary of test conditions and observed results for model validation

	I	II	III	IV
Test conditions:				
Oil inlet velocity	1.67 m/s	1.67 m/s	1.67 m/s	0.14–1.16 m/s
Water inlet velocity	3.21 m/s	3.21 m/s	3.21 m/s	0.06-0.65 m/s
Pipe configuration	horizontal straight with sudden expansion	horizontal straight with sudden expansion	horizontal straight with sudden expansion	horizontal straight with uniform diameter
Pipe Diameter	21/30 mm	21/30 mm	21/30 mm	15.9 mm
Pipe length	0.5 m (upstream) 0.8 (downstream)	0.5 m (upstream) 0.8 m (downstream)	0.5 m (upstream) 0.8 m (downstream)	6.35 m
Oil viscosity	0.838 Pa s	0.838 Pa s	0.838 Pa s	200-900 Pa s (waxy crude oil) 2.7 Pa s (fuel oil)
Initialization method	water initialization	-	water initialization	-
Observed results:				
Oil holdup	0.275	-	0.307	0.263
Upstream pressure gradient (kPa/m)	9.39	9.29	6.3	-
Downstream pressure gradient (kPa/m)	1.67	1.54	1.45	-

* I: convergence test case, II: experimental work (Babakhani, 2017), III: CFD simulation (Babakhani Dehkordi et al., 2018), IV: semi-empirical correlation based on large database (Arney et al., 1993)
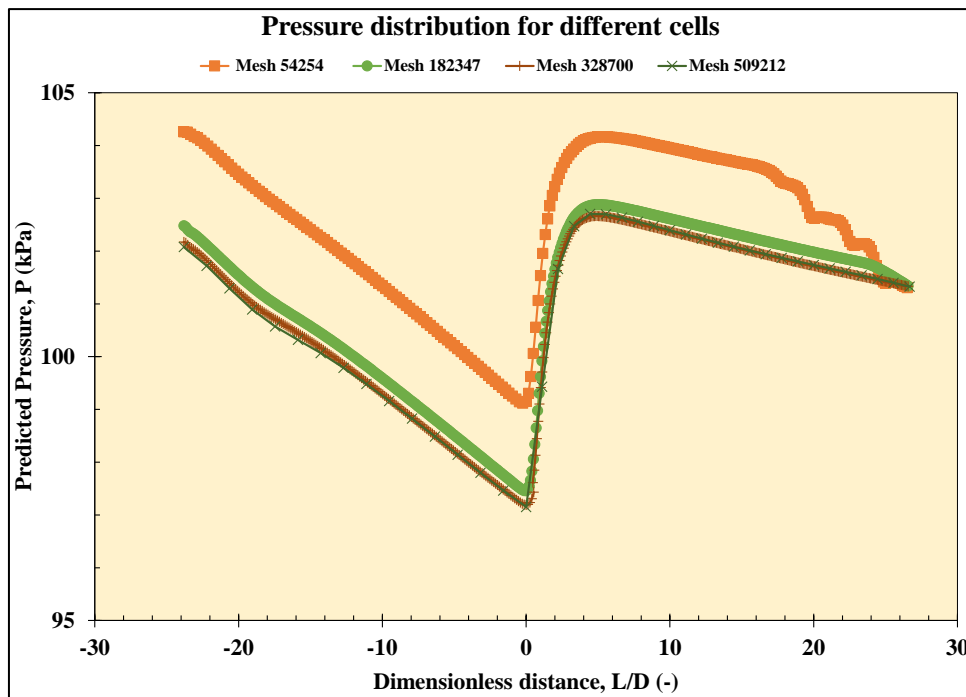
Fig. 8 － Cross-sectional time-average pressure predictions along the pipe's axis for both the downstream and upstream regions for re-simulation work using various computational cells

As a comparison to the result of experiment, the deviation or error of re-simulation work ranged from 1% (328,700 cells) to 5% (54,254 cells) for upstream pressure gradient as illustrated by Fig. 10. With relative errors of 9% and 12%, respectively, the cells 328,700 and 509,212 produced excellent findings for the downstream pressure gradient when compared to experimental data. This successfully verifies the model utilized and verifies the simulation results' correctness. The quantitative computational outputs of the re-simulation work were closer to experimental result compared to the simulation finding given by Babakhani Dehkordi et al. (2018) for the identical experimental study by (Babakhani, 2017), mainly for upstream pressure gradient. The pressure gradient results from the work completed by (Babakhani Dehkordi et al., 2018) were 6.30 kPa/m (for upstream region) and 1.45 kPa/m (for downstream region)

around 32% and 6% below experimental results, respectively. Additionally, according to the results of this simulation, the straight sudden expansion pipe's oil holdup forecast was roughly 4.2% higher than the figure determined by (Arney et al., 1993) correlation. This correlation was developed using a large database derived from high viscosity oil-water tests. With superficial velocities ranging from 0.14 to 1.16 m/s for oil and 0.06-0.65 m/s for water, waxy crude oil (viscosity 200-900 Pa.s) and fuel oil (viscosity 2.7 Pa.s) were utilized. The very thick oil and water mixture was carried via a 15.9 mm internal diameter, 6.35 m of length.

In addition, the oil holdup prediction of the straight sudden expansion pipe of this current simulation result was about 4.2% higher than the value calculated by (Arney et al., 1993) correlation. This semi-empirical correlation was generated by (Arney et al., 1993) by utilizing a big database derived from high viscous oil-water experiments. Waxy crude oil (viscosity 200-900 Pa s) and fuel oil (viscosity 2.7 Pa s) were used, with superficial velocity varying from 0.14-1.16 m/s for oil and 0.06-0.65 m/s for water. The very viscous oil-water system passed through a 6.35 m long pipe with an internal diameter of 15.9 mm.
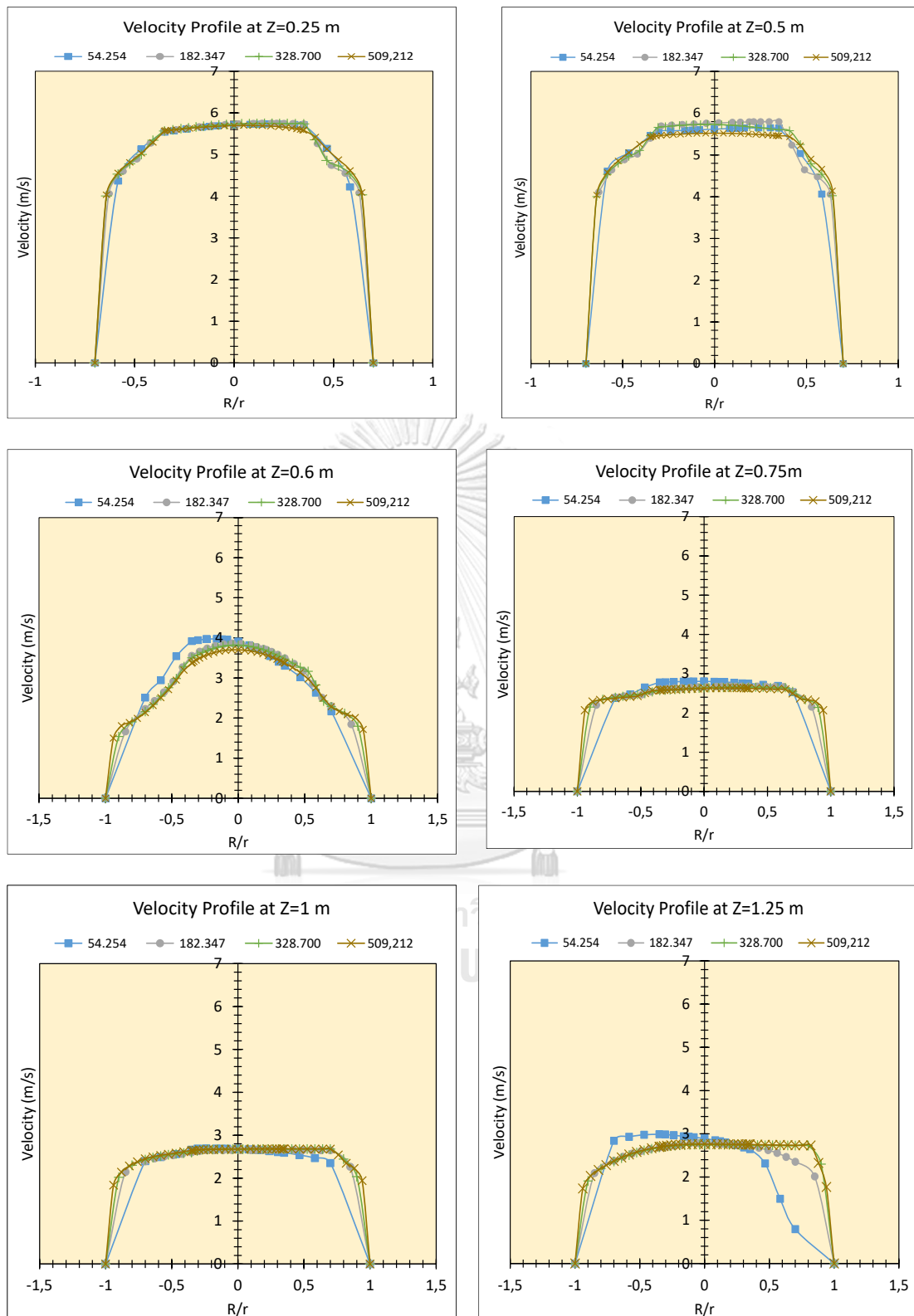
Fig. 9 – Velocity profiles of the upstream and downstream due to sudden expansion for re-simulation work using various computational cells
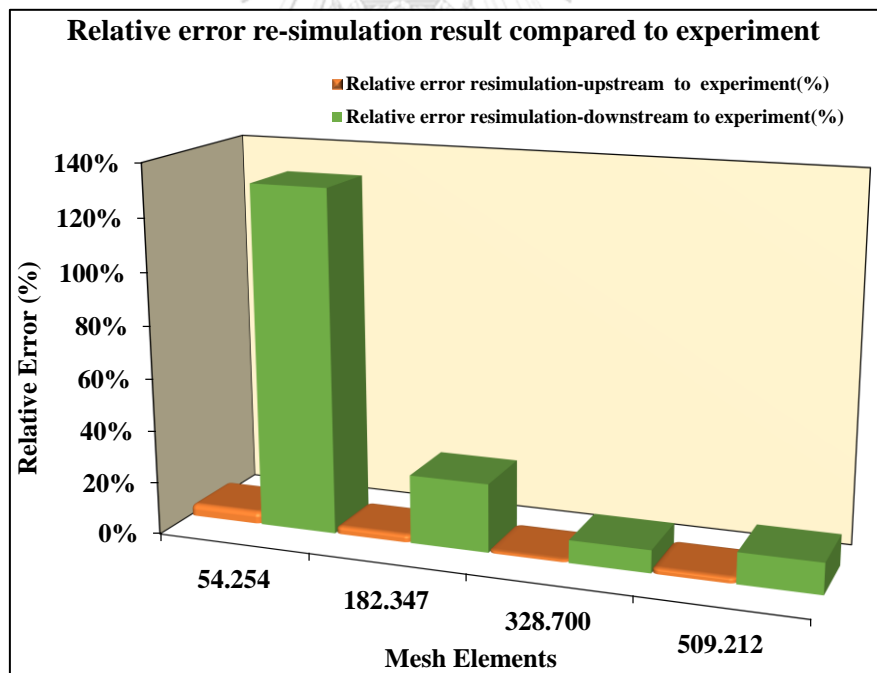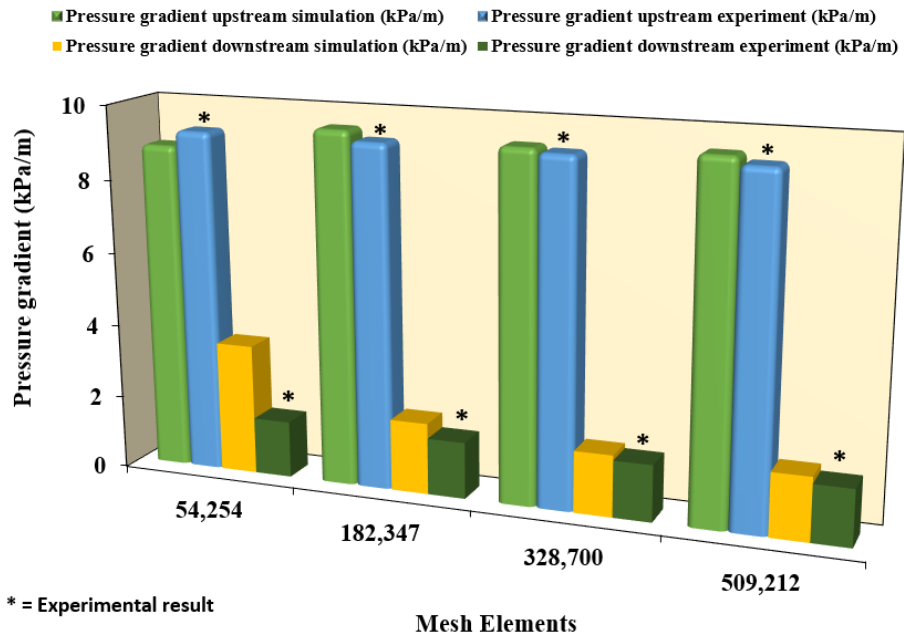
Fig. 10 − *Pressure gradients for re-simulation result with various mesh number (a) Pressure gradients of re-simulation result compared to experimental data* (*b*) *Deviation of re-simulation result compared to experimental data.*

3.3.2   Time Independence Study

The velocity profile of the final mesh elements was generated for a certain time interval as part of the model validation process to perform a time independence test. The criteria for temporal independence was met once the value of velocity started to become stable. Time independence was examined for both the shaped pipes and referred horizontal sudden expansion pipe. While the velocity data for T-shaped junction pipes and Y-shaped junction pipes were retrieved at the intersection area and the downstream points close to the pipe outlet, the velocity data for the reference case was gathered at the downstream site. At t = 0.4 s, the velocity value in this investigation had stabilized or reached a constant value. Using the same interval, the profile of velocity inside the T- and Y-shaped connection pipes was also assessed and show constant result at t = 0.5 s. Therefore, this study selected 4.0 s as the simulation time by using the parameter simulation of the cited work.

3.4   Core Annular Flow in T-Junction and Y-Junction for Oil-Water System: Constant Viscosity of Oil

In the current work, the pipe with configuration of straight horizontal with sudden expansion in the research carried out by Babakhani Dehkordi et al. (2018) and Babakhani (2017) was adopted as the basis to develop the simulation. One of the conclusion that can be highlighted from Babakhani (2017) experimental work is that modify the pipe section's diameter impacted the behavior of the flow. As a result, changes in the flow hydrodynamics from the previous condition as well as shifting velocity and pressure profiles were observed. In this research, the flow "disturbance" caused by changing diameter, as shown in Fig. 6, was assumed to be similar to the

presence of intersection in T and Y-junction, as shown in Fig. 11. As stated in Section 3.3, the grid independence study results indicate that 328,700 mesh elements are the optimal number to be chosen as the selected mesh number for the next computational work.

3.4.1 Computational Geometry

The factorial designs method was used in this research to determine the impact of configuration of pipe on flow and hydrodynamics behavior within various pipe geometries. When many factors are expected to be investigated, the method of 2^k factorial design is especially useful in the initial stages of experimentsThis experimental design provides the minimum number of runs necessary to study k factors in a complete factorial design. The value of k in this study is set to 3, as three specific design factors, namely junction angle, inlet diameter, and outlet diameter, were selected. Consequently, a total of 8 distinct pipe geometries were generated, encompassing two primary pipe configurations, namely T-shaped and Y-shaped pipes. All potential combinations of the levels of the factors were investigated using the factorial designs technique. This technique is additionally useful in determining the primary effects of each independent factor as well as the interaction effects of the factors on the parameters being assessed. Table 4 summarizes the structure of the 2^3 factorial statistical experimental design analysis. As shown in Fig. 11, the length of the upstream section is 500 mm before hitting the intersection point and entering the downstream section, which is 800 mm long.
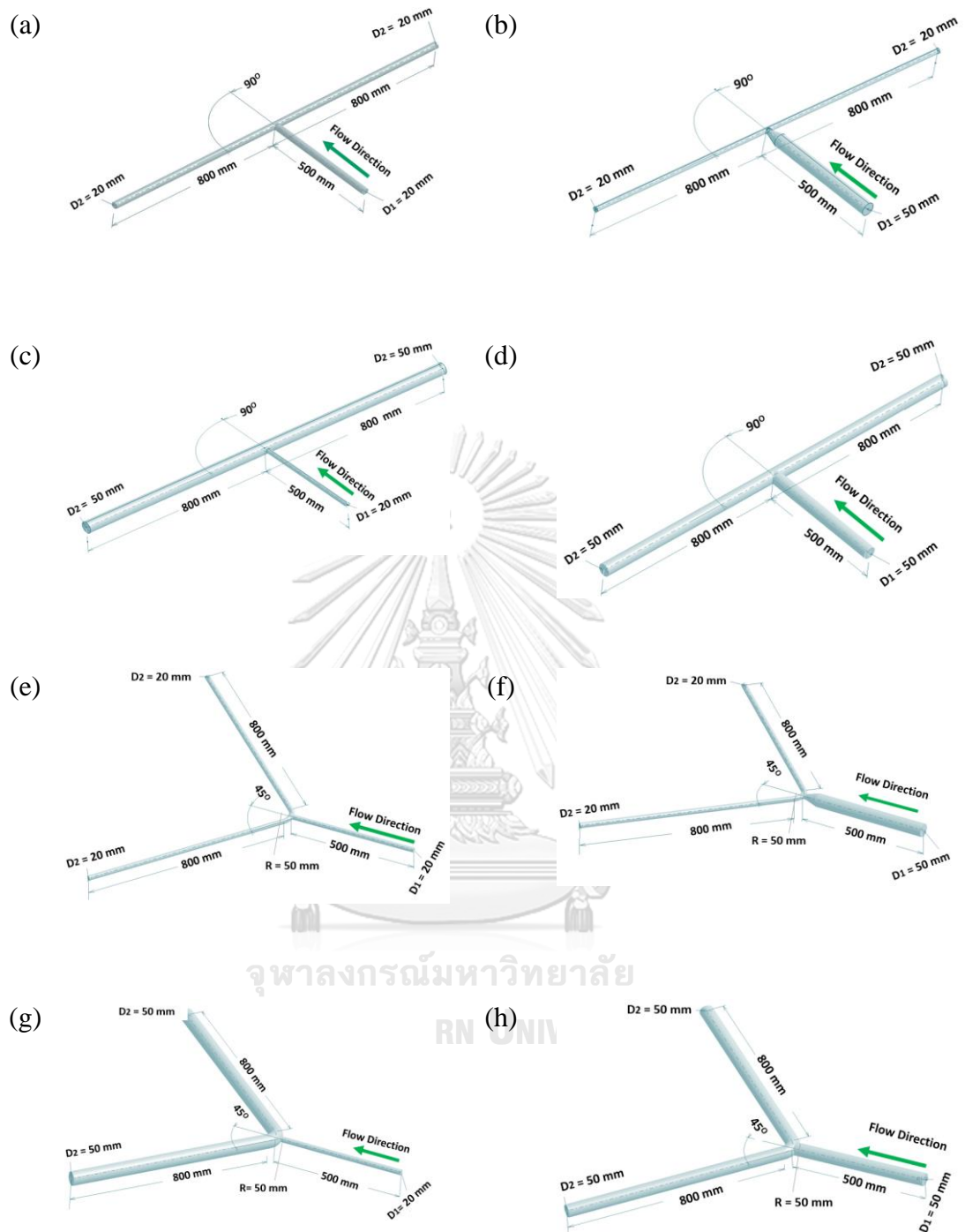
Fig. 11 −The schematic drawings of T and Y− shaped pipe configurations

Table 4— The parameters governing the 2^3 statistical experimental design

Case	Geometry	Bend Angle (º) (A)	Inlet Diameter (mm) (B)	Diameter Ratio (mm) (C)
1	T20-20	90	20	20
2	T50-20	90	50	20
3	T20-50	90	20	50
4	T50-50	90	50	50
5	Y20-20	45	20	20
6	Y50-20	45	50	20
7	Y20-50	45	20	50
8	Y50-50	45	50	50

The factors' levels were chosen to be between low (-1) and high (+1). The angle at the junction, denoted as variable (A), was modified to 45 degrees (represented as "-1") and 90 degrees (represented as "+1") in order to create the T and Y-shaped junction pipes. The computation of the junction angle involves the utilisation of the angle formed between the branch and the point of intersection in a bifurcation. Based on the data presented in Table 5, it was observed that in specific experimental investigations pertaining to oil-water flow, the dimensions of the inlet and outlet diameters were appropriately modified to accommodate the various pipe sizes under consideration. The parameters for the intake diameter (factor B) and outflow diameter (factor C) in the present study were subsequently modified to 20 mm (-1) and 50 mm (+1), respectively. However, the effects of these diameter factors were not considered as separated variables. For analysis purpose, both inlet and outlet diameter were used as unity to represent the diameter ratio effect on the flow performance. The detail of how the diameter effect was interpreted as unseparated variables is presented in Section 3.4.

Table 5 – Previous experiments on oil–water system with various pipe design and viscosity of oil

No	Author	Inlet diameter (mm)	Viscosity of oil (Pa.s)	Pipe Design
1	(Charles et al., 1961)	26	0.00629 0.0168 0.065	Straight
2	(Oliemans et al., 1987)	50	3	Straight
3	(Hwang et al., 1997)	20.37/41.24	0.3 0.0027	Sudden expansion & contraction
4	(A. C. Bannwart et al., 2004)	41.24/20.37	2.7 0.488	Straight
5	(Grassi et al., 2008)	28.4	0.8	Straight
6	(Sotgia et al., 2008)	21	0.9	Straight
7	(Strazza et al., 2011)	21-40	0.9	Slightly inclined
8	(Chen et al., 2012)	21	0.0284	Combined T-junction
9	(Colombo et al., 2015)	40	0.2 0.838	Sudden expansion & contraction
10	(Shi et al., 2017)	50/30	3.3–16.0	Straight
11	(Loh et al., 2016)	50/40	0.03	Straight
12	(Ingen Housz et al., 2017)	25.4	2.2-2.7	Straight
13	(Babakhani Dehkordi et al., 2018)	27.86	0.838	Sudden expansion
14	(van Duin et al., 2019)	21	0.36–2.74	Straight
15	(Garmroodi et al., 2020)	21/30	0.12–0.85	Sudden expansion & contraction (inclined)

3.4.2 Model Validation

The setting of simulations parameters was checked to ensure the quality of model. In this simulation, the mesh quality showed the values with category

of good quality mesh, primarily from the parameter of skewness, aspect ratio, and orthogonality. This work also confirmed the boundary layers occurred near the wall. The turbulent boundary layer has various layers depending on the value of y+. In CFD, y+ is represented by the distance between the wall and the first cell center of the mesh. Theoretically, the closer to the wall, the more accurate the calculation will be. As the best practice, the model of enhanced wall treatment is suggested to show y+ value less than 5 or in the sub layer region to avoid floating point problem that can lead to error or unaccurate results. In this simulation, the y+ value was recorded under 5 Additionally, employing both wall functions and the near-wall model in the buffer region leads to inaccurate computations, hence it is advised to avoid it (Salim et al., 2009).

3.4.3 Results and Discussion

A. 2^3 Factorial Statistical Experimental Design Analysis

One of the reasons for using CAF in heavy oil transport is to minimize total pressure reduction. All flow efficiency parameters, such as hold-up ratio, maximum volumetric flow rate, and lowest pressure gradient at specified flow capacity, can be predicted for this idealized CAF (Churchill, 1988).

Hold-up value are described as the fluids' in-situ volumetric fractions. As reported by (A. C. Bannwart et al., 2004), oil holdups greater than 0.5 were required for the presence of CAF. (Rodriguez et al., 2006) observed the tendency of lower drag level for two-phase system in vertical pipe with core flow using 500-cP oil in a glass tube with an internal diameter of 2.84 cm. When the value of oil holdup was 0.92, the author noticed a stable core flow

pattern, confirming a small quantity of water needed. The performance of heavy oil transportation through the pipe was evaluated in the current work using the important findings of earlier studies and the results of numerical pressure drop and oil hold up. The goal of oil transportation is to get the highest oil fraction at the end point of the pipeline with the lowest pressure gradient in order to reduce pumping costs. As a result, the lower pressure gradient and deviation of pressure, as well as the higher value of oil hold up, represent a more effective technique in oil transportation. Table 6 shows an outline of the collected data, while Fig. 12 shows the areas of data extraction.

Table 6 − Derived CFD simulation results for the 2^3 factorial statistical experimental design analysis

Case	Geometry	Pressure gradient, average value (kPa/m)	SD of pressure (-)	Oil holdup, average value (-)	Obtained flow regime [*]
1	T20-20	66.674	16.451	0.440	stratified
2	T50-20	535.374	85.876	0.421	stratified
3	T20-50	4.824	0.743	0.600	slug
4	T50-50	18.179	3.658	0.502	stratified
5	Y20-20	45.302	10.486	0.463	stratified
6	Y50-20	661.774	120.580	0.394	stratified
7	Y20-50	5.590	0.760	0.552	slug
8	Y50-50	12.988	3.106	0.521	stratified

([*]) visually captured by oil volume fraction contours in Fig. 16

(a)

(b)
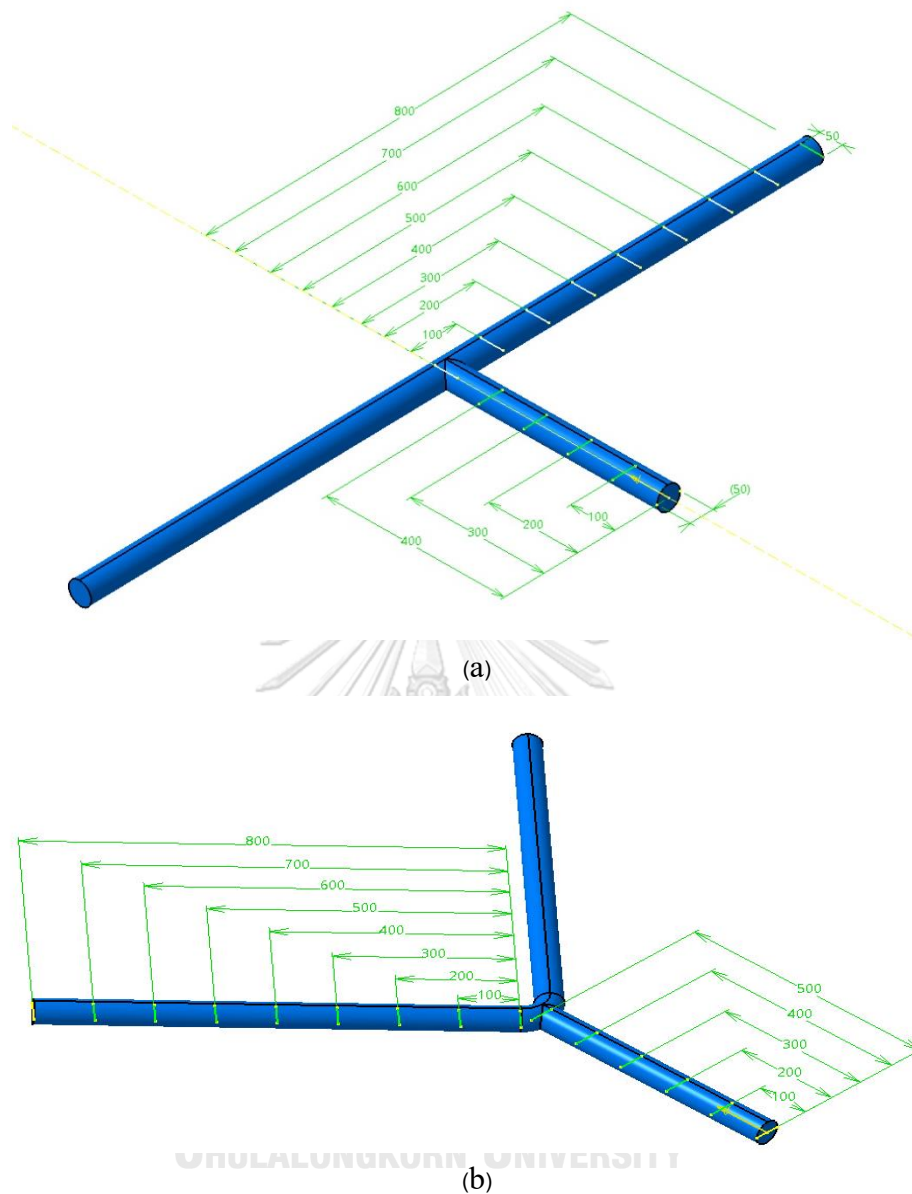
Fig. 12 － Coordinates of data retrieval for the values of pressure and oil holdup (a)
T-shaped pipe and (b) Y-shaped pipe

Present work used a statistical technique to perform the analysis of

variance (ANOVA). The ANOVA method was implemented to identify the

significant variables. The change in defined response caused by the adjustment

of the level of a factor is described as the main effect or effect of that factor.

Meanwhile, it is strongly necessary to assess all significant interactions (Myers et al., 2011).

The ANOVA results from the 2^3 factorial experimental design analyses are listed in Table 7. The deviation level from the resulting mean is determined for the sum of squares. The total sum of squares in an analysis of variance (ANOVA) serves the purpose of identifying the overall variation that may be attributed to different factors. Variance, a statistical measure, is obtained by dividing the sum of squares by the degrees of freedom. The utilisation of mean squares in analysis of variance (ANOVA) is employed to determine the statistical significance of various factors. The concept of degrees of freedom pertains to the quantity of information derived from data, enabling the estimation and calculation of undetermined population characteristics.

The modelling statistics were used to compare the predicted R squares and modified R squares for the three response variables. The difference between the two measures was found to be less than or equal to 0.2.In the event that the gap value surpasses 0.2, it is imperative to investigate potential anomalies within the data or model. This may involve identifying outliers, considering data transformations, or exploring alternative polynomial orders. The statistical method known as R-squared is employed to assess the extent to which an independent variable or variables within a regression model contribute to the variability observed in a dependent variable.Consequently, it is possible to ascertain the proximity of the data points to the regression line. The adjustment of R-squares in relation to the number of components in the model is done to account for the number of points in the design. When the inclusion of an

additional predictor variable is advantageous to the model, it will result in an increase in the adjusted R-squared value. The adjusted R-squared values will exhibit an increase when the additional predictor variable plays a significant role in the model. The experiment also included testing the sufficient accuracy (signal to noise ratio) with a value ratio greater than 4. The determination of the necessary precision was made by comparing the range of predicted values at the design points to the average prediction error. Model discrimination is considered acceptable when the ratio exceeds 4.

The variables in Table 7 with significant impacts, as shown by a p-value less than 0.05, were the ones used to choose the source variationsThe effects of the factors were classified into two distinct categories: major effect and interaction effect. The primary impact, also known as the singular factor impact, demonstrates the linear influence of modifying the quantity of an independent factor. The process involves predicting the outcomes for the negative (-1) and positive (+1) magnitudes or levels of a variable. The junction angle (A) is represented by the low level (-1) and high level (+1) on the x-axis, corresponding to 45 degrees (for Y-pipes) and 90 degrees (for T-pipes), respectively. The smaller (20 mm) and bigger (50 mm) diameter (C) inlet and outlet diameters, respectively, are denoted by the labels (-1) and (+1) on the x-axis. On the other hand, interaction effects are designed to identify how the behavior of one variable is affected by the value of another. Interaction effects occur when two non-parallel lines intersect. The intensity of the interaction increases as the lines of interaction effect chart become more nonparallel. The anticipated outcomes (responses) of statistical study might be influenced by a

variety of circumstances. As a result, adjusting these variables can have a direct impact on the outcomes.

The statistical analysis revealed that the intake diameter (B) and outlet diameter (C) were the primary factors that exerted a substantial influence on the pressure gradient of the flow system in the T and Y-shaped junction pipes. The statistical analysis indicates that the p-values provide evidence of a significant influence of the interaction between input diameter B and outlet diameter C on the flow system. The outlet diameter (C), intake diameter (B), and BC interaction revealed the most remarkable effects when the same procedure was also used to determine the major parameters that influenced the pressure parameters. Table 7 also includes the ANOVA findings for the average oil hold up from pipe input to outflow. The p-value indicated that B and C were significant model terms. Despite the fact that the p-value for the main effect of junction angle (A) exceeds the threshold of 0.05, indicating a lack of statistical significance, it should be noted that the interaction between junction angle (A), inlet diameter (B), and outlet diameter (C), denoted as ABC, exhibits a significant and meaningful impact. According to Montgomery (2006), however, even though the first order effects of the variables (A, B, and C in this example) had p-values higher than 0.05, they should still be taken into account if the interaction (ABC in this case) produced a significant impact. According to the oil holdup response variable results reported in Table 7, parameter C had the most influence, followed by B and ABC.

The average pressure gradient, the standard deviation of pressure, and the average oil hold up, respectively, were estimated using the Eqs. 3.14, 3.15, and 3.16 as given below.

$$dP/L = 168.84 + 138.24X_B - 158.44X_C - 133.05X_BX_C \qquad (3.14)$$

$$SD\ dP = 30.21 + 23.10X_B - 28.14X_C - 21.78X_BX_C \qquad (3.15)$$

$$H_o = 0.4867 + 0.0041X_A - 0.0272X_B + 0.0571X_C \qquad (3.16)$$
$$- 0.0148X_AX_BX_C$$

where the coded variables of X_A, X_B, X_C, X_BX_C, and $X_AX_BX_C$ represent the factors A, B, C, BC interaction, and ABC interaction, respectively.

Equations 3.14 to 3.16 show how to anticipate the reaction for certain amounts of each factor using equations in terms of those factors (X_A, X_B, and X_C). As a result, these equations may be used to optimize a system or design. The simulation results and projected reaction were also contrasted, as shown in Fig. 13.

It is very important to be highlighted that when interpreting main and interaction effect, any statistically significant interaction is the real result because the interaction tells more about the levels of each independent variable than any main effect can (Oja, 2023). Another literature also states that if there is a significant interaction, the effect of simultaneous changes cannot be determined by examining the main effects separately. If there is not a significant interaction, then proceed to test the main effects (Kiernan, 2021).

Table 7 – The ANOVA result for the response variables: the average of pressure gradient, standard deviation of pressure, and average of oil holdup

Response Variable	Source of variation	Sum of squares	Degree of freedom	Mean square	F-value	p-value
Average of pressure gradient	B-B	1.529E+05	1	1.529E+05	74.30	0.0010
	C-C	2.008E+05	1	2.008E+05	97.60	0.0006
	BC	1.416E+05	1	1.416E+05	68.83	0.0012
	Error	8230.67	4	2057.67		
	Total	5.036E+05	7			
Standard deviation of pressure	B-B	4267.97	1	4267.97	27.53	0.0063
	C-C	6335.22	1	6335.22	40.86	0.0031
	BC	3795.68	1	3795.68	24.48	0.0078
	Error	620.12	4	155.03		
	Total	15018.98	7			
Average of oil holdup	A-A	0.0001	1	0.0001	1.25	0.3453
	B-B	0.0059	1	0.0059	55.19	0.0050
	C-C	0.0261	1	0.0261	244.01	0.0006
	ABC	0.0018	1	0.0018	16.42	0.0271
	Error	0.0003	3	0.0001		
	Total	0.0342	7			

จุฬาลงกรณ์มหาวิทยาลัย

CHULALONGKORN UNIVERSITY
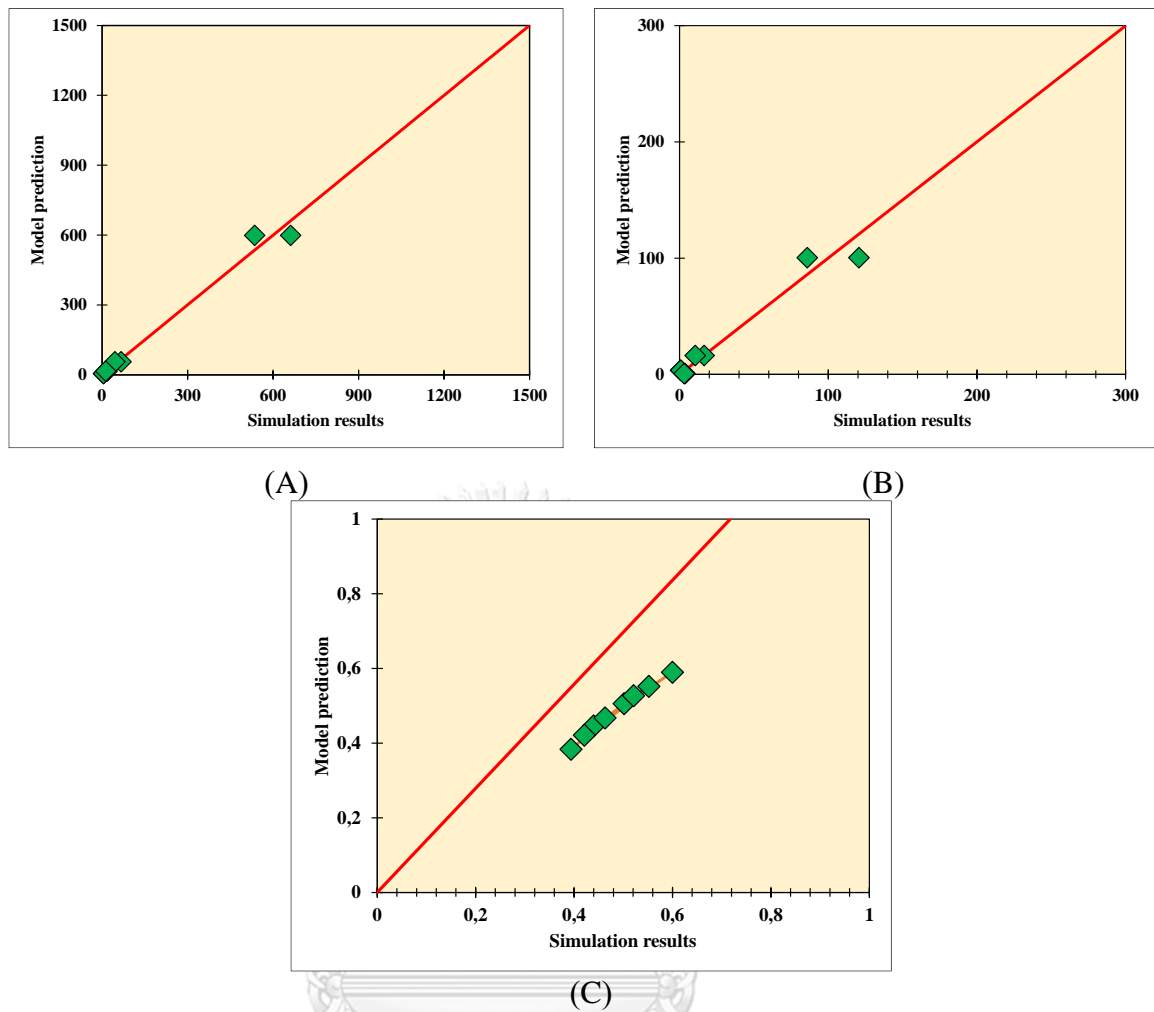
Fig. 13 – Comparison of model predictions and simulation outcomes for (A) the average pressure gradient, (B) the average pressure deviation, and (C) the average oil holdup

The inlet and output diameters should be regarded as one variable when analyzing the impact of diameter factors. The relationship between the two diameters is crucial for illustrating how the diameter ratio affects the effectiveness of the flow. As seen in Fig. 14(a), the optimum result was projected to be attained by a geometry with small intake diameter and large exit diameter or greater diameter ratio as the average of the pressure gradient should be as lower as possible. Pressure drops were found to be greater for geometry with a diameter ratio less than one. According to some studies,

one of the major geometrical parameters involved in flow distribution within junctions
is the diameter ratio of T-junction and Y-junction (Ejaz et al., 2021; Memon et al., 2020;
Saieed et al., 2018; Yang et al., 2019). The downstream section of the small diameter
ratio T-junction and Y-junction experienced a significant pressure drop due to the
Bernoulli effect. Moreover, it can be anticipated that the liquid, primarily composed of
water as the annular fluid, will encounter a narrower cross-sectional area as it reaches
the branches of the downstream region. This will lead to an increase in pressure drop
due to the reduction in diameter of the side branches at the junctions. However, the
critical interaction was also looked at in order to come to a more certain conclusion.

Based on the recorded average pressure measurements at different axial locations
within the flow system, it is deemed most advantageous to sustain a consistent pressure
magnitude from the upstream inlet to the downstream exit. The zero-pressure drop
cannot be sustained naturally, though. The pressure decrease in T-junctions and Y-
junctions is influenced by various factors, including the smoothness of the inner pipe
wall, flow direction, junction angle, and cross-sectional area. (Li et al., 2013). The
pressure loss was indicated by a change in the average pressure number, which was
computed as the pressure standard deviation. The data presented in Figure 14(b)
demonstrates the relationship between BC interaction and the standard deviation of
pressure. It is observed that the impact of outlet diameter on pressure deviation is
relatively insignificant when the inlet diameter is small. However, this effect becomes
more pronounced as the inlet diameter increases. Consequently, the attainment of the
minimum standard deviation in pressure can be facilitated by employing a smaller inlet
diameter in conjunction with a larger outlet diameter or a greater diameter ratio. The
effects of BC on the response variables of average pressure gradient and standard

deviation of pressure were found to be in line with the findings presented in Table 6. The table indicated that expansion geometries with a diameter ranging from 20 to 50 mm exhibited the lowest pressure gradients.

As mentioned earlier, the flow efficiency of T and Y-junctions was influenced by various factors, such as the angle and cross-sectional area of the junction, which was found to be associated with the diameter ratio. The influence of these parameters, namely the junction angle and diameter ratio, exhibited variability contingent upon the specific values assigned to the angle and pipe diameter. Based on the established equations for determining friction loss resulting from junction structures, it can be observed that the loss coefficient associated with the junction angle and pipe wall friction is comparatively lower for a T-junction in comparison to a Y-junction (Li et al., 2013). Another work also stated in their study that the smaller the branch angle of the kerosene-water flow system in vertical T-junction, the more water enters the branch (Puspitasari et al., 2014).

However, it has been observed that within a specific range of pipe diameters, the resilience of oil flow may not be influenced by the diameter of the pipe (Hughmark et al., 1961). Figure 14(c) illustrates the ABC interaction, presenting the observed effects resulting from different outlet diameter values, specifically low and high values. The results indicate that a decrease in outlet diameter resulted in advantageous outcomes at high inlet diameter, while yielding unfavourable consequences at low inlet diameter. When the outlet diameter is larger, an increase in the junction angle has an advantageous impact on the flow at low inlet diameters, but negative consequences at high inlet diameters.

Figures 15(a) to 15(d) depict the response surface of the average pressure gradient, pressure standard deviation, and average oil hold up, considering different significant factors. The utilisation of three-dimensional plots facilitates the visual analysis of the interdependent associations among the response variables. The utilisation of 3D surface plots as a visual tool can contribute to the optimisation process by facilitating the identification of the optimal region within the surface's curvature where the projected results reach their maximum value. The present study identified optimal conditions as those characterised by a low average pressure gradient, a low standard deviation of pressure, and a high oil hold up. Consequently, it can be observed that the optimal design configurations for T and Y-shaped junction pipes are achieved when the junction angle and outlet diameter are increased, while the inlet diameter is decreased. In this study, it was determined that the optimal junction angle for T-shaped pipes, with an inlet diameter of 20 mm and an outlet diameter of 50 mm, is 90 degrees.

(a)   (b)   (c)
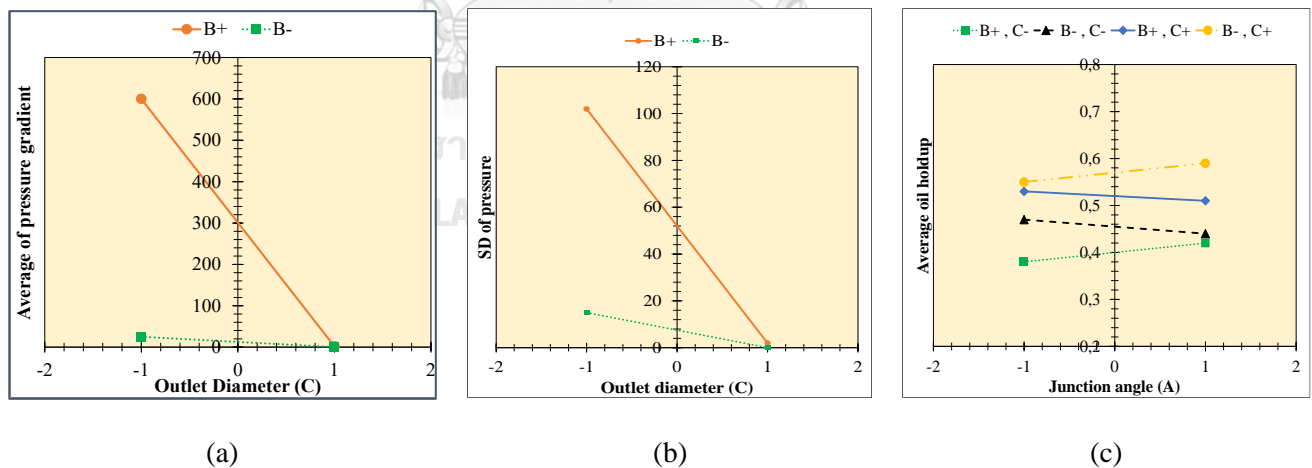
Fig. 14 – The current research examines the interaction effects of various factors on three key parameters: (a) the average pressure gradients, (b) the standard deviation of pressure, and (c) the average oil holdup
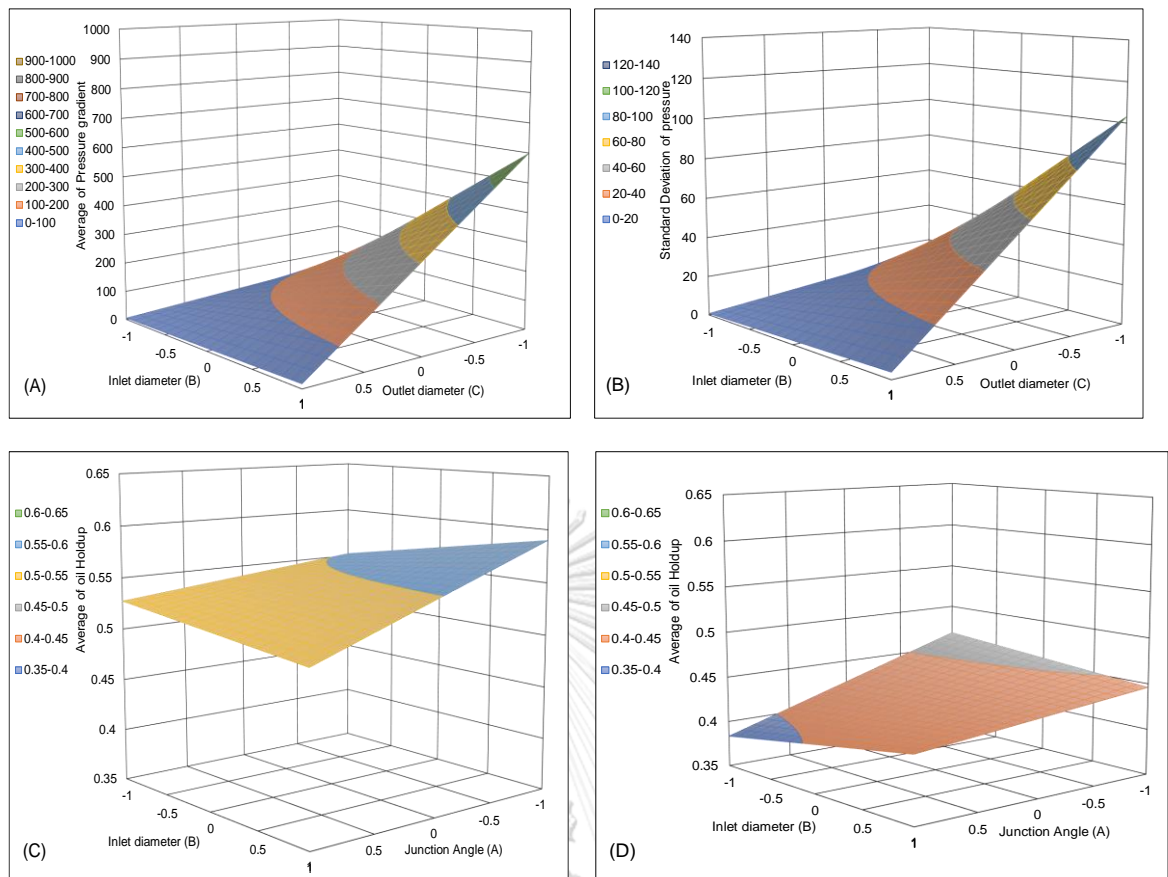
Fig. 15 – The response surface of (a) the average pressure gradient is visualised with respect to the variation in inlet diameter and outlet diameter, while (b) the standard deviation of pressure is visualised with respect to the variation in inlet diameter and outlet diameter. (c) The study examines the relationship between the average oil holdup and the variations in junction angle and inlet diameter, specifically focusing on a high value (+1) of the outlet diameter. (d) The investigation explores the average oil holdup in relation to the variations in junction angle and inlet diameter, with a specific emphasis on a low value (-1) of the outlet diameter.

B. System Hydrodynamics

According to the data presented in Table 6, the average pressure gradient, standard deviation of pressure, and average oil hold up values exhibited a consistent trend across the eight modifications. The performance of Y-shaped junction pipes was found to be superior to that of T-shaped junction pipes in pipe designs characterised by consistent diameter sizes. Moreover, when comparing cases with smaller diameters (Y20-20 and T20-20) to those

with larger diameters (Y50-50 and T50-50), it was observed that the geometries with greater diameters exhibited enhanced flow efficiency in the process of oil transfer.

According to a prior study on vascular junctions (Mynard et al., 2015), fluid behaves as though it will lose more pressure while crossing a Y junction. This study presents a comprehensive analysis of the loss coefficients associated with T- and Y-shaped junction pipes, encompassing various values. The aforementioned loss coefficients exhibit a correlation with pressure losses in the context of diverging flow, which varies depending on the Reynolds numbers involved. For all selected Reynolds numbers, it was observed that the Y-shaped junction pipes exhibited lower loss coefficients compared to the T-shaped junction pipes. The numerical results presented in Table 6 indicate that T-shaped junction pipes outperformed Y-shaped junction pipes in cases where there were variations in diameters between the upstream and downstream areas. This is evident from the observation of lower pressure gradients and higher oil hold up values associated with T-shaped junction pipes. When comparing the configurations of pipes with sudden expansion (20-50) and sudden contraction (50-20), it was observed that the designs featuring sudden contraction exhibited the highest pressure drop and the lowest oil hold up. Balakhrisna et al. (2010) conducted an experimental study, while Wu et al. (2020) combined computational fluid dynamics (CFD) modelling with experimental data. Both studies demonstrated that annular flow within sudden contraction and 90° elbow structures exhibits a greater pressure gradient when the geometry has a smaller diameter. This phenomenon occurred due to the fluid's passage through a

reduced cross-sectional area, resulting in an increase in velocity and a corresponding decrease in internal pressure, or an increase in pressure drop. The investigations of phase separation in T-junction and Y-junction involved the declaration of lower diameter ratios in order to enhance the performance of phase split and modify the flow pattern. The aforementioned ratios were attained through the reduction of the diameter of the downstream or branching components, while keeping the diameter of the main upstream component constant (Azzopardi et al., 1999; Azzopardi et al., 1982; Ejaz et al., 2021).

Based on the findings presented in Table 6, it is observed that the predicted oil holdup values exceed the input volume fraction of oil ($\varepsilon_o = 0.34$). This suggests that either the effective average water velocity surpasses the velocity of oil, or the slip ratio is less than one. This particular scenario may pose challenges in establishing the concept of CAF (continuous annular flow) and transitioning the fluid dynamics to one of several plausible regimes, such as stratified, slugs, bubble, or dispersed flows. Figure 16 displays the two-dimensional representations of the flow patterns corresponding to eight distinct geometries. The presence of CAF in the upstream region was evident based on the observed contours, as the oil-water mixture moved from the inlet towards the end of the junction region prior to branching.

Upon encountering the junction wall and subsequently dividing into two outlet directions, it was observed that stratified flow patterns emerged for variations 1, 2, 4, 5, 6, and 8. Andrade et al. (2013) also reported the almost similar finding in their simulation work for CAF within T-junction for heavy

oil-water flow (ρo = 989 kg/m3, ρ_w = 997 kg/m3, μ_o = 10.0 Pa s, μ_w = 8.89 x 10-4, σ = 0.072 N/m) with diameter of inlet and outlet were 14 cm and 15 cm, respectively. Their results showed that the pressure drop increased during the flow and that the annular to stratified flow pattern altered starting at the bend connection zone. In the downstream region (1,2,4,5,6,8), the flow characteristics at the two branches of each geometry in this study exhibited a general similarity in the case of stratified flow. A small oil layer close to the wall and stratified flow downstream were consistently seen along the Y20–50 geometry contour (case 6). The Y50-20 geometry was found to have the thinnest oil layer in relation to the other geometries, as well as the lowest oil holdup, as shown in Table 6. The T50-50 pipe in case 4 exhibited a slightly undulating interface in the upstream segment near the junction, while the Y20-20 pipe in case 5 displayed a similar wavy interface in the vicinity of the pipe outlets. These waves were generated as a result of the interaction between heavy oil and water in the interface zone. A clear pattern was observed in the morphology of T20-50 (example 3) and Y20-50 (case 7), both of which displayed slug flow within their respective branches. The oil velocity exhibited a decrease in magnitude as the flow pattern transitioned into slug flow. The utilisation of three-dimensional contoured photographs allows for enhanced visualisation of the slug flow phenomena in the aforementioned geometries, as depicted in Figure 17. According to the 3D pictures, oil smashes the rear wall at the junction before flowing incoherently into the sidewall. The 2D illustration did not adequately depict the problem.

Changing flow rates and volumetric flow ratios typically disrupt the annular flow in a straight pipe system (Dessimoz et al., 2008). Nevertheless, the presence of an intersection that separated the upstream and downstream sectors had a detrimental effect on the stability of the previously built CAF in this study. The contour representations illustrate that once the primary flow structure reached the termination point of the upstream length and started to approach the downstream region, it bifurcated into two distinct branches. At the point of convergence, the velocity of oil was observed to be higher than that of water. It is unlikely that water made contact with the intersection wall, as oil exhibited greater velocity and ultimately collided with the wall at the termination point of the intersection. The oil was distributed to each outlet direction within the annulus, while the water was directed towards the nearest outlet side in the downstream area. As a consequence of the sudden occurrence, the oil came into contact with the inner surface of the pipe, leading to a significant increase in pressure drop. However, the shape of examples 3 and 7 implied a specific type of flow occurring downstream. The impact of geometry on the flow pattern was evident, despite the similarity in velocity trends at the junction region to other scenarios, where the velocity of oil exceeded that of water.

In the present study, the superficial velocities remained unaltered. On the other hand, the experimental study examined the impact of varying surface velocities on the pressure gradient, oil holdup, and flow pattern. In their research, Babakhani Dehkordi et al. (2018) and Babakhani (2017) conducted experiments and developed models to investigate the impact of their interventions on the flow characteristics in a sudden expansion horizontal pipe.

The pipe had an upstream diameter of 21 mm and a downstream diameter of 30 mm. The researchers were able to increase the J_o for CAF from 1.67 m/s to 3.35 m/s, as well as modify the J_w range from 3.21-3.24 m/s.

Based on the findings from experimental observations and computational fluid dynamics (CFD) simulations, it can be inferred that higher values of the dimensionless parameter J_o are associated with an increased pressure gradient in both the upstream and downstream regions. Furthermore, higher oil holdup values were observed for higher J_o values, based on both simulation work and the Arney et al. (1993) correlation. A transition flow pattern from core-annular flow (CAF) to dispersed flow was observed across all surface velocity ranges, characterised by the presence of a thicker oil core at higher values of the dimensionless flow rate (J_o). Jiang et al. (2021), Joseph et al. (1997), and Sotgia et al. (2008) all discussed various oil and water superficial velocities. In the aforementioned works, the development of the flow pattern based on the oil and water superficial velocities was forecasted using the flow pattern map that was created after studying the evolution of the flow pattern according to the oil and water superficial velocities. In their study on flow regimes and pressure drop reduction in horizontal pipes for oil-water mixtures, Sotgia et al. (2008) observed that increasing the oil superficial velocities beyond a critical value resulted in the transformation of flow patterns from various water superficial velocities to core annular and wavy annular patterns. This transformation occurred across a wide range of water superficial velocities.

The present study revealed that certain variables, including the superficial velocity of each phase, mixture flowrate, pipe dimension, and structures, exerted an influence on the transition of flow pattern from upstream to downstream regions. The stratified flow observed in this study can be attributed to the gravitational separation of the fluid, leading to the formation of distinct oil and water layers that exhibit a smooth interface. The slug flow observed in geometry with sudden expansion, specifically cases 3 and 7, exhibited an augmentation in the velocity of water within the system. The slug flow phenomenon in oil transportation was investigated in an experimental study, which found that at low mixture velocities, an intermittent phase occurred. This phase was characterised by the presence of water slugs and was observed to reduce the pressure gradient of heavy oil flow (McKibben et al., 2000). The significance of water slugs in facilitating the transportation of a substantial volume of oil through a pipeline characterised by a low pressure gradient has been ascertained. This discovery indicates that the establishment of counter-current air-water flow (CAF) may lead to a reduction in pressure drop during the occurrence of slug flow in the oil-water system. Based on the data presented in Table 6, it can be observed that cases 3 and 7, characterised by slug flow patterns, exhibited comparatively lower pressure gradients in the downstream region when compared to other geometries featuring stratified flow. The observed low pressure gradient is indicative of the relatively low velocity of the mixture.

High momentum transfer capacity, low buoyancy effects, low free energy at the interface, fewer dispersed phase droplet sizes, wettability, and the

volume fraction and droplet distribution of the dispersed phase due to the density difference between the oil and water phases are the primary causes of variations in liquid-liquid flow characteristics (Ismail et al., 2015). Shi (2017) found that when flow system characteristics such viscosity, density, and pipe diameter were quantitatively changed, the flow structure will fundamentally change Nevertheless, previous studies conducted on flow systems in T-junctions and Y-junctions have specifically examined stratified liquid-liquid flow and gas-liquid flow. These investigations have revealed that both the branch angle and flow direction significantly influence the flow performance, encompassing flow pattern, holdup, and pressure drop. The modelling results of this study revealed that phase separation and alterations in the flow pattern were observed for all potential adjustments in pipe geometry. Therefore, it is not recommended to utilise the geometries and conditions employed in this simulation study to establish the CAF (core annular flow) for an oil-water system with the intention of benefiting from water lubrication around the oil core. The stability of the CAF (Cyclically-Assisted Filtration) was not sustained upon traversing the junction, resulting in the core phase coming into contact with the inner surface of the pipe.
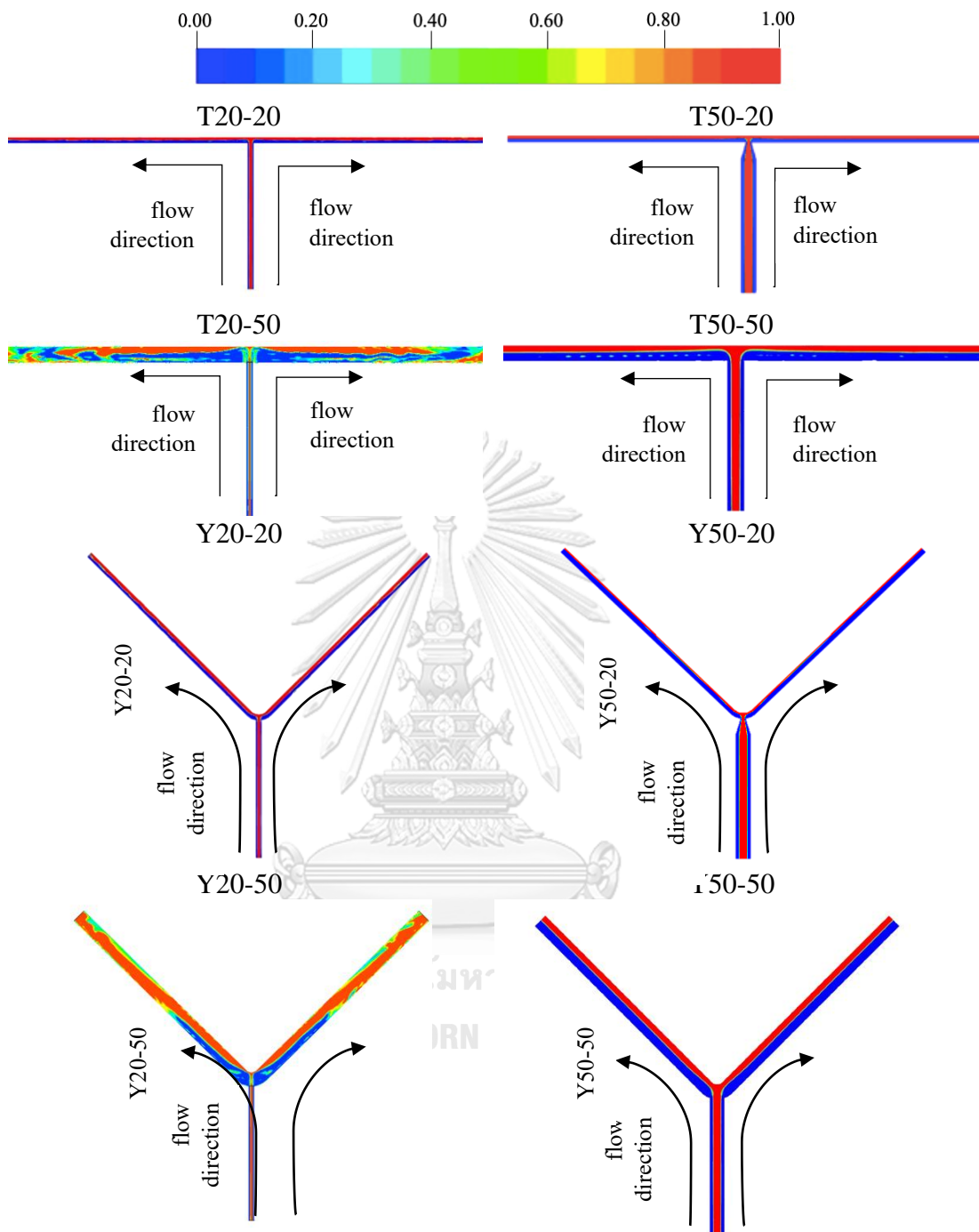
Fig. 16 – Two-dimensional visualisation of oil fraction contours for eight different cases involving T and Y-shaped junction pipes.

(a)

(b)
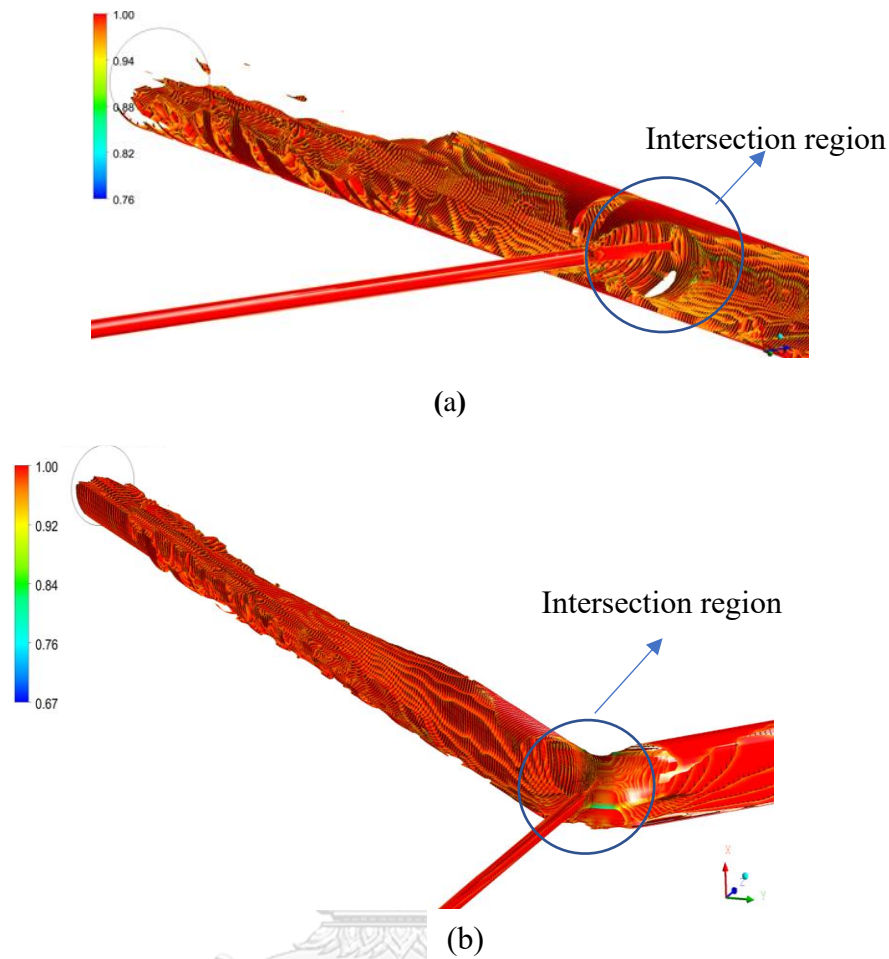
Fig. 17– The three-dimensional contour plot illustrates the distribution of the oil phase fraction in the downstream region, specifically at two locations: (a) T20-50 and (b) Y20-50.

3.4.4 Conclusion

The computational fluid dynamics (CFD) analysis was conducted to simulate the flow of heavy oil and water in T and Y-shaped junction pipes. Various combinations of junction angle, inlet diameter, and outlet diameter were considered during the modelling process. Based on the outcomes of the simulation, it can be observed that the establishment of CAF stability was not observed in the downstream region subsequent to traversing the intersection area. Upon the introduction of fluids into the downstream region, the flow system exhibited two discernible patterns of

behaviour. Initially, the dense oil came into contact with the inner surface of the conduit during its flow. Furthermore, the movement of the oil exhibited irregular patterns, with the denser heavy oil being enveloped within the flow system composed primarily of water. Consequently, the flow pattern underwent a transition from core annular to stratified and slug flow. The present study observed that instances of abrupt expansion exhibited a slug flow pattern characterised by the lowest pressure gradient and the highest oil holdup in comparison to stratified flow. In contrast, the suddencontraction configuration demonstrated resistance to an increase in pressure gradient and a reduction in oil holdup.

Based on the factorial statistical experimental analysis, it was observed that the average pressure gradient and the standard deviation of pressure were significantly influenced by the parameters of inlet diameter, outlet diameter, and the interaction between inlet and outlet diameter. However, it was determined that the outlet diameter made a more significant contribution. The variation in junction angle did not yield any discernible impact on the mean pressure gradient, standard deviation of pressure decline, or average oil holdup.

The average oil holdup was significantly influenced by the interaction effect of junction angle, inlet diameter, and outlet diameter, as well as the main effects of junction angle, inlet diameter, and outlet diameter. The present study aimed to establish the optimal condition, which was characterised by a low average pressure gradient, a low standard deviation of pressure, and a high oil hold up. Hence, optimal design configurations for T and Y-shaped junction pipes are attained by increasing the junction angle and outlet diameter, while decreasing the inlet diameter. However,

the combined effect of junction angle, inlet diameter, and outlet diameter, as well as the individual effects of junction angle, inlet diameter, and outlet diameter, had a statistically significant impact on the average oil holdup. This study aimed to establish the optimal condition, which was characterised by a low average pressure gradient, a low standard deviation of pressure, and a high oil hold up. Therefore, the optimal design configurations for T and Y-shaped junction pipes are attained by increasing the junction angle and outlet diameter while decreasing the inlet diameter.

3.5   Core Annular Flow In T-Junction And Y-Junction For Oil-Water System: Oil As Non-Newtonian Fluid

This Sub-Chapter discusses the simulation results that was developed from previous simulation work in Section 3.4. This section examines the occurrence of crossflow amplification (CAF) in a non-Newtonian high viscous oil-water system, specifically through horizontal T and Y-junctions with symmetrical dividing flow. The Carreau viscosity model is utilised for this analysis. Previous experimental, theoretical, and numerical CAF studies have been performed on highly viscous oil-water. The primary focus of the research conducted is applicable to the behavior of Newtonian fluids within a pipe. Infact, the heavy crude oil exhibits non-Newtonian characterization. Heavy oil is classified as a non-Newtonian fluid due to its shear-thinning rheological properties, wherein the effective viscosity decreases as the shear rates increase. However, due to their non-Newtonian properties, heavy oils are difficult to transport. CAF is the preferred method of non-Newtonian oil transportation (Jiang et al., 2018). In particular, the rheology of non-Newtonian fluid affects the CAF characteristics (Picchi et al., 2018).

Almost all investigations on CAF have been undertaken under the assumption that the core fluid's viscosity is constant, despite the fact that there is an extensive amount of literature on CAF involving very viscous oil or non-Newtonian liquid. (Tripathi et al., 2015). Only a few CAF theoretical investigations have up till now taken into account the presence of shear-thinning fluids (Jiang et al., 2016; Jiang et al., 2018; Picchi et al., 2016; Picchi et al., 2018; X. Sun et al., 2010; X. W. Sun et al., 2012; Tripathi et al., 2015). The rheological characteristics of non-Newtonian liquids were expressed in these experiments using the Ostwald de Waele power law model. However, this approach is only useful in a small number of operating circumstances due to the limitless rise in viscosity value forecast at low shear rates. In order to better understand the structure and flow characteristics of activated sludge, a prior study assessed the predictive power of seven different models for the viscosity of Non-Newtonian fluids (Power law, Bingham plastic, Herschel-Bulkley, Casson, Sisko, Carreau, and Cross) (Khalili-Garakani et al., 2011). In terms of predicting viscosity throughout the whole range of MLSS (mixed liquid suspended solids) concentrations, the Cross model and the Carreau model came out on top. Despite their lower level of precision, the Herschel-Bulkley and Casson models still proved to be appropriate for the given context. Picchi et al. (2018) employed a shear-thinning Carreau fluid in their prior research to present a comprehensive solution for laminar fully formed concentric annular flow (CAF) in both horizontal and inclined pipes. The observed behavior of the two-phase annular flow, characterized by a combination of non-Newtonian and Newtonian properties, was found to persist across a range of operational conditions. This behavior was observed even in the presence of complex rheological properties exhibited by the liquid, as described by the Carreau fluid model.

The simulation conducted in this section was an extension of the simulation work discussed in Section 3.4. It employed comparable geometries, multiphase flow simulation parameters, grid independence test outcomes, simulation duration, convergence criterion, and flow system response variables. However, it is important to note that the heavy oil studied in this particular section was categorized as a non-Newtonian Carrreau fluid, exhibiting rheological properties comparable to an untreated crude oil sample as described by Montes et al. (2018). The heavy oil had a viscosity (μ_o) of 170.811 Pa.s at zero shear rate and a density (ρ_o) of 976 kg/m3. The calculated parameters of the Carreau rheological model for viscous oil are presented in Table 1.

3.5.1   Carreau Viscosity Model

.For this simulation part, the Carreau model was selected to facilitate the non-Newtonian fluid's rheological behavior. The flow behavior number (N) describes the fluid's behavior, and values less than one indicate that the fluid is pseudoplastic. This equation explains the rheological behavior of a shear thinning fluid at low and high shear rates, with zero shear rate viscosity (μ_0) and infinity shear rate viscosity (μ_∞). Eq. 3.17 depicts the equation relating to the Carreau model.

$$\mu = \mu_{\infty,\dot{\gamma}} + \frac{\mu_{0,\dot{\gamma}} - \mu_{\infty,\dot{\gamma}}}{(1 + (\lambda_c \dot{\gamma})^2)^N} \tag{3.17}$$

3.5.2   Model Validation

The calculation of oil holdup for straight sections of pipe involved the utilization of the semi-empirical correlation developed by Arney et al. in 1993. The correlation presented in this study is based on an experimental investigation conducted using waxy crude oil with a viscosity range of 200 to 900 Pa.s, as described in Section 2.9. The outcome of this study indicated a decrease in error of

approximately 5 to 10% when comparing the model that incorporated variable viscosity to the model that assumed constant viscosity. This difference was observed specifically in the predicted oil holdup values for the upstream straight segment (from the inlet to near the junction) and the downstream straight segment (located 200 mm after the intersection to the pipe outlet).

The time step and simulation time utilized in this study were 1×10^{-4} s and 4 s, respectively, as indicated in the computational domain section. Furthermore, the selection of these numbers was made with the intention of regulating the Courant number. The duration of a particle's residence in a single mesh cell can be quantified using a dimensionless parameter known as the Courant number. The stability of the numerical method employed in the solver can be evaluated by utilizing the Courant number, which is contingent upon the local flow velocity, the mesh size, and the time increment. In order to precisely represent the alterations in the flow variables, it is imperative that the Courant number remains below a value of one. The Courant number for all geometries in this research ranged from 0.6 to 0.8. When the Courant number surpasses unity, the information propagates through multiple grid cells within each time step. Certain integration schemes can lead to inaccurate solutions and solution divergence. In instances where the simulation failed to converge or when the Courant number exceeded unity, adjustments were made to the under-relaxation factors (URF) setting to effectively control the Courant number. The control of the iterative process is achieved by the utilization of the Under-Relaxation Factor (URF), which effectively mitigates the impact of numerical errors on the flow solutions, thereby preventing fluctuations in the flow.

The evaluation of the mesh's quality involved the assessment of the skewness ratio and orthogonal quality rate. In this particular instance, the orthogonal quality rate ranged from 0.8 to 0.95, while the skewness ratio ranged from 0 to 0.3. The numerical data presented in this study indicates that the mesh quality employed in the research falls within the spectrum of very good to excellent.

To validate the differentiation between the mass entering and exiting the system, an analysis of the mass balance within the system was conducted. In the conducted simulation, it was observed that the mean disparity between the mass flow rates upstream and downstream across all geometries amounted to a mere 3×10^{-3}. This suggests that the mass balance system's requirement has been fulfilled.

3.5.3   Results and Discussion

A. 2^3 factorial statistical experimental design analysis

The same input factors and response variables that were discussed in Section 3.4 are used in this part. Table 8 provides a summary of the results collected for the response variables. For the results, similar and different phenomenon were observed compared to the first case in Section 3.4. The same phenomenon occurred that for pipe with similar diameter ratio, pipes with smaller diameter (20-20) have higher pressure drop and lower oil holdup than bigger pipes (50-50) . The same phenomenon also occurred for geometries with sudden contraction (smaller diameter ratio) that showed lower oil holdup. However, different trend was observed for configurations with diameter combination of 50-50 that have comparatively high oil holdup and low pressure drop compared to other diameter ratios for the same junction angle.

In order to identify variables that are statistically important, an analysis of variance (ANOVA) was also performed as shown by Table 9. As previously discussed in Section 3.4.3, the statistical value indicating the significant variables should be interpreted not only referred to the p-values but also the indicated flow phenomenon that might be occurred mainly because of the interaction between the independent variables.

Table 8 − Derived CFD simulation results for the 23 factorial statistical experimental design analysis (oil as Carreau fluid)

Case	Geometry	Average of pressure gradient (kPa/m)	SD of pressure (-)	Average of oil holdup (-)
1	T20-20	369.83	96.802	0.657
2	T50-20	496.61	82.636	0.518
3	T20-50	857.12	130.481	0.605
4	T50-50	67.08	14.326	0.699
5	Y20-20	1336.68	379.717	0.575
6	Y50-20	1156.02	220.726	0.512
7	Y20-50	1000.24	268.408	0.522
8	Y50-50	76.61	18.151	0.603

According to Fig. 18(a), interactions between A and other factors is not considered significant. The best result of oil holdup can be achieved for larger diameter value. This prediction could come to accurate, especially in the context of the shape and flow conditions discussed in this paper. The findings align with the conclusion drawn from Table 8, indicating that T or Y-shaped pipe designs with 50 mm inlet and outlet diameters exhibit superior oil hold up compared to alternative geometries, when considering the same junction angle. The presented interaction chart indicates that there is no significant difference in oil holdup between uniform smaller diameter (20-20) geometries and uniform larger diameter geometries, even when the diameter ratio of T50-50 and T20-20 or Y50-50 and T20-20 is approximately equal to 1. However, the

data presented in Table 8 indicates that designs with a diameter ratio of 1 exhibit a relatively higher oil holdup in comparison to designs with different diameter ratios, while maintaining the same connection angle. The geometries exhibiting the highest diameter ratio (D1/D2 = 2.5) demonstrate the lowest oil holdup values in both T and Y-shaped pipe configurations.

According to the p-values associated with the various source changes, it was anticipated that the interaction effect between variables B and C would exert the most significant impact on the pressure gradient value, in comparison to the effect of variable AC. This observation is particularly evident in Table 9, particularly with regard to the average pressure gradient. In order to provide further elucidation on the interplay between various components and their impact on the average pressure gradient, Figure 18(b) illustrates the interactions involving components AC and BC. According to the AC interaction, it is anticipated that the impact of the outlet diameter will be more pronounced when the junction angle is at a lower level (i.e., a smaller angle), while it will be less significant when the junction angle is at a higher level (i.e., a larger angle). The simulated flow system achieved the lowest pressure drop when both diameters were increased to a high level or a larger diameter with a higher junction angle (A). Furthermore, the study revealed a significant correlation between BC and setups characterized by larger input diameters, while the impact was comparatively less pronounced for designs featuring smaller exit diameters. If the diameters of both the inlet and outflow are increased, the desired condition will be achieved regardless of the junction angle. The potential reduction of fouling in lubricated oil-water systems due to the impact of a larger diameter in the CAF through abrupt contraction and expansion

has been suggested to have an effect on system pressure drop (Kaushik et al., 2012). According to the study conducted by Li et al. (2013), it was observed that T-junctions exhibited a lower loss coefficient compared to Y-junctions, with the variation being dependent on the inclination of the junction and the friction of the pipe wall. The present study observed the minimum pressure drops of T-shaped pipes, specifically T50-50, resulting from the combined influences of variables on the mean pressure gradient, as depicted in Figure 18(c).

Table 9 presents varying results pertaining to the standard deviation (SD) of pressure. The standard deviation of fluid system pressure in the pipe was found to be significantly influenced by three factors, namely A, B, and C. Among these factors, A exhibited the most substantial impact, as evidenced by its lowest p-value of 0.0121, while B and C had comparatively smaller effects. The standard deviation of pressure was affected by modifications in the AB, AC, and BC interactions, which were in turn influenced by the interaction of two components. Although the p-values of AB and AC were nearly equivalent, the p-value of BC was comparatively higher.

The phenomenon of pressure loss was identified and quantified by calculating the standard deviation of pressure measurements taken at different points along the length of the pipe, where the average pressure value exhibited variation. The pressure standard deviation is generally reduced when A, B, and C have higher values, as demonstrated in Figure 18(c) and (d). The findings of this study indicate that it is feasible to achieve a gradual pressure shift along the length of a pipe without experiencing a sudden drop in pressure, by utilizing a larger pipe diameter and an appropriate junction angle as implemented in the simulation. The interaction effects of AB (Fig. 18(c)) indicate that

a larger junction angle, particularly when combined with a larger intake diameter, leads to a decrease in the standard deviation of pressure. The impact of the smaller outlet diameter (C) on the larger junction angle (A) is minimal, as depicted in Figure 18(d). In order to optimize the outcome of the AC interaction, it may be advantageous to consider modifying the design by increasing the junction angle and enlarging the outlet diameter. Based on the findings of the BC interaction (Figure 18(d)), it can be inferred that a design featuring a greater outlet diameter and a smaller inlet diameter, or a higher diameter ratio, will result in an increase in the standard deviation of pressure. Optimal flow performance, as indicated by the minimal standard deviation of pressure, can be attained by selecting larger inlet and outlet sizes for any given junction angle. Optimal flow performance, as indicated by the minimal standard deviation of pressure, can be attained by selecting larger inlet and outlet sizes for any given junction angle. The maximum attainable minimum pressure standard deviation (SD) can be achieved by selecting a high junction angle, regardless of the intake diameter.

Table 9 — The ANOVA result for the defined response variables : the average of pressure gradient, standard deviation of pressure, and average of oil holdup

Response variable	Source of variation	Sum of squares	Degree of freedom	Mean square	F-value	p-value
Average of oil holdup	A	0.0089	1	0.0089	13.64	0.0209
	C	0.0035	1	0.0035	5.40	0.0808
	BC	0.0179	1	0.0179	27.40	0.0064
	Error	0.0026	4	0.0007		
	Total	0.0330	7			
Average of pressure gradient	A	1.58E+08	1	1.58E+08	23.55	0.0337
	B	1.92E+08	1	1.92E+08	28.62	0.0341
	C	1.07E+08	1	1.07E+08	15.98	0.0559
	AC	1.43E+08	1	1.43E+08	21.39	0.0480
	BC	3.50E+08	1	3.50E+08	52.23	0.0385
	Error	13405,09	2	6702.54		
	Total	9.64E+08	7			
Standard deviation of pressure	A	39587.07	1	39587.07	2754.80	0.0121
	B	36391.92	1	36391.92	2532.45	0.0126
	C	15182.86	1	15182.86	1056.55	0.0196
	AB	9725.06	1	9725.06	676.75	0.0245
	AC	9747.74	1	9747.74	678.33	0.0244
	BC	4668.50	1	4668.50	324.87	0.0353
	Error	14.37	1	14.37		
	Total	1.5E+08	7			

The shape of the T and Y- shaped pipes was shown to have a significant impact on the flow performance of the system under study, according to the overall findings of the statistical experimental design analysis. In contrast, the line gradient depicted in Figure 18 demonstrates that the impact of junction angle, inlet diameter, and outlet

diameter as individual main effects was not as significant as the interaction effects between these design factors in relation to the majority of correlations observed between design factors and response variables. Of all the interaction effects deemed statistically significant, the interaction involving the inlet and outlet diameter, specifically the diameter ratio, emerged as a prominent factor consistently influencing all the response variables. This discovery aligns with previous findings that have indicated the significant role of the combined diameter ratio in governing the flow distribution of a two-phase system as it passes through a T-junction (Ejaz et al., 2021; Memon et al., 2020; Saieed et al., 2018). For variables related to pressure gradient, there were more design parameters affecting pressure than oil holdup. Several factors contribute to pressure losses in T and Y-pipes, such as the junction angle, pipe material, direction of flow, inner pipe wall smoothness, and cross section area (Guangbin et al., 2010; Li et al., 2013). As a result, in order to control the pressure gradient value, design considerations should be more stringent in effort accommodate geometrical variables.

A quantitative relationship (equation) between the response and the primary design parameters is generally highly beneficial for describing the findings of several trials for the purpose of design selection. It should be noted, however, that statistical approaches can only serve as guides for the trustworthiness and validity of the data; they cannot prove causality. We can gauge the likelihood of a mistake in our conclusions or the reliability of a claim by employing statistical procedures correctly (Montgomery, 2012). The formulas written as Eqs.3.17, 3.18, and 3.19 are regression models developed from the ANOVAs to forecast the values of pressure gradient, pressure standard deviation, and oil hold up.

$$\frac{dP}{L} = 670.02 - 222.36X_A - 220.94X_B - 169.76X_C + 184.20X_AX_C$$

$$- 207.47X_BX_C \tag{3.18}$$

$$SD\ dP = 151.41 - 70.34\ X_A - 67.45X_B - 43.56X_C + 34.87X_AX_B$$

$$+ 34.91X_AX_C - 24.16X_BX_C \tag{3.19}$$

$$H_o = 0.5864 + 0.0334X_A + 0.0209X_C + 0.0471X_BX_C \tag{3.20}$$

where coded variables of X_A, X_B, X_C, X_AX_B, X_AX_C, and X_BX_C are presented the factors of A, B, C, AB interaction, AC interaction, and BC interaction, respectively.

The accuracy of the regression model was evaluated by examining the residuals, which represent the differences between the predicted values of the model and the actual values obtained from the experimental data. (Fig. 19). The parity plot in Figure 19 illustrates the concordance between the simulation outcome, represented on the x-axis, and the expected model, represented on the y-axis. In instances where the outcomes of simulations precisely align with the predictions made by the model, thereby accurately representing the actual targets, it can be inferred that the data and model exhibit complete concordance, as visually demonstrated by the 45° line. The model verification revealed no discoveries related to anomaly, outliers, variance inequalities, or a pronounced trend with the projected values. The resulting regression model might thus be acknowledged as a legitimate model.
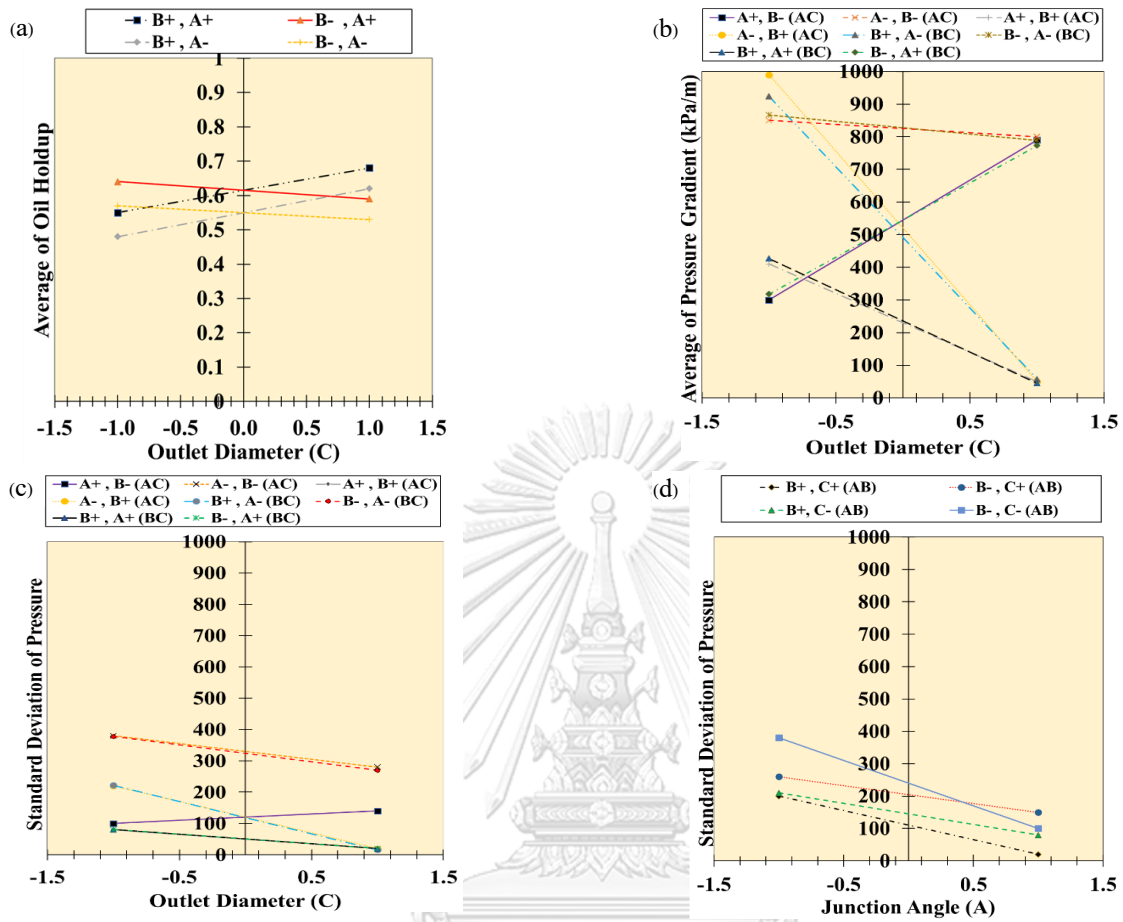
Fig. 18 – The influence of interaction effects on various parameters, including (a) oil holdup, (b) pressure gradients, (c) pressure deviation (AB), and (d) pressure deviation (AC and BC).
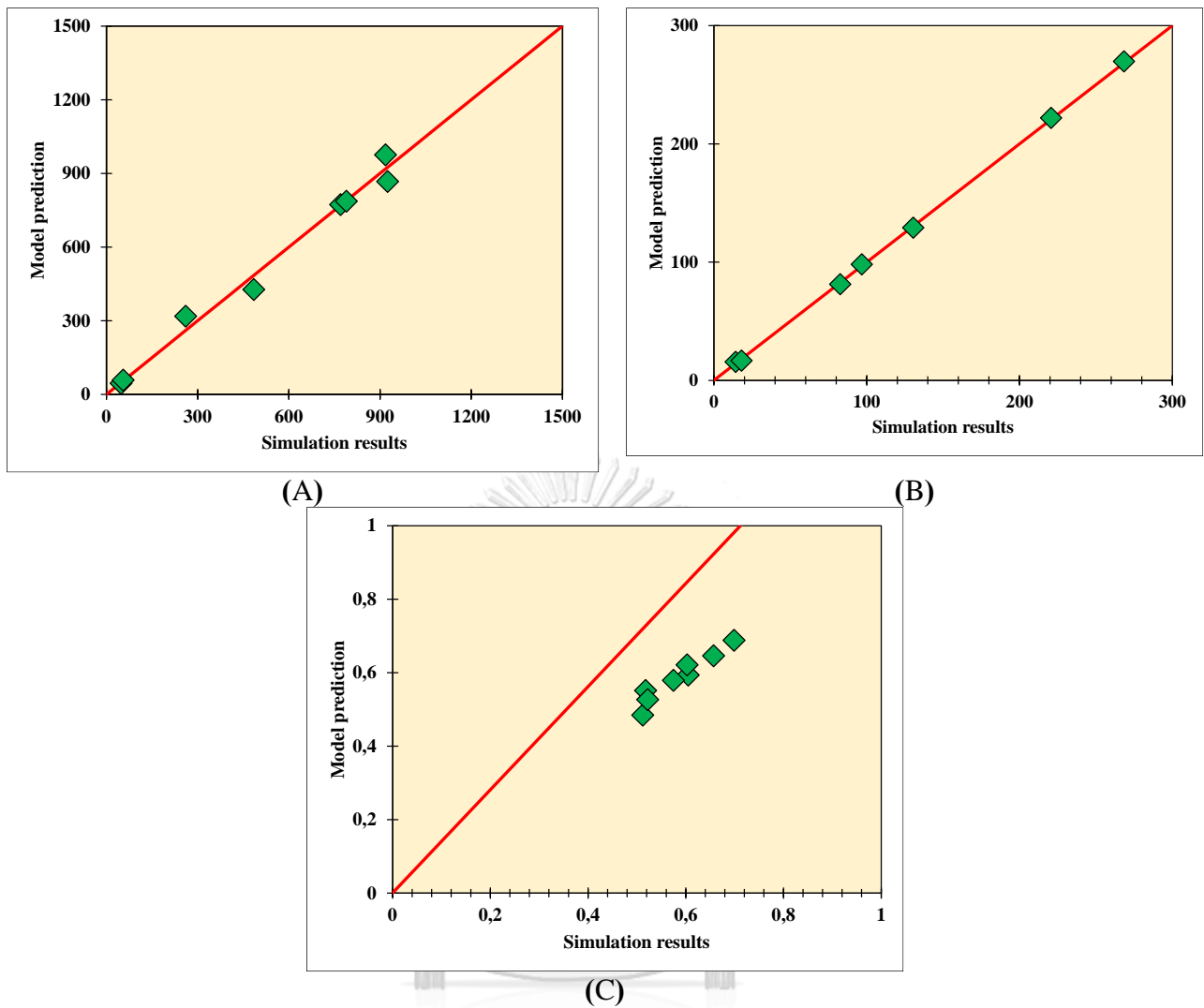
Fig. 19 – Comparison of model predictions and simulation outcomes for (A) the average pressure gradient, (B) the average pressure deviation, and (C) the average oil holdup
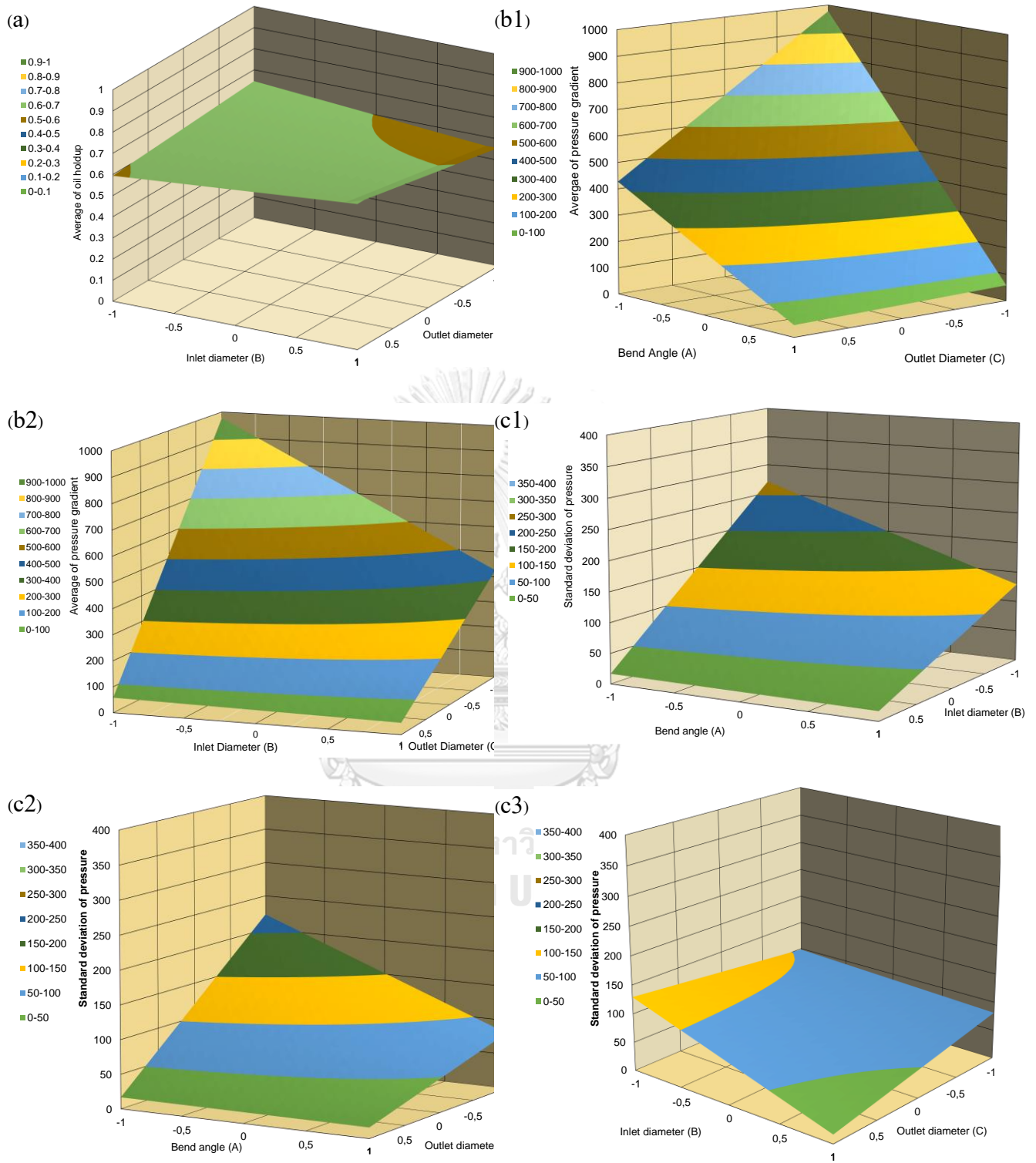
Fig. 20 – An illustration of the three-dimensional response to changes in (a) oil holdup average, (b) pressure gradient average, and (c) standard deviation of pressure as a function of (a) junction angle and inlet diameter, (b) junction angle and outlet diameter, and (c) both diameters, respectively.

The 3D response surface of the average of the pressure gradient, the average of the oil hold, and the standard deviation of the pressure are shown in Figs. 20(a) through 20(c), together with their significant variables. In this investigation, the best conditions were attained when the oil hold up value was maximum and the average pressure gradient value and standard deviation of pressure were at their lowest values. Therefore, the configuration with high values of junction angle, inlet diameter, and outlet diameter was the preferred design generally for the T and Y-pipes to provide the optimal condition. Therefore, the arrangement with a 90° connection angle, 50 mm inlet and outlet diameters, and T50-50 pipe geometry was suggested.

B. Comparison of ANOVA Results For 1st Simulation (Newtonian) and 2nd Simulation (Non-Newtonian)

As the ANOVA results for the 2 simulation cases have been discussed, then these 2 conditions can be compared as Table 10. From Table 10, for both cases, the interaction between ID and OD has main role in impacting the value of oil holdup and pressure parameters. However, for Newtonian case, the interaction of junction angle is absent for oil holdup and pressure gradient, while for Non-Newtonian case, junction angle has important effect for all variables. In addition, the 3 design factors should be interacted to give significant effect to pressure deviation for Newtonian case. For Non-Newtonian case, more interaction effects between 2 factors are involved that give big contribution to the pressure variables.

It can be emphasized that in the case of Non-Newtonian fluid, the pipe geometry plays an important role in the observed responses that were not observed for a Newtonian fluid. This phenomenon occurred because the effect of shear rate is significant for flow performance of Non-Newtonian fluid. Shear rate is determined by

both the geometry and speed of the flow. The geometry of T and Y pipe with intersection region can contribute to bigger shear rate and change the fluid properties (viscosity of fluid). As described by Fig. 23 and Fig. 24, sudden change of viscosity is captured when the flow passing the intersection because of remarkable change of shear rate.

Table 10 – Significant effects of design factors on flow performance for Newtonian and Non-Newtonian cases

Response variable	Significant effect	
	1st case	2nd case
Average of oil holdup	-	A
	B	-
	C	C
	BC	BC
Average of pressure gradient	-	A
	B	B
	C	C
	-	AC
	BC	BC
Standard deviation of pressure	A	A
	B	B
	C	C
	-	AB
	-	AC
	-	BC
	ABC	

C. Hydrodynamics

For all geometries, CAFs were found across the upstream region, as seen in Fig. 21. The CAF, however, was compelled to disperse when it passed through

the roadblock and abrupt curve of the intersection. As a result, the flow pattern and velocity in the downstream region changed. Furthermore, the phenomenon of reverse flow and the generation of vortices due to the shift in velocity, particularly at the junction, could potentially result in the confinement of fluid within a specific region, as depicted in Figure 21. Consequently, the development of the CAF may give rise to more complex flow patterns, potentially leading to a significant decrease in pressure. Moreover, the escalating fluid dynamics pose a difficulty in effectively directing the fluid flow towards the branches. The occurrence of vortices and reverse flow was more prevalent for the Y20-20 and Y50-20 geometries, leading to a higher pressure drop, as depicted in Figure 22 and summarized in Table 8.

As visualized by Fig. 21, the oil can be maintained in the center of the pipe from inlet to near intersection. In all designs of the T and Y pipes, the flow separation followed by recirculation at the junction region affects the oil-water interface's stability. In classical hydrodynamics, recirculation zones are typically attributed to the separation of boundary layers. This phenomenon can be observed in various structures, such as angular walls, T junctions, L junctions, and pipes with disturbances. The re-circulation zone occurs in the classical backward-facing step situation, i.e., (i) flow separation occurs at the sharp upstream intersection corner, (ii) a zone of re-circulation is produced where instabilities develop, producing detached vortices, and (iii) the flow reattaches at the downstream wall after a certain length. In the context of a stable core-annular flow (CAF), the oil exhibits a central flow pattern within the pipe, while the water forms a thin film along the inner wall of the pipe. This film is characterized by

small amplitude waves and ripples at the interface between the oil and water phases (Jiang et al., 2022). This condition could not be maintained when the flow passed through the intersection because the sudden change of momentum affected the water cut and the fluctuation of interface wave amplitude. It contributed to the floating of the oil core above the pipeline with different interface wave amplitudes between the upper and lower parts of the flow system. As a further effect, the oil core will break through the water film in the case of large interface fluctuations, causing wall adhesion.

In the case of inviscid flow within a straight pipe, a prediction according to Bernoulli's principle demonstrated a positive impact of sudden enlargement design that resulting a reduction of the pressure gradient. However, in the simulated scenarios in this section, this tendency was not seen. It was expected that the additional total pressure drop in the fluid system would predominantly arise from a combination of minor losses attributed to the configuration of the pipes (T and Y shapes) and the frictional effects induced by the oil's elevated viscosity. The T50-50 and Y50-50 combinations exhibited a comparatively reduced pressure gradient when compared to the remaining combinations, as indicated in Table 8. The investigation of volume fraction contours (Fig. 21) revealed that the downstream sections of T50-50 and Y50-50 exhibited intricate flow patterns. In contrast, the CAF pattern was observed in certain downstream sections of T50-20 and Y50-20, despite the occurrence of thin oil fouling in certain geometries within these sections. It is important to acknowledge that enlarging the diameter of the downstream region (with a diameter ratio greater than 1) has the potential to elevate the probabilities of an oil spill, despite the fact

that the uniform and larger diameter geometry displayed a reduced pressure gradient (Babakhani Dehkordi et al., 2018). The issue of oil fouling should be mitigated due to the consequential increase in pressure gradient along the axis of the pipe resulting from the accumulation of oil on the pipe wall. If the gradual accumulation of oil fouling is not effectively managed, it can lead to disruptions in the flow, as evidenced by the fouling observed in the San Tomé test loop when exposed to Zuata crude oil. (ρ = 0.996 g/cm3, m = 115 Pa.s at 25˚C. Oil fouling might cause simulations to overestimate the pressure gradient, especially in the downstream region.. (Shi et al., 2021) demonstrated significant pressure gradient discrepancies between simulation and experimental findings due to poor prediction of oil fouling on the pipe wall. When connecting the flow pattern and pressure loss results, it needs to consider the limitations of 2D contour in capturing the detail of the flow pattern, as shown in Fig. 22. For instance, the pressure gradients of T50-50 and Y50-50 are lower than T50-20 and Y50-20, despite the more complex flow pattern of T50-50 and Y50-50.

The occurrence of CAF within upstream region shown by the oil volume fraction visualization in Fig. 21. With the exception of a few T50-20 and Y50-20 outlet locations that captured the CAF area but were inconsistent, the situation for downstream regions, however, usually indicated uneven or variable oil volume fraction along pipe segments. Based on the viscosity contours displayed in Fig. 23, it was discovered that the oil's viscosity was practically constant from the entrance to the vicinity of the junction. As the fluid traveled to the junction area and subsequently downstream, its viscosity significantly changed. The viscosity of Non-Newtonian shear thinning or pseudoplastic fluids tends to decrease

primarily as the shear rate of flow increases. The behavior described in the text was captured in a graphic (Fig. 24) that depicted the relationship between oil viscosity, shear rate, and a steady-state T50-20 flow system.

Due of the multiple elements involved, the flow regime in fittings is incredibly complex, which severely limits the ability of the current theory to describe it. The flow structure was influenced by factors such as density, viscosity, and pipe diameter. Moreover, previous studies examining the flow behavior at T and Y-junctions have revealed that the flow direction and branch angle significantly influence the formation of flow patterns, as well as the holdup and pressure drop characteristics in stratified liquid-liquid and gas-liquid flows. The simulation results of this section indicate that careful consideration should be given to the use of CAF for transporting high viscosity oil through T and Y-pipes. Following the traversal of an intersection, it was observed that the self-sustaining stability of oil flow within the core and water flow within the annulus was not achieved. Consequently, there was an occurrence of oil interacting with the inner surface of the pipe, leading to the detection of oil fouling. Additionally, this interaction resulted in the formation of an intricate flow pattern characterized by the presence of vortices.
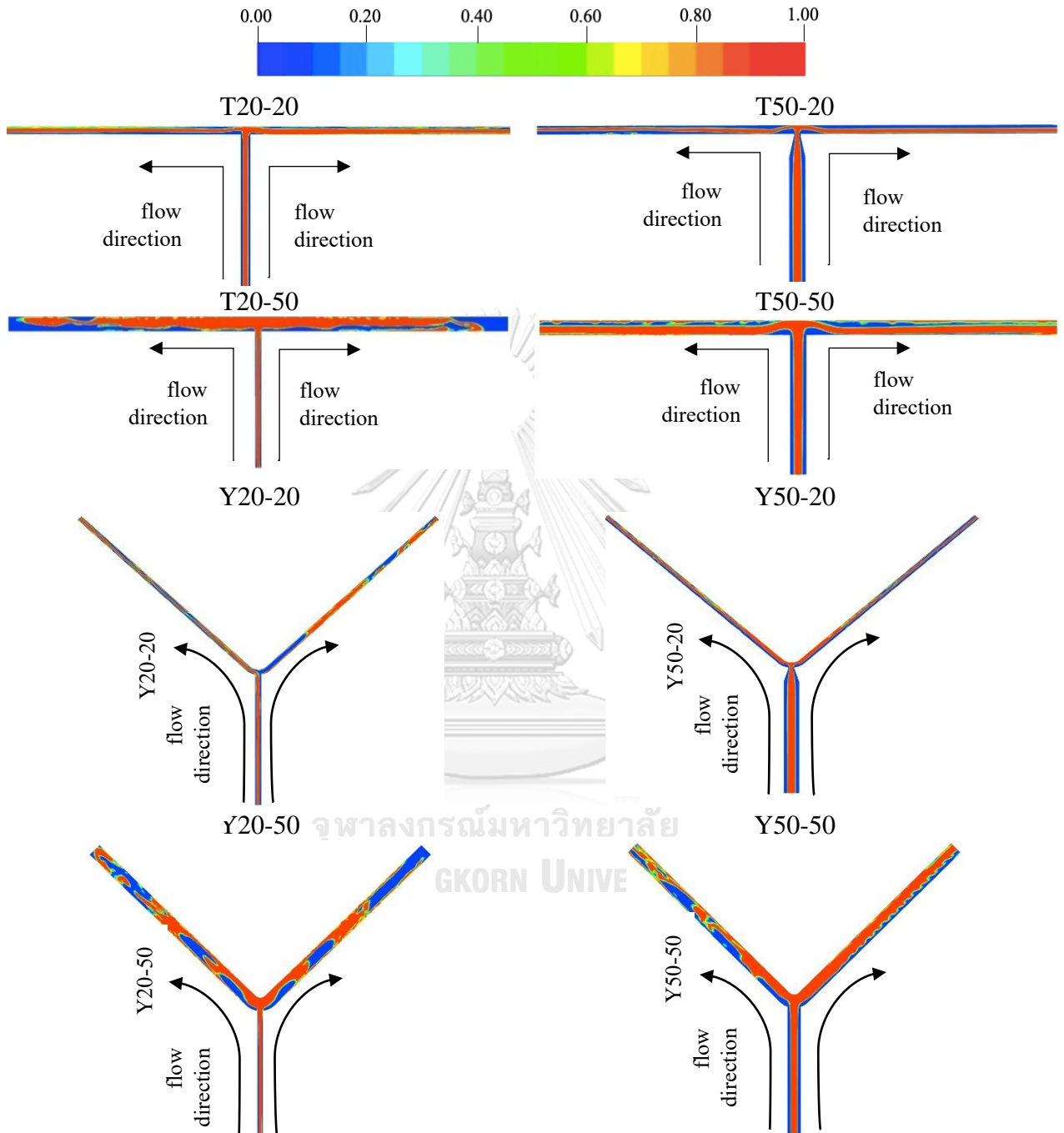
Fig. 21 – Visualization of oil volume fraction of 8 configurations of T and Y-shaped pipes

T20-20

T20-50

T50-50

T50-20

Y20-20

Y20-50

Y50-50

Y50-20
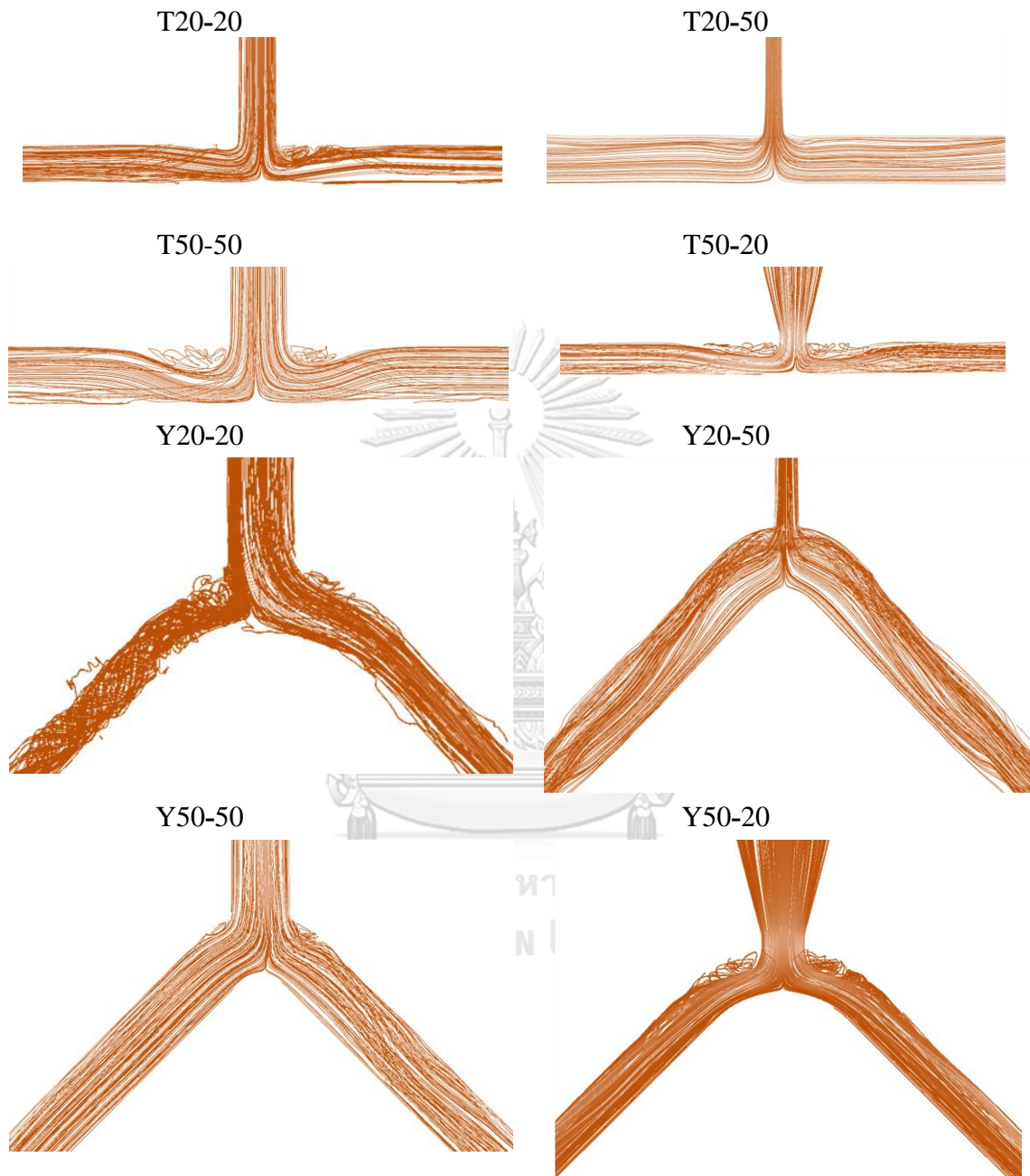
Fig. 22 ─ Streamlines of the flow capturing areas of vortices and reverse flow at intersection
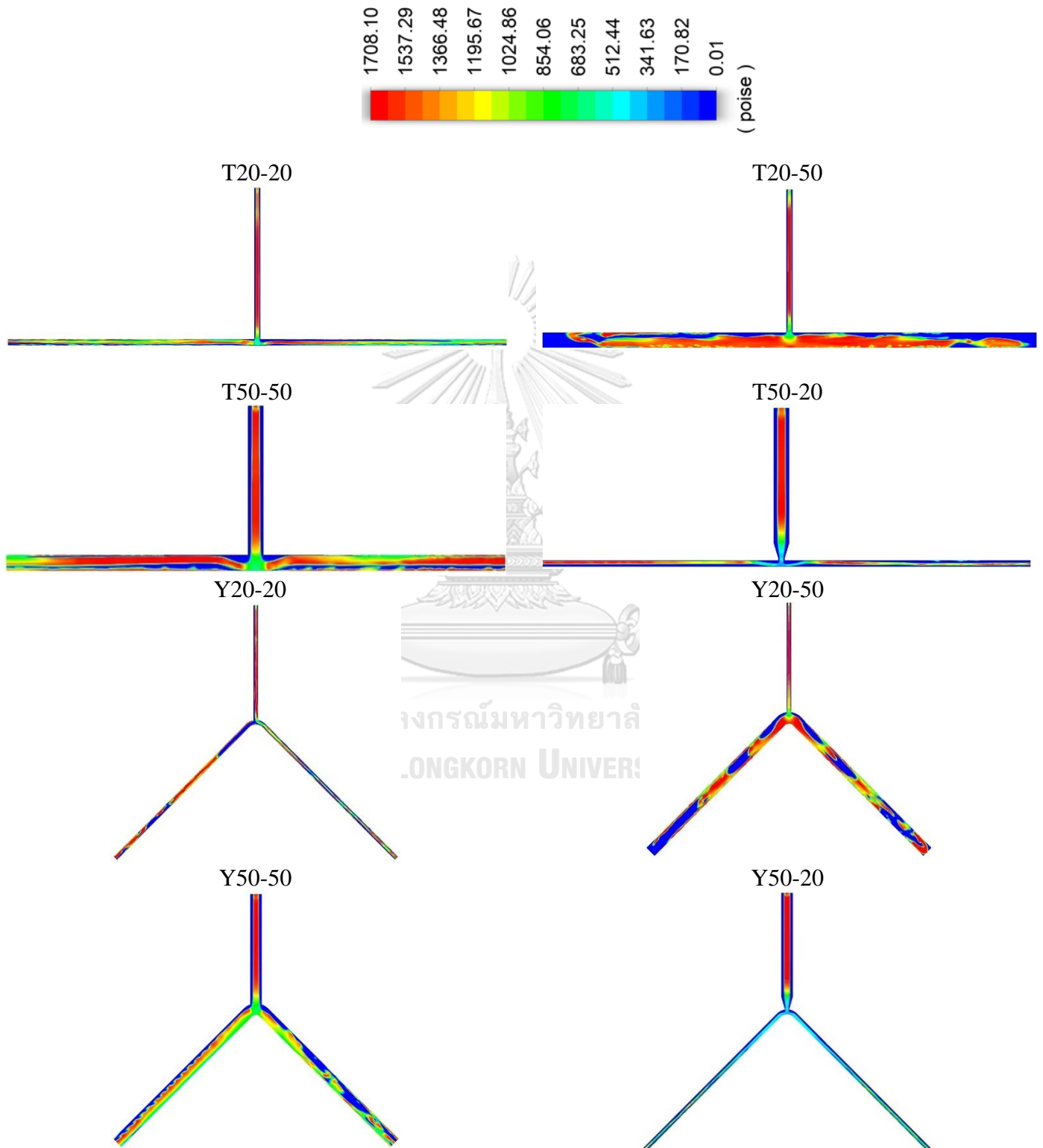
Fig. 23 ─ Visualization of viscosity contours of 8 variantss of T and Y-shaped pipes
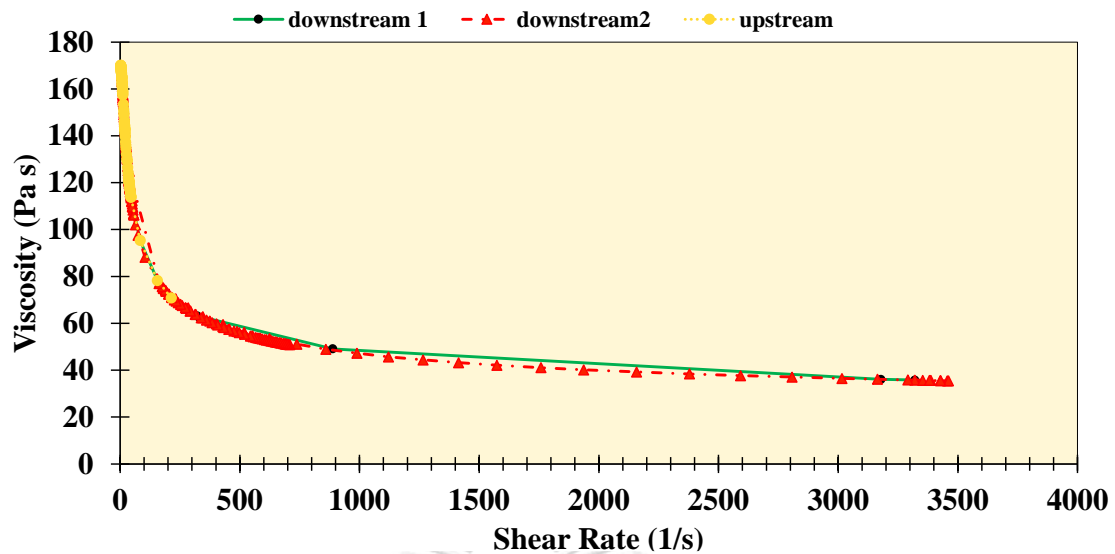
Fig. 24 −Profile of viscosity of heavy oil extracted for T50‑20

It should be noted that there is still more to be done in terms of the procedure and fix for recovering the CAF after deformation, particularly in T and Y-shaped pipes. However, a lot of studies on phase separation for industrial applications also look at the problem of flow pattern change in upstream to downstream zones at T and Y junctions (Lu et al., 2018; Memon et al., 2020; Yang et al., 2019; B. Yang et al., 2020; L. Yang et al., 2020). The phenomenon of phase separation has been demonstrated to be significantly affected by factors such as mass rate, flow regime, operating conditions, and the geometry and orientation of the test section (Azzopardi et al., 1982). When simulating oil-water flow to examine separation behavior in combined T-junctions, modifying the pipe length and branched pipe intervals can be considered to change the flow pattern (Chen et al., 2012). The flow evolution of CAF in horizontal straight pipe was noted by Joseph et al., 1997, Sotgia et al. (2008), and Jiang et al. (2021). Joseph et al. (1997) and Sotgia et al. (2008) identified the boundary region of flow regimes and made predictions regarding the evolution of flow patterns by considering the superficial

velocities of oil and water. In their study, Jiang et al. (2021) determined the watercut and mixture velocity thresholds at which the oil in the core flow would make contact with the inner wall of the pipe. For a pipe diameter of 21 mm, these thresholds were found to be 9.6% for the watercut and 1.1 m/s for the mixture velocity. On the other hand, for a pipe diameter of 10.5 mm (with a viscosity ratio of 1040), the corresponding thresholds were 14% for the watercut and 0.3 m/s for the mixture velocity. Additional studies have also indicated the necessity of employing larger quantities of water to maintain the integrity of the continuous aqueous phase (CAF) structure. However, this approach proves to be unfeasible in situations where the oil content is exceptionally high, surpassing 70% (Coelho et al., 2020; van Duin et al., 2019). According to Jing et al. (2021), it is crucial to maintain the water input fraction at the critical threshold and optimize the oil flow rate in order to achieve optimal efficiency in oil-water coalescence-assisted flotation (CAF) within a horizontal pipe containing a 90-degree elbow. However, further investigation is necessary for cases involving T and Y-shaped pipes, as the existing studies are restricted to straight horizontal pipes and horizontal pipes with 90° elbows.

When comparing the simulation results of the flow system applied in this Section with the case in Section 3.4, both works showed that CAF could not be maintained after passing the intersection. Furthermore, the analysis of 2^k factorial experimental design also showed the that geometry of pipe affected the flow performance of the both systems. However, different oil rheological behavior showed different influence of all experimental factors and their interaction effects on the response. In the case of previous section (Newtonian oil, μ_o = 0.838 Pa.s, ρ_o = 890 kg/m³The optimal design configurations for T and Y-shaped junction pipes are typically achieved when the

junction angle and outlet diameter are set to high values, while the inlet diameter is set to a low value. This configuration can be denoted as T20-50. On the other hand, this result of this section (Non-Newtonian oil, $\mu_o = 170.811$ Pa.s, $\rho_o = 976$ kg/m^3) showed that optimum design will be achieved by for geometries with high values of junction angle, inlet diameter, and outlet diameter, as represented by the geometry T50-50. The case of oil as Non-Newtonian fluid also showed that geometry with sudden enlargement did not contribute to the better flow performance as indicated in the previous simulated case as recorded in Section 3.4. This might show that the shearing force of very viscous oil (non-Newtonian in this case) across the lateral surfaces of stream pipe should be considered for this phenomenon. In Section 3.4, the Newton's second law can be simplified and derived to Bernoulli equation for inviscid flow case without significant viscous force. In flow of a real fluid, sometimes the viscous forces are small enough outside the boundary layer that the Bernoulli equation is a good approximation. However, the advantage of sudden enlargement according to Bernoulli equation could not be obtained for current case with Non-Newtonian oil.

3.5.4 Conclusion

This section presents a study on the flow of Carreau model viscosity fluids in T and Y-shaped pipes, specifically focusing on the effects of varying junction angles, inlet diameters, and outlet diameters. The occurrence of the cross-sectional area flow (CAF) was observed in the upstream region for all geometries simulated in this study. However, the stability of the CAF could not be sustained beyond the intersection area. Upon traversing the intersection area, a multifaceted flow pattern characterized by the presence of vortices and reverse flow materialized. While the presence of CAF was observed in specific downstream regions of T50-20 and Y50-20, its occurrence was not

found to be consistently present. Consequently, under the specific geometries and conditions examined in this section, the efficacy of water as a lubricant for oil in the core region was not sustained.

A 2^k factorial statistical experimental design was employed to investigate the impact of design parameters, specifically junction angle and pipe diameter (diameter ratio), and their interactions on flow performance. As a result, it was determined that the most favorable configuration for simulated pipe geometries would be attained by employing geometries characterized by elevated values of junction angle, inlet diameter, and outlet diameter, exemplified by the T50-50 geometry. The anticipated primary factors impacting the intricate flow patterns and overall pressure drop in the system were the pipe designs and the friction associated with high viscosity oil. The simulation results indicated that there were additional design factors that influenced the flow performance parameter in the Non-Newtonian case, which were not observed in the Newtonian case. The influence of shear rate is a significant factor in the flow behavior of Non-Newtonian fluids, as it is primarily influenced by the flow's geometry and velocity.

CHAPTER IV RECOVERY OF CORE ANNULAR FLOW STRUCTURE IN A HORIZONTAL T-PIPE USING CFD APPROACH

4.1 Pipe Geometry Modification for CAF Recovery

One of the important issues that still being an attention in CAF research is how to maintain the stability of CAF formation along the pipe. The CAF stability is defined as an uninterrupted steady and continuous CAF regime. However, the oil fouling phenomenon frequently occurs in the middle of flow process initiated by some oil droplet attach on the pipe inner wall and it may continue to prevail, creating thick layer of oil at the wall followed by sharp increase in the pressure drop. The fouling condition may reach more severe condition and eventually blocks the pipeline.

Several experimental and theoretical studies have been carried out to propose strategies to maintain the CAF stability in pipe. Joseph et al. (1997) determined the particular velocity range where CAF regime could be stable. Another work also applied cement-lined pipes as a promising strategy to reduce oil fouling (Arney et al., 1996). In their work, the oleophobic properties of the cement materials was considered as a practical solution to the problem of fouling. Some other works also emphasized that water fraction, mixture velocity, and oil flow rate should be adjusted to certain values to maintain the CAF stability. Jiang et al. (2021) dealt with a simulation work concerning on the oil-water CAF system in a horizontal pipe, generated the wall-touching line to describe the value of critical water cut below which the oil in the core flow can reach the pipe wall, as a function of the mixture velocity. In addition, an

experimental work provided evidence of more stable CAF structure by supplying higher amount of water in a system of three consecutive test sections (horizontal vertical horizontal) connected by several hydraulic fitting (Coelho et al., 2020). However, the feasibility of this condition was need to be reviewed for flows with oil cuts more than 70%. Another experimental work by Jing et al. (2021) was also completed to evaluate the stability in CAF evolution by the influence of the elbow in a horizontal pipeConsequently, it is essential to maintain the water input fraction at a specific critical level and optimize the oil flow rate in order to achieve optimal efficiency in oil-water transportation using the CAF technique. Two simulation works by Kaushik et al. (2012) and Babakhani Dehkordi et al. (2018), both involving pipe geometry with sudden diameter change, showed how geometry variation with larger diameter pipe could reduce the fouling tendency.

Regarding the pipe geometry effect on the stability of CAF structure, some experimental and theoretical studies have been carried out. Joseph et al. (1997) reported that the experiments in Venezuela showed the increase of oil fouling and the decrease of CAF stability at certain areas i.e., near pumping stations (where the pressure is highest) and around line irregularities (union, bends, flanges, and curves). Coelho et al. (2020) also monitored the appearance of oil fouling zones near the hydraulic accessories from the experimental works involving pipe with several pipe fittings as valves, unions, elbows, 90° long bends, nipples, and couplings. CFD simulation works performed by Andrade et al. (2013) concluded that the CAF structure could not be maintained after the oil-water flow hitting the bend connection and oil fouling started to grow at the wall with huge pressure drop detected. However, the strategy on how to

prevent the CAF deformation or how to recover the breaking CAF has not been explained yet.

Principally this section was a further development of previous simulation in Chapter III to solve the problem of CAF deformation that occurred after passing intersection. Many studies concerned about stop (shutdown) and restart methods when CAF regime cannot be maintained as the solution to get back the CAF in the system (Arney et al., 1996; Livinus et al., 2017; Peysson et al., 2007; Strazza et al., 2012). However, current study was expected to propose a strategy to recover the stability of CAF particularly after passing the intersection area of the T-pipe without interrupting or stopping the flow process.

The system simulated in this study referred to the flow system and geometry of a horizontal T-pipe with similar diameter of 50 mm (T50-50) which was concluded as the most desired design as reported in Section 3.5. In this part of simulation work, an additional water insertion was introduced at the intersection point that considered as critical region for CAF stability to support the recovery of CAF structure by suppressing fouling. Two main geometry candidates of additional water insertion with variation of water velocity were simulated as a part of this work.

4.1.1   System Description

The basic geometry was T-shaped pipe with horizontal orientation and diameter of 50 mm (both for inlet and outlet) with detail geometry and flow condition as described in Section 3.5. Since the goal of this simulation was to assess the possibility of recovering the CAF after passing through the intersection, an extra water tapping point was added at the intersection area in the reverse direction of the upstream section

coming flow. According to the results of the previous simulation in Chapter III, the intersection point of T50-50 was a crucial area where the stability of CAF could not be naturally retained, resulting in oil fouling spread at the intersection pipe inner wall and the generation of a flow pattern with vortices. Thus, installing water insertion at this location was meant to remove the attached oil at the intersection inner pipe wall while also increasing water fraction to provide enough additional force to push the oil to the core. As shown in Fig. 25, the additional water insertion was divided into two geometries: V-insertion and ducting insertion. The CAF system with V and ducting geometry of additional water insertion are coded as VI and DI, respectively.

Some candidates for additional water velocity value ($u_{w,a}$) were considered in the first stage of simulation work. The trials were finished by using a smaller $u_{w,a}$ than the inlet water introduced into the annulus at a velocity of $u_{w,inlet}$. A small amount of extra water was preferred to save energy and cost during the pumping and dewatering procedure. Only certain values of additional water velocity and simulation time demonstrated the probability of stable CAF structure formation in the trial results, which are summarized in Table 11.

4.1.2 Simulation Setup

As shown in Fig. 26, the present study used polyhedral cells for the outer area and hexahedral cells for the inner area of pipe. The choice to use both types of cells was made specifically to decrease computational time. Polyhedral cases are more precise than tetrahedral cases but are comparable to hexahedral cases. However, because the cell counts in polyhedral cases are less than half of those in hexahedral cases and less than a quarter of those in tetrahedral cases, the polyhedral mesh requires the fewest computational resources (Wang et al., 2021).

After creating the T50-50 geometry with polyhedral and hexahedral cells, testing was performed to ensure that the outcome would be the same as obtained when using hexahedral cells as simulated in Section 3.5. As a consequence, the pressure drop and volume fraction contour were nearly identical. Mesh quality was evaluated using the skewness ratio and orthogonal quality rate, with very good to excellent category findings.

To avoid pressure overprediction, the CFD simulation used water initialization, as recommended by Babakhani Dehkordi et al. (2018). Water entered the system through two points: the inlet section and the intersection via extra water insertion (V-insertion or ducting insertion). As captured in the upstream region, oil flowed to the core area to create CAF. After establishing a steady CAF pattern along the upstream section and finally transitioning to a more complex flow regime directly after passing the intersection, the additional installed water insertion was intended to immediately get back the CAF pattern. Thus, data extraction from 3 separate locations in the downstream region was required to ensure that the irregular flow pattern had returned to the CAF structure. The flow had been steady for most velocity values at t = 2 s for all types of water insertion geometry mentioned in Table 4.1, except for ducting insertion geometry with $u_{w,a}$ = 2 m/s, which took longer time to be steady, i.e., 8 s. This simulation work ensured that the applied simulation time was appropriate for allowing the Courant number to be less than 1. The Courant number is a dimensionless value representing the number of mesh cells traveled at a given timestep. When Courant number is less than unity, fluid particles move from one cell to another within one time step. High Courant number (more than 1) can lead to a decrease in accuracy.

(a)

(b)
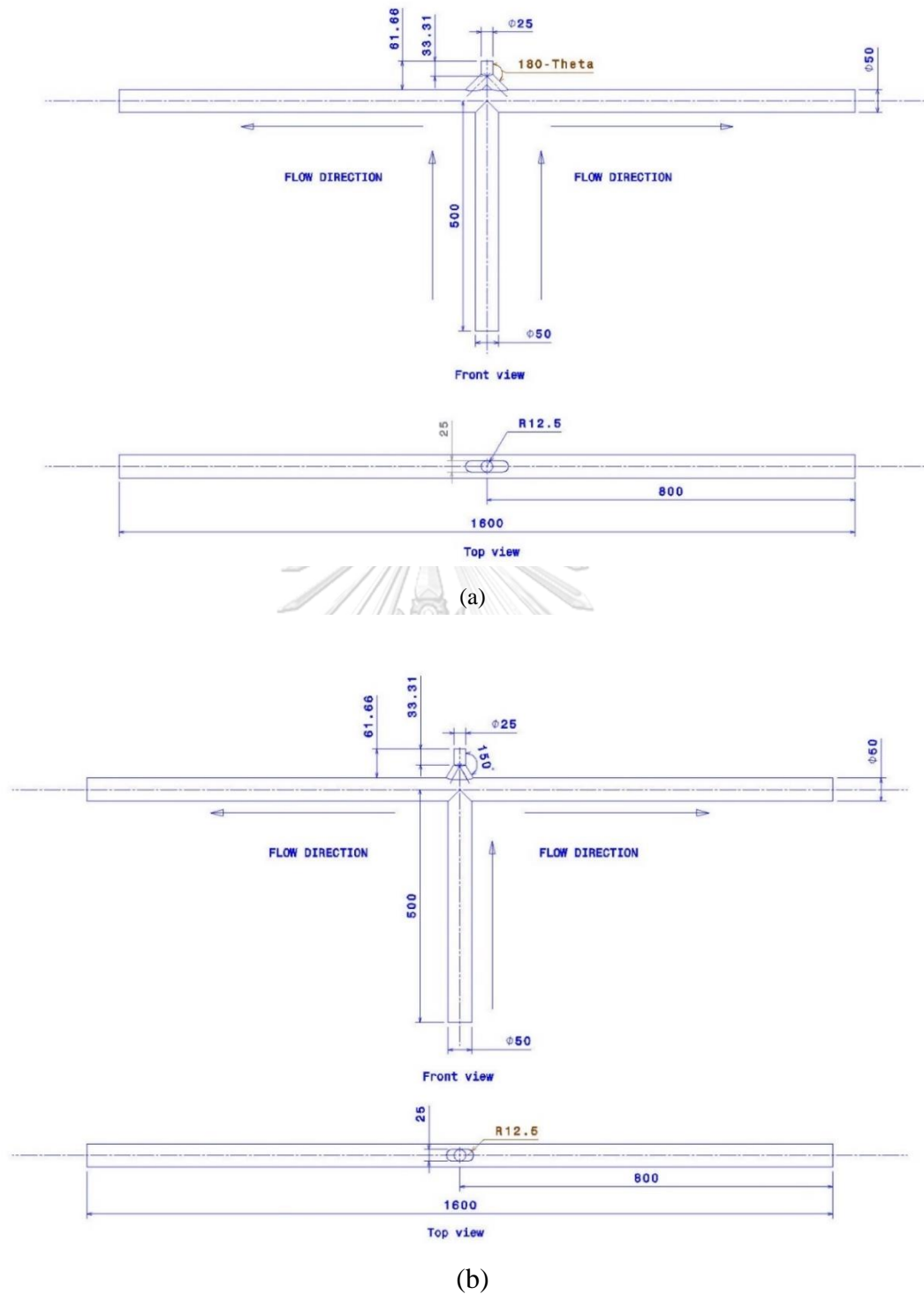
Fig. 25 — Proposed model for T-shaped pipe with additional water insertion: (a) V-insertion model; (b) ducting insertion model
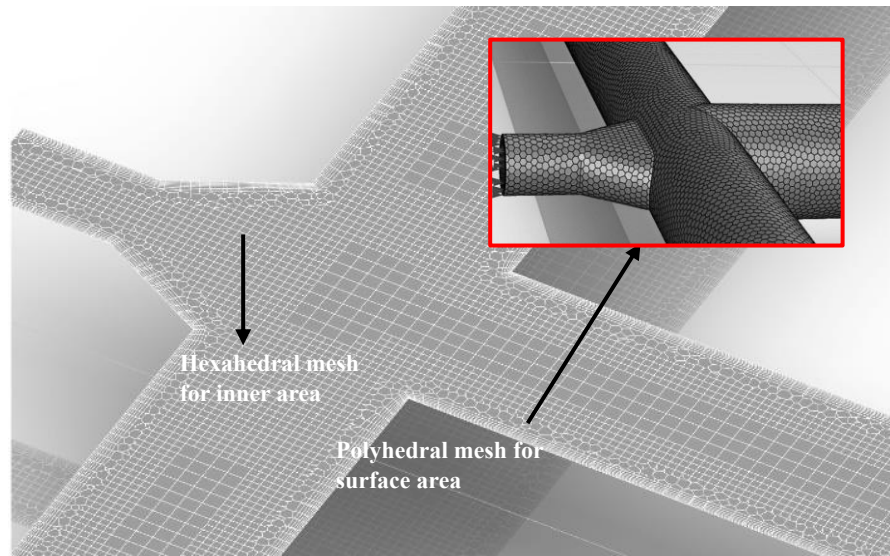
Fig. 26 － Schematic of meshed geometry used in the model simulations

Table 11 － Variation of simulation runs for water insertion geometry, additional water velocity, and simulation time

Type of water insertion	Angle (º)	Tube geometry	Additional water velocity – $u_{w,a}$ (m/s)	Simulation time – t (s)	Code
V-insertion	30º	Smaller tube	2	2	VI-30-S
	30º	Bigger tube			VI-30-B
	45º	Smaller tube			VI-45-S
	45º	Bigger tube			VI-45-B
Ducting insertion	-	-	5.35	2	DI-5.35-
			4.35		DI-4.35-
			2.35		DI-2.35-
			2	4	DI-2-4
				8	DI-2-8

4.1.3 Results and Discussion

As concluded by previous simulation results in Chapter III, using CAF to transport high viscosity oil through T and Y-pipes should be reconsidered because the intersection area appeared as an obstruction, interrupting the CAF into a more complicated flow pattern. As shown in Table 10, the current CFD simulation was performed to modify the previous geometry with four variations of V-insertion type and five variations of ducting insertion type at intersection. Figures 27 and 28 show the phase configurations at cross-section for the region near the pipe outlet, with red representing the oil fraction and blue representing the presence of water.

The additional water velocity, $u_{w,a}$, was set to 2 m/s for all proposed designs with V-insertion. This velocity value (2 m/s) was chosen based on simulation findings that demonstrated the tendency of CAF formation after several trials with different values of additional water velocity (1 m/s, 3 m/s, 4 m/s, and 5 m/s with simulation times of 2 and 4 s). When this number ($u_{w,a}$ = 2 m/s) is used, the flow pattern tends to reshape to the eccentric core-annular, as illustrated in Fig. 27. It is necessary to emphasize that in the absence of additional levitation force, the eccentricity of CAF can be increased and the tendency of oil fouling is estimated to be greater, as illustrated in Figs. 27(a) and 27(b) for V-insertion with an angle of 30° (VI-30-S and VI-30-B). When the superficial velocity of the oil is low, the probability of eccentric CAF formation is high. The density difference between oil and water creates buoyancy in this situation (Ooms et al., 2007). The degree of oil core eccentricity can be calculated using a dimensionless number, the Froude number, by calculating the ratio of inertial force to buoyancy force.

Figures 27(c) and 27(d) demonstrate a strategy to increase the angle of V-insertion. The CAF structure in Fig. 27(c) or VI-45-S is still eccentric, but the tendency of oil to touch the wall has been reduced when compared to VI-30-B. When a wider angle is applied, the difference in CAF structure for V-insertion with a smaller tube is not significant. The core irregularity of VI-45-B is captured to be reduced (Figs. 27(d) and 28(b)). Experiment results show that under typical conditions, a steady eccentric core-annular state is possible because gravity pushes the core (oil) off-center. The pressure distribution of the liquid would intensify in the narrow portion of the annulus while relaxing in the wide part. The core would rise as a result of the higher positive pressure produced in the narrow annulus (Ooms et al., 2003).

In this simulation method, the simulation time for VI-45-B was increased from 2s to 4s, but the contour of volume fraction was not drastically changed. The geometry with 45° and larger tube (VI-45-B) was estimated to enable a better recovery flow regime of CAF after passing the intersection among all simulated geometries with V-insertion. When $u_{w,a}$ was set at 5.35 m/s and 2.35 m/s, the oil fouling condition almost occurred for the geometries with ducting insertion (DI-2.35-2) shown in Fig. 28(a) and Fig. 28(c). A decrease in oil fouling tendency is indicated when $u_{w,a}$ was set at 4.35 m/s for DI-4.35-2 as shown by Fig. 28(b). However, as demonstrated by the volume fraction contour, eccentric CAF is still observed in DI-4.35-2. The additional water velocity was then reduced to 2 m/s by considering the velocity condition of VI-45-B, which could provide more concentric CAF. The phase configuration at pipe outlet for variant DI-2-4 (Fig. 28(d)) still shows eccentric CAF structure when $u_{w,a} = 2$ m/s and t = 4s. Further trial was arranged to expand the time simulation to 8s with the same

additional water velocity as the previous run ($u_{w,a}$ = 2 m/s). As a result of this, the CAF structure of DI-2-8 was significantly improved. The phase configuration, as shown in Fig. 28(e), exhibits significant concentric CAF.

Some studies stated that when the inertial force dominates, the oil in the water is more likely to be concentric (Hu et al., 2019; Macías-Hernández et al., 2016; Ooms et al., 2007). When the oil superficial velocity rises further, the proportion of oil phase in the pipes rises, leaving only a thin coating of water films between the oil core and the upper-layer pipe walls. The increased inertia force at that stage causes the oil core to become more concentrically shaped. Higher core inertia can prevent the core from rising because of buoyancy and makes it easier for the core to stabilize (J. Sun et al., 2022).

(a)	(b)	(c)	(d)
30° smaller tube	30° bigger tube	45° smaller tube	45° bigger tube
(VI-30-S)	(VI-30-B)	(VI-45-S)	(VI-45-B)
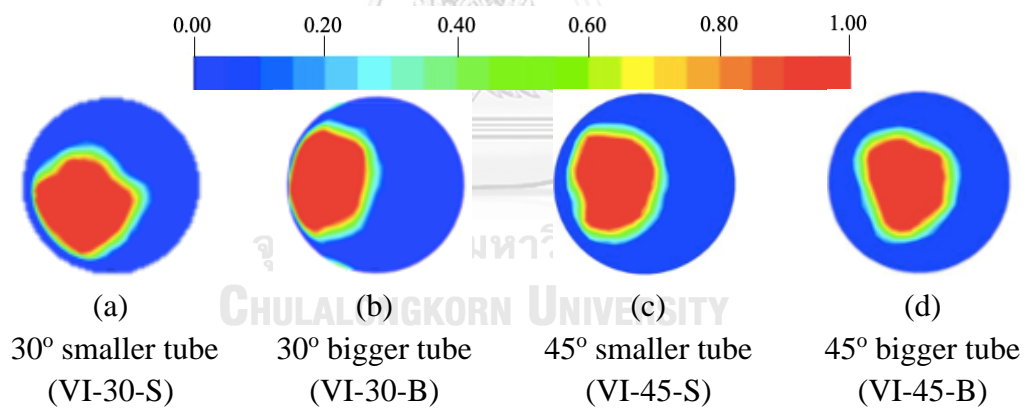
Fig. 27 － The cross-sectional phase configuration at near outlet location for CAF simulation with additional water insertion using various angle of V-insertion type at water velocity = 2 m/s.
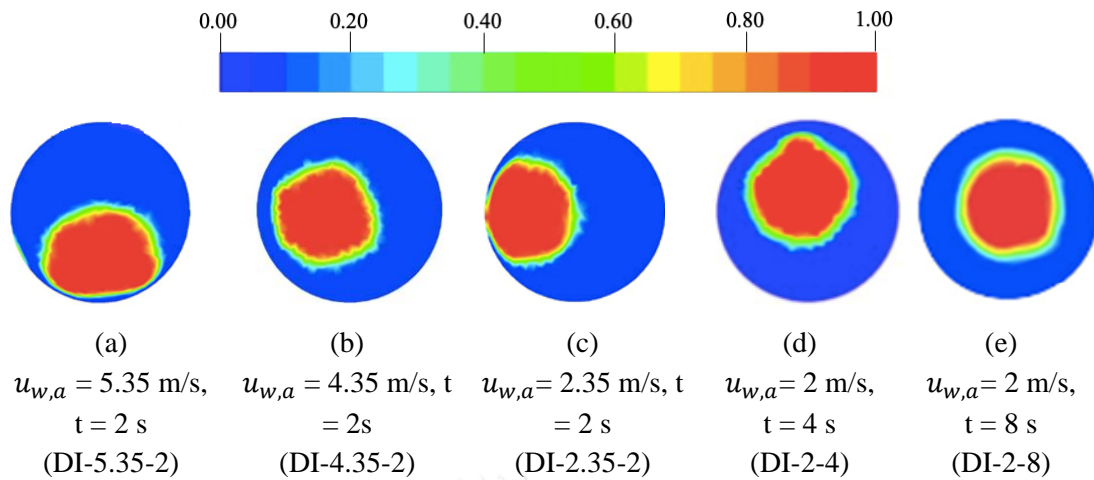
Fig. 28 — *The cross-sectional phase configuration at area near to pipe outlet for CAF simulation with additional water insertion using ducting-insertion type at different water injection velocity and simulation time*

The contours showing the flow pattern along the pipe's length are collected in Fig. 29. For geometry of T50-50 without additional water insertion, as shown in Fig. 29(a), the oil can be maintained within the center of the pipe from the inlet to the area near intersection before entering downstream. When the CAF structure cannot be kept after passing the intersection, oil strikes the pipe wall, penetrates the water layer, and distributes to the pipe wall. According to Fig. 29(c), different conditions were observed for VI-45-B and DI-2-8. The addition of water injection through VI-45-B ($45°$ bigger tube V-insertion at $u_{w,a} = 2$ m/s and t = 2 s) and DI-2-8 (ducting insertion $u_{w,a} = 2$ m/s and t = 8 s) could support the presence of CAF based on the cross-sectional phase configuration at area near pipe outlet. However, the consistency of the CAF structure after passing the intersection point had to be taken into account in order to select the most stable CAF regime. From the cross-sectional phase configuration at three axial positions of the downstream region, as shown in Fig. 29(b) and Fig. 29(c), the difference between phase configurations of the three positions of the ducting insertion

DI-2-8 run is not significant. On the other hand, for all axial locations, the oil core tends to be more eccentric for V insertion (VI-45-B) than for ducting insertion DI-2-8. The degree of oil core eccentricity for VI-45-B is found to be greater than that of DI-2-8. Even when the pressure gradient over the pipe was big enough, a balance between the buoyancy force and the hydrodynamic force led to the formation of steady eccentric core-annular flow in the instance of VI-45-B eccentricity (Ooms et al., 2007). However, it should be noticed that as the pressure gradient decreases or the buoyancy force increases, the eccentricity of the core may increase. The current work only considered the situation where the pipe diameter did not change, represented by T50-50 pipe. At $u_{w,a}$ = 2 m/s and t = 8 s, the geometry of T50-50 with ducting insertion of the additional water inlet was considered to enable a more stable and concentric oil core flow.

Fig. 30 depicts the averaged local oil holdup for both sides of downstream region at various pipe axis for comparing the consistency of CAF in T50-50 after modification as geometry of DI-2-8 to the original geometry of T50-50. According to Figs. 4.6(a) and 4.6(b), the value of oil fraction is one or close to unity at the center region and near the pipe wall, with a fluctuating pattern. The ideal condition of CAF is represented by the unity value of oil holdup for core region of pipe (at smaller value of R/r) and almost zero for area near to pipe wall (at bigger value of R/r), which means that no oil fouling is occurred and CAF at core region has been established. Fig. 30(c) and 30(d) capture the desired condition with the trend of oil holdup is high (equals to 1) at central region and going smaller for locations near to pipe wall. These charts clearly emphasize that the geometry of CAF-2 can facilitate a more stable lubricated flow in an oil core after the deformation at intersection

(a)

without additional water insertion (CAF-1)

(b)

with V-insertion (VI-45-B)

(c)

with ducting insertion (DI-2-8)
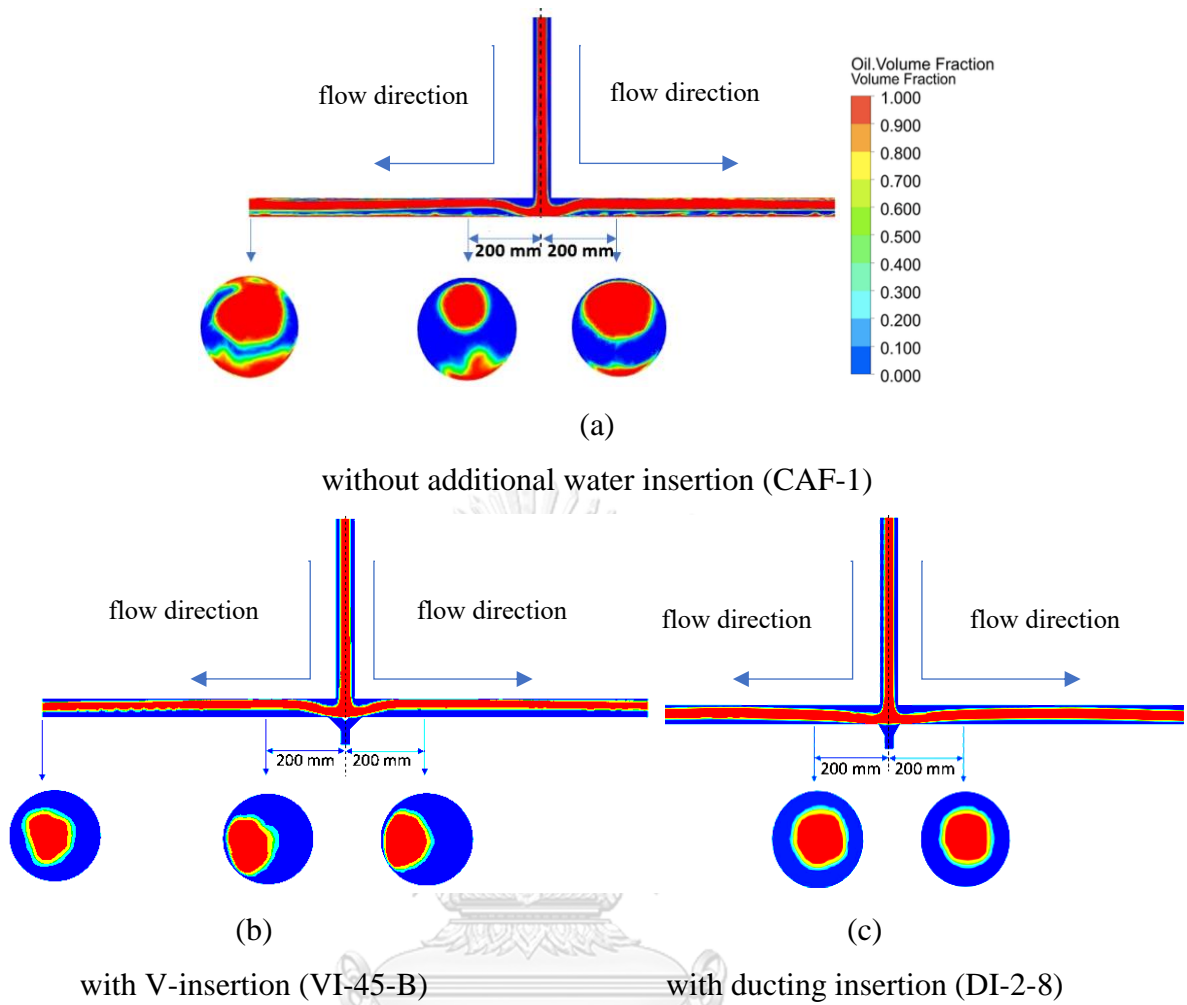
Fig. 29 － The cross-sectional phase configuration at 3 different downstream locations for CAF simulation.
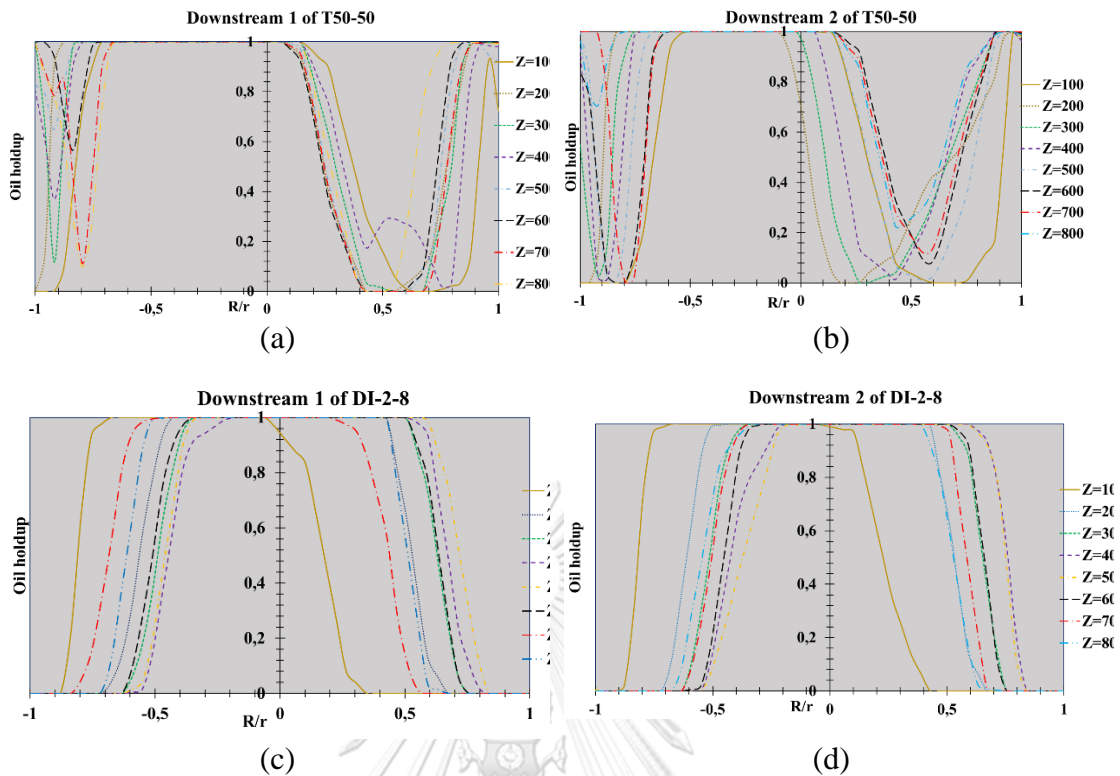
Fig. 30 ─ Time-averaged local oil holdup for both sides of downstream region at various pipe axis (a) Downstream 1 of T50-50 without additional water; (b) Downstream 2 of T50-50 without additional water; (c) Downstream 1 of DI-2-8 (d) Downstream 2 of DI-2-8.

Fig. 31 shows the pathlines as a tool to visualise the complex 3D flows for the area near the junction for the proposed design of DI-2-8. From this figure, a re-circulation flow phenomenon was observed for the downstream area near the intersection. As illustrated by Fig. 31, the re-circulation zone of DI-2-8 occurs near the junction, and the length of the re-circulation zone is about 200 mm from the intersection. The vortices produced reduce the flow momentum and fluid particle velocity. As a further effect of the vortices, the interfacial tension increased, causing an increase in the interfacial wave instability of oil and water. However, after 200 mm measured from the intersection point, the flow stability is recovered. The addition of water allowed the generation of sufficient hydrodynamic lifting force to facilitate the

levitation while at the same time resisting interfacial deformation. As reported by Ooms et al. (2007), the levitation could not take place without hydrodynamic lifting action due to the fluctuation at the oil-water interface. The re-circulation phenomenon is also observed for the flow from the additional water inlet to the downstream region of the main pipe. However, this zone is very short and almost disappears when entering the downstream region. The width and length of the recirculation zone increase as the momentum ratio and discharge ratio rise, and the recirculation zone range is affected by junction angle changes. The momentum ratio and discharge ratio are computed based on the flow rate ratio of the main pipe (upstream section or additional water inlet) to the branch pipe (downstream section right after intersection) and represented by the contour of flow velocity, as shown in Fig. 32.
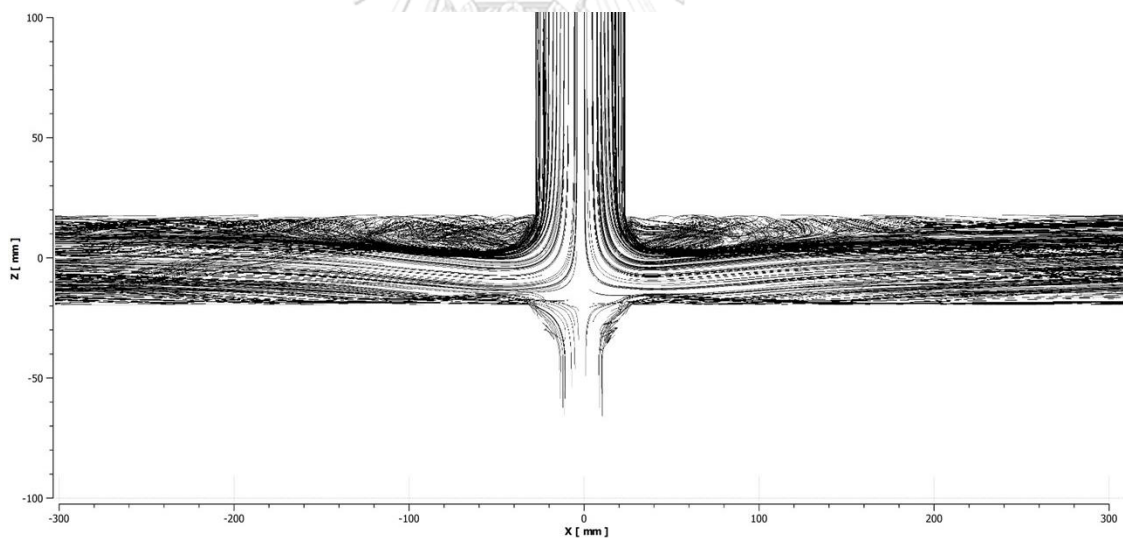
Fig. 31 － Streamlines of the flow capturing the re-circulation zone at area near junction
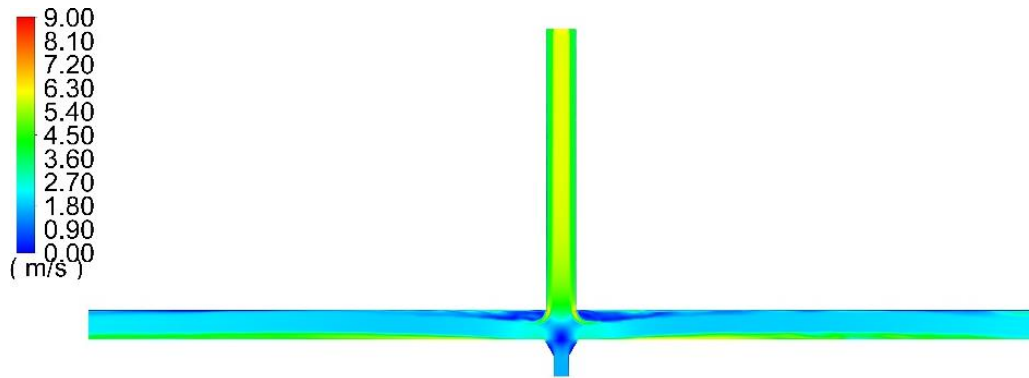
Fig. 32 － Velocity contour of the flow system in a modified T50-50 pipe with additional water injection through ducting insertion DI-2-8

Table 12 － Fluid velocity at inlet, intersection, and outlet of DI-2-8

Position	Oil (m/s)	Main water (m/s)	Add water (m/s)
Inlet	6.3	4.3	0
Intersection	2.1	0.9	2
Outlet	2.5	0.9	3.6
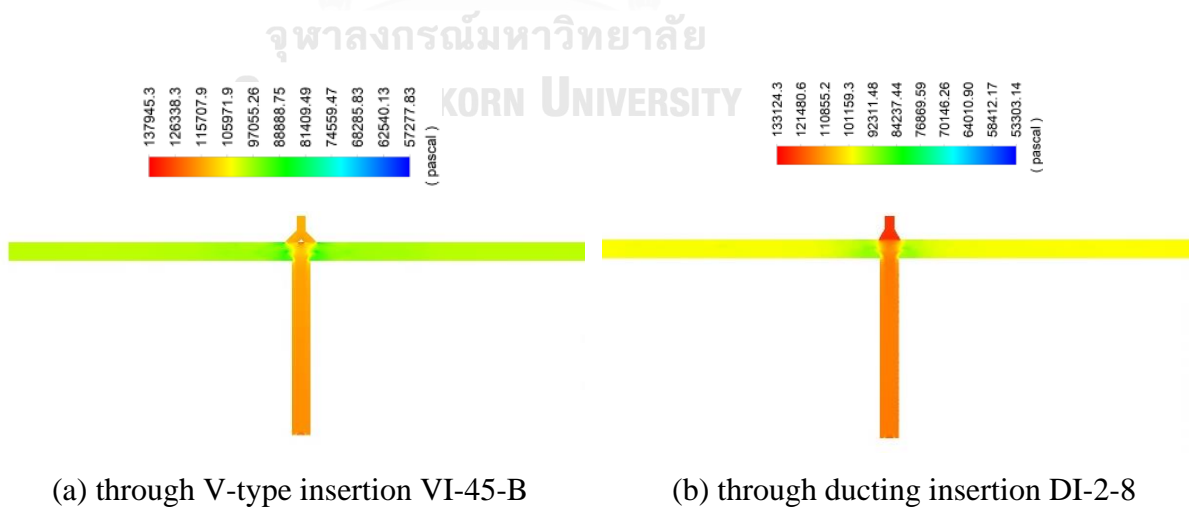
(a) through V-type insertion VI-45-B   (b) through ducting insertion DI-2-8

Fig. 33 － Pressure contour of the flow system in a modified T50-50 pipe with additional water injection

From pipe manufacturing side, unlike the ducting shaped pipe, the V-type application is uncommon in the pipeline transportation unless it is as a custom product. To obtain the most appropriate geometry design of additional water insertion, the design should be capable of allowing the water to consistently push the attached oil on the wall surface to the center area of the pipe at a specific water flowrate without getting in to oil flow system. The geometry of ducting insertion allows for more extensive pressure distribution to all areas of the pipe junction than V-type insertion. Furthermore, as shown by the pressure contours in Fig. 33, the overall pressure loss of the flow system through DI-2-8 was found to be lower than that of VI-45-B.

From Table 12, the sudden drop of velocity values is observed for oil and water at intersection region because fluid hits the junction obstruction. The decrease in the velocity of fluid causes a decrease in the fluid's kinetic energy, and finally decrease the fluid's pressure as shown by Fig. 33. The decrease in pressure is generally calculated as the head loss. The addition of water at intersection was predicted to recover the velocity of fluid system. The velocity of additional water at outlet was higher than intersection because additional water flowed from the constricted area created by the viscous oil (assumed as solid body) at area near intersection directed to downstream region. The velocity of the fluid system after additional of water changed the ratio of inertial force to buoyancy force. After passing intersection until outlet, higher velocity of water was needed to facilitate the lifting force to prevent oil – wall contact. Regarding the ratio of water that should be applied to the flow system, Coelho et al. (2020) revealed the need to apply higher amount of water to keep CAF structure in flow through hydraulic fittings. With this, flows with very high oil cuts (above 70%) were unfeasible. However, condition with minimum water cuts would be commercially more

interesting because it can reduce the energy consumption by volume of transported oil and required costs for the separation of fluids. In this study, the initial water cut was 40% and after additional water injection, the ratio of water at outlet was 44%.

The effect of pipe modification by installing additional water insertion to solve a huge pressure drop is also summarized by Fig. 34 illustrating the predicted cross-sectional time-average pressure along pipe axis. Three distinct areas can be identified: (I) the upstream section, (II) the transitional region, and (III) the downstream section. According to Fig. 34(a), the pressure of the flow system constantly declines with fluctuating pressure at one side of downstream sections after intersection. On the other hand, different result is presented by Fig. 34(b). Initially, it shows a pressure reduction because the CAF structure is still developed. When the CAF has been developed, a stable pressure trend is detected at almost all area of upstream. The CAF structure can be maintained until the flow reaches the area near intersection (II). An indication of sharp pressure reduction is shown when the flow reached the area near the intersection until passing the intersection and continue entering downstream sections (transitional zone). The injected additional water has a role to progressively force the oil to core. The positive effect of additional water injection is documented by the area III with gradual rise of pressure and then the pressure is relatively constant until pipe outlet. The typical pressure profile is also reported by Babakhani Dehkordi et al. (2018) with the transitional zone was the expanded pipe section that promoted thicker core flow. Andrade et al. (2013) conducted a simulation for CAF in T-junction with 1 injection flow inlet and 2 outlet directions (one of the outlet flows had same direction as inlet. The pressure difference as a function of time for the T-junction of that work was generated with similar trend as resulted by this study specifically for proposed modified

design DI-2-8. This outcome emphasizes how the presence of pipe intersection can be considered as barrier for stable CAF and the strategy to use the modified T50-50 with DI-2-8 ducting insertion to inject additional water at intersection can be a strategy to recover the CAF structure.
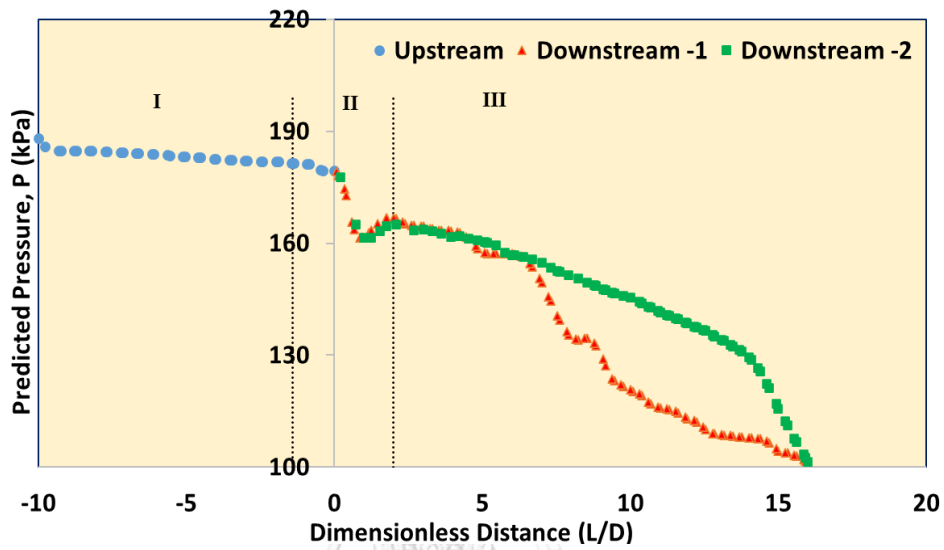
(a)
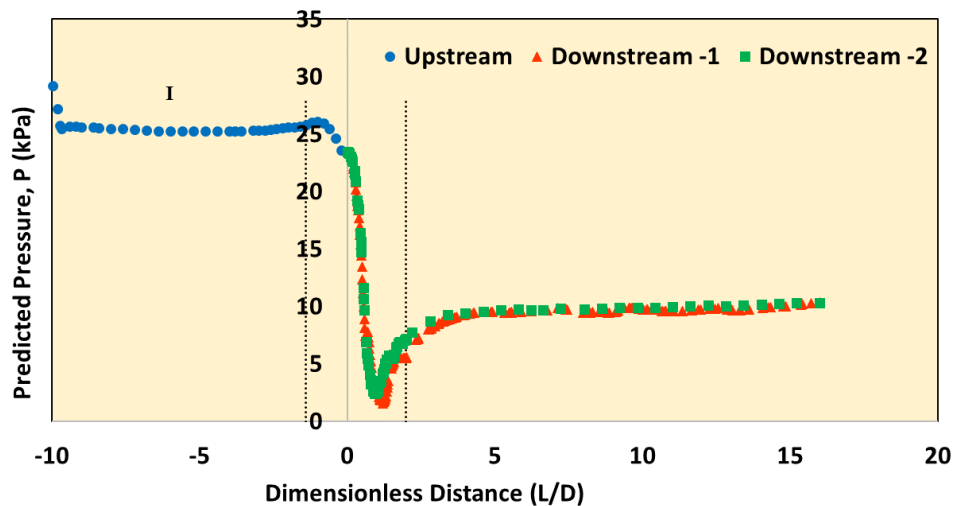
(b)

Fig. 34 − Predicted cross-sectional time-average pressure along pipe axis for (a) T50-50 without additional water and (b) T50-50 with additional water insertion (proposed design coded as DI-2-8)

4.1.4   Conclusion

A simulation work to propose strategy to recover the CAF through horizontal T50-50 pipe has been completed. The result confirms that the effectiveness of CAF can be maintained by installing water insertion at intersection to inject additional water. From some variants of water insertion geometry and velocity of additional water, the ducting insertion with water velocity of 2 m/s (DI-2-8) was selected to promote a more stable condition of CAF recovery started at about 200 mm from intersection point to final downstream exits. The predicted cross-sectional time-average pressure along pipe axis was also generated for T50-50 without additional water injection and proposed design of T50-50. The positive effect of additional water injection was observed at downstream region with gradual rise of pressure before relatively steady until reached the pipe outlet. The re-circulation zone was observed at the near junction area, where vortices phenomena occurred. However, the additional water at the junction allowed the generation of sufficient hydrodynamic lifting force to facilitate the levitation while at the same time resisting interfacial deformation.

4.2   Simulation of CAF with Scaled-Up Pipe Size

Commercial establishing for CAF systems involves not only technical questions but also operational methodologies to increase their feasibility and flexibility. The effectiveness of the commercial implementation of CAF is related to its adaptability to existing pipeline systems. The parameter which is of greatest practical interest is undoubtedly the pipe diameter, the effect of which refers to the problem of scale-up. Limited works are available for the issue of scaled-up pipe sizes. Previous work had developed predictive tool in the basis of experimental works to evaluate the correlation of pressure drop ratio and pipe diameter for case of slightly inclined horizontal pipe

(Brauner, 1991). This work also presented the maximum pressure drop reduction and the corresponding input water fraction as the function of the tube diameter. For pipes with a D > 5 cm, the required fraction of water for achieving the maximum pressure decrease varies slightly with tube diameter and, on average, is between 8 and 9 cm, which were nearly identical as reported by Oliemans (1987).

In this section, a CFD simulation is reported in order to obtain the prediction of CAF formation after scaling up to larger diameter. The selected diameter refers to the common range of crude oil pipeline dimension.

4.2.1 System Description

The scaled-up pipe size simulations were dedicated for T50-50 geometry without additional water inlet (as proposed in Section 4.1) and T50-50 with ducting additional water insertion or coded as DI-2-8 (as proposed in Section 4.1). Both geometries of pipes have same diameter i.e., 50 mm and for scaling up purpose, the diameter was set to be larger i.e., 50 cm. According to the U.S. Department of Transportation's Pipeline and Hazardous Materials Safety Administration (PHMSA), the pipe used in oil pipeline systems generally range in size from 2 inches (5.08 cm) to 42 inches (106.68 cm) in diameter. As the consequence of larger pipe diameter application, the length was also adjusted to get the same dimensionless distance L/D as previous dimension.

There were two conditions of fluid velocities that applied for the systems. First, Reynolds number was set as fix variable and the fluid velocities were calculated using the new diameter value. As the result, lower fluid velocities were obtained i.e., 0.6349 m/s for oil and 0.4355 m/s for water. The second condition was fluid velocities were maintained to be the same as the condition for smaller pipe diameter i.e., 6.349 m/s and

4.355 m/s for oil and water, respectively. Except for the simulation time, all the simulation parameters were set to be identical to the previous simulation in Section 3.5 and Section 4.1.

4.2.2   Results and Discussion

The Reynolds Number (Re) is a ratio between the mass of a fluid stream and the inertia possessed by the material in the flowing fluid. Re is used to determine whether the flow in a system is in a laminar or turbulent flow regime. Furthermore, many phenomena that occur in the internal flow are also heavily influenced by Re. However, the similar Re showed unsatisfying result of current scale up simulation for both geometries. It was observed that by setting certain values of fluid velocities for generating same Re value was not able to provide sufficient velocities to facilitate CAF formation as depicted by Fig. 35.

Different results were obtained when applying the similar fluid velocities as previous smaller diameter case. From Fig. 36(b) and 36(d), the contours were considered to be similar to the condition before scaling up at t = 6s. Simulation time at t = 6s was selected because it has reached stable condition after applying longer simulation time (t = 13s).
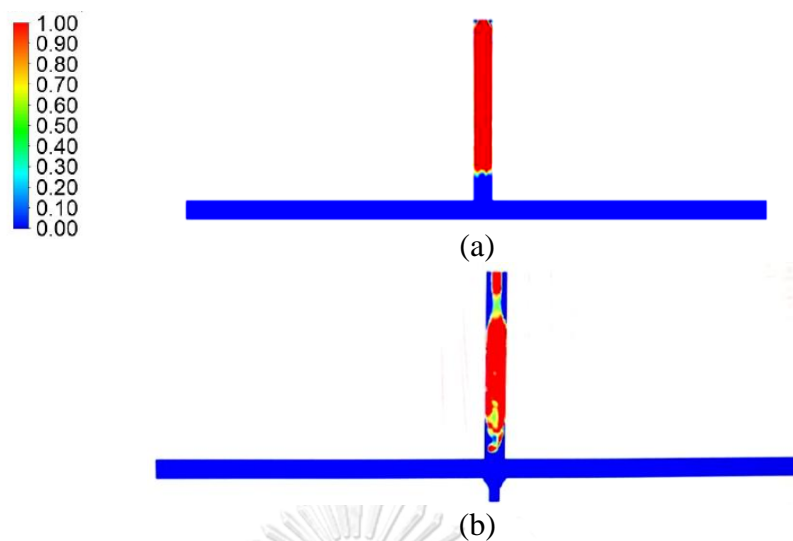
Fig. 35 ─ Contours of oil fraction after scaling up with $u_{o,inlet}$ = 0.6349 m/s and $u_{w,inlet}$ = 0.4355 m/s for (a) T50-50 (b) DI-2-8
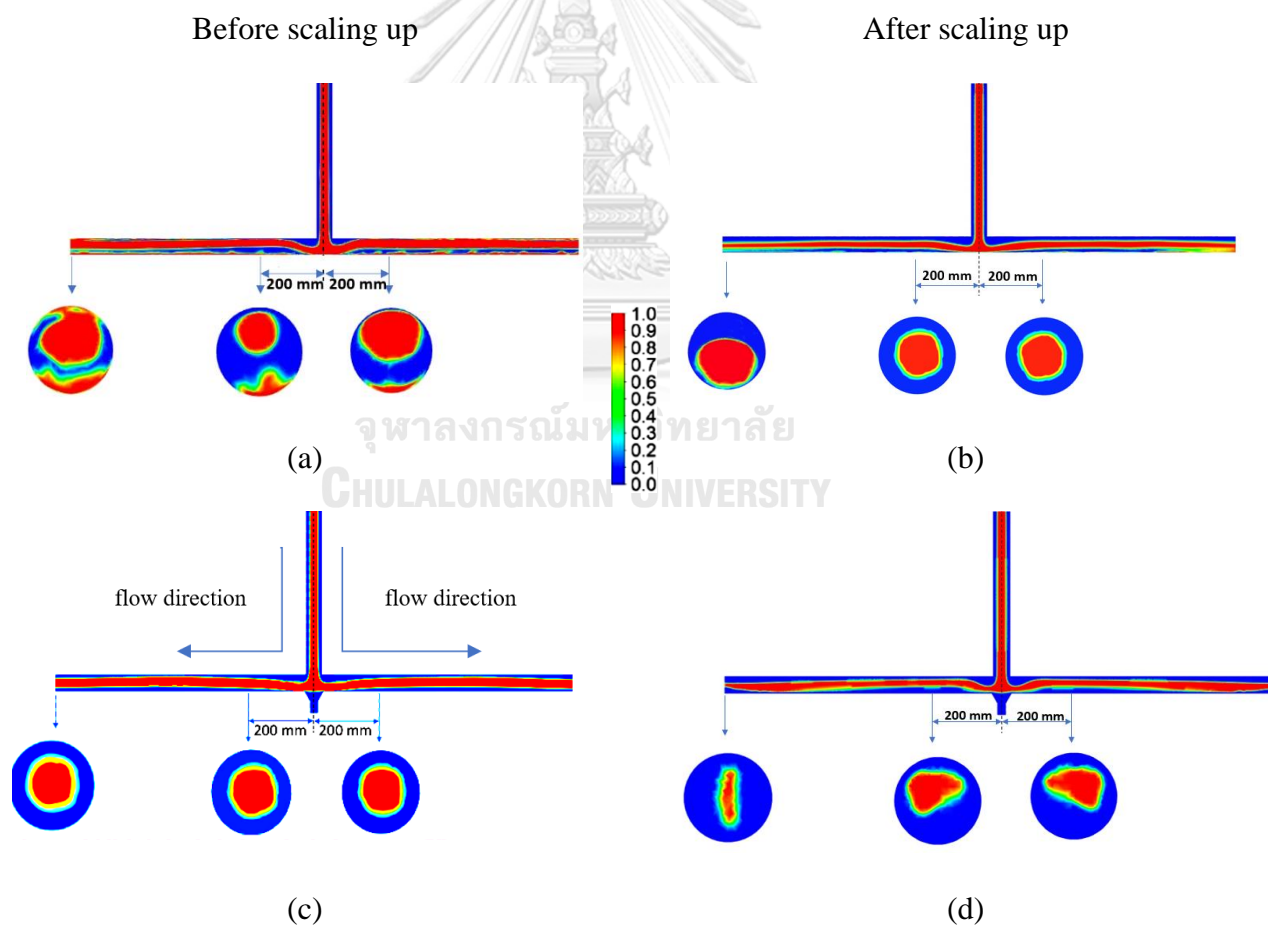
Fig. 36 ─ Contours of oil fraction before and scaling up with $u_{o,inlet}$ = 6.349 m/s and $u_{w,inlet}$ = 4.355 m/s for T50-50 without additional water inlet (a and b) and T50-50 with additional water inlet DI-2-8 (c and d)
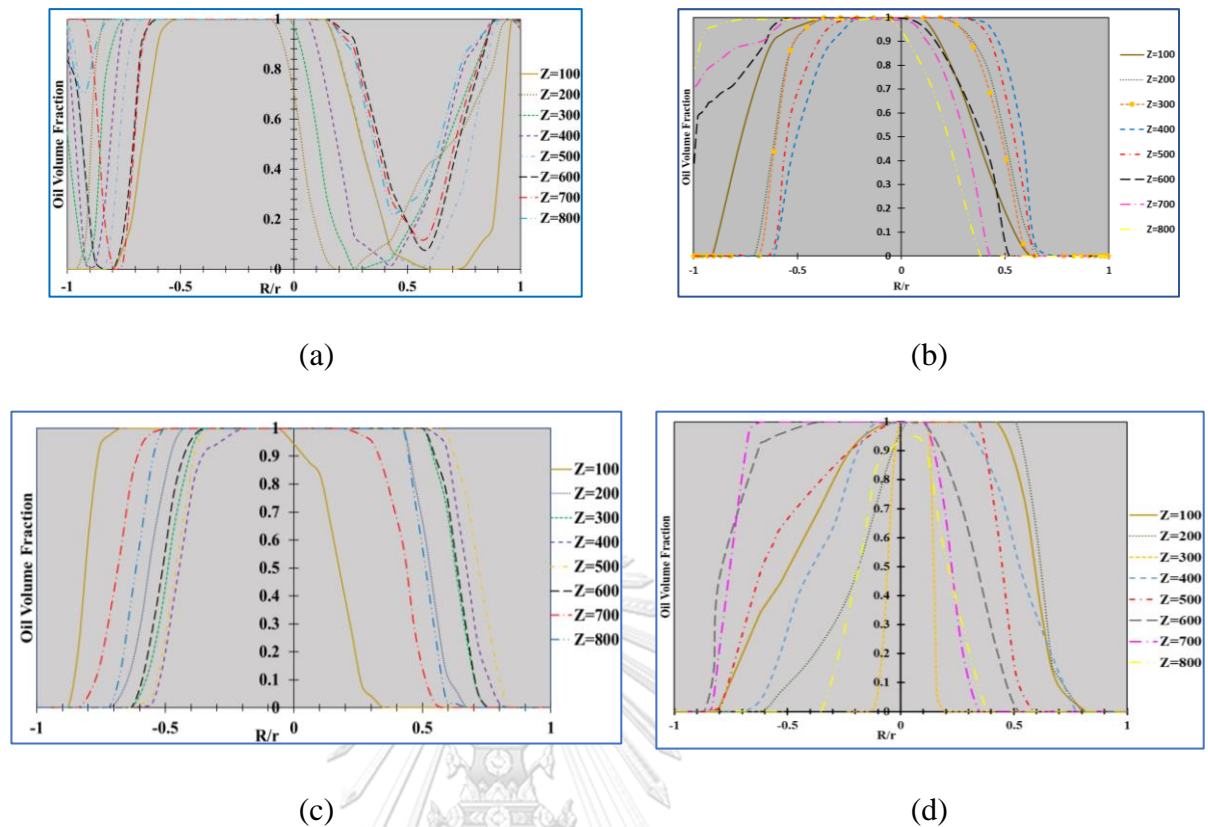
Fig. 37 ─ The averaged local oil holdup for downstream region at various pipe axis (a) T50-50 before scaling up, (b) T50-50 after scaling up, (c) DI-2-8 before scaling up, (d) DI-2-8 after scaling up

From Figs. 36(a), 36(b), 37(a), and 37(b), although the CAF is detected to be formed at downstream near junction but at the end, the condition is similar to smaller dimension that CAF stability cannot be maintained and oil fouling occurred in the area near the outlet. The oil volume fraction profile on the right side also explains the oil fouling occurred near wall or when the ratio of R/r is almost -1. However, from the oil volume fraction contour, it can be observed that in this geometry case, bigger diameter affects the flow pattern as the bigger pipe size show less complex flow pattern compared to the smaller pipe size. It should be noted that in the oil–water flow system, CAF does not always appear. It exists under certain circumstances, affected by the flow rate,

density, viscosity ratio, and interfacial tension between fluids. Some literature state about Eotvos number that also might be considered. This number shows that the existing boundaries of CAF are affected by the density difference between oil and water, pipe diameter, and the interfacial tension between oil and water.

An experimental study about liquid-liquid flow pattern prediction, using pipe diameter of 10-100 mm states that the multiphase flow behaviors in small diameter pipes are significantly different from that in the pipes of conventional or industrial scales, as the Eötvös numbers in the small pipes are small hence the interfacial tension is critically significant (Osundare et al., 2020). Previous study also reported that behaviors of multiphase flows in large diameter pipes (or measured as diameter bigger than 100 mm) pipes could be substantially different from that in smaller pipes (Cheng et al., 1998). In the case of CAF through smaller pipes, there is certain interfacial tension needed to prevent the core layer from splitting into smaller pieces, but its importance decreases in larger pipes.

From the visual of oil fraction contours as shown by Figs. 36(c), 36(d), 37(c), and 37(d), CAF still occurs in DI-2-8 downstream even with more eccentric and thin oil core result. As we can see from oil fraction contour, the oil fraction is almost 1 at small R/r (pipe center) and 0 at big R/r (pipe wall). From this phenomenon, it can be seen that CAF occurred after passing junction is changed dramatically until pipe outlet for pipe with big diameter. In some literatures discussed about the hydrodynamic force of CAF, the ratio of fluid velocity to diameter has important role in the formation of concentric or eccentric CAF. The bigger diameter of pipe has tendency in resulting larger buoyancy force.

4.2.3 Conclusion

The scaled-up pipe size simulation was completed for T50-50 with ducting additional water insertion (DI-2-8) and T50-50 geometry without additional water inlet by setting the dimension to 10 times bigger according to real oil pipeline size. The first simulation was run by keeping similar Reynold Number of the flow and second simulation was set to use the same fluid velocities. As the result, the first simulation indicated unsatisfying contours of CAF. On the other hand, the obtained CAF contours are captured by applying similar fluid velocities as previous smaller diameter case.

It is very important to remark that the boundary layer in smaller pipe size is more intensive than in the larger pipes. This fact also become a challenge to accurately predict the behaviour of flow, particularly multiphase flow, in larger pipes. For the scale up simulation, generally it needs to consider several similarities such as geometry similarity, physical similarity, mechanical similarity, thermal similarity, and chemical similarity. In addition to the Reynolds number, there are other dimensionless parameters that must be satisfied in order to scale up the process. Because of this, developing a process that is identical to the experimental one requires more than just the Reynolds number. Further work to scale up the pipe dimension for CAF of heavy oil-water system can also consider the application of Bingham number to facilitate the shear force and viscosity factors.

CHAPTER V ENERGY SAVINGS EVALUATION OF CAF IN A HORIZONTAL T-PIPE

5.1 Introduction

Several studies have reported that the utilization of water (annulus fluid) as a lubricant for oil (core fluid) can result in a significant reduction in energy consumption during oil transportation (Bensakhria et al., 2004; Coelho et al., 2020; Jing et al., 2021; McKibben et al., 2000; Peysson et al., 2007; Silva et al., 2020; Strazza et al., 2011). Prior research recommended for the utilization of the CAF methodology in order to attain a pressure gradient reduction of at least 80% through appropriate operational parameters. The attainment of substantial drag reduction necessitates the presence of a stable water lubrication surrounding an oil core. The formation of CAF necessitates specific requirements, including fluid properties, superficial velocities of fluids, volume fraction of water, pipe roughness, wettability, and geometry of the pipe (J. Sun et al., 2022). Despite the existence of prior research on the lubricated flow technique, the analysis and reporting of the CAF effect in energy reduction for heavy oil-water systems in T-shaped pipes remains limited.

A CFD simulation work in previous chapters stated that the geometry of the T-pipes contributes in the difficulties to maintain the flow pattern of multiphase flow mainly after passing the junction region. In this chapter, the energy saving of CAF of heavy oil-water system through similar diameter (D = 50 mm) of a horizontal T-pipe was investigated. Principally, this study was the development of previous result from Section 3.5 and Section 4.1. In these two sections, the most optimum designs for CAF were proposed. In order to obtain more comprehensive conclusion about the advantage

of CAF, this chapter will focus on the quantitative energy evaluation of studied flow system by using the power consumption and pressure drop parameters. The energy savings discussed in this section has considered the power to pump additional water. However, this discussion set the boundary to exclude the energy consumption for dewatering process in the calculation

5.2 System Description

For energy savings evaluation, there were 2 geometries that was being evaluated. The first system was CAF through T50-50 pipe, coded as CAF-1 (as previously proposed in Section 3.5), and the other geometry was T50-50 pipe modified with additional ducting water insertion, coded as DI-2-8 (the preferable geometry to recover the CAF as concluded in Chapter IV).

As described in previous chapters, oil as core fluid was injected with $u_{o,inlet} = 4.36$ m/s while water flowed circumferentially with $u_{w,inlet} = 6.35$ m/s as annulus fluid. For the simulation with the single phase oil condition, the inlet mass flow rate data was extracted and set to $\dot{m}_{inlet,o} = 2.763$ kg/s as the input for the amount of transported oil. Untreated sample of crude oil observed by Montes et al. (2018) was still used as the input for core fluid with viscosity (μ_o) of 170.811 Pa.s at zero shear rate and density (ρ_o) of 976 kg/m^3. The oil was surrounded by water with viscosity (μ_w) of 0.001 Pa.s and density (ρ_w) of 999 kg/m^3.

5.3 Computational Domain

The computational domain was similar to the previously applied for work in Chapter III and IV. In order to assess the energy conservation, it was necessary to

compare the result with the scenario where entirely oil flow was present within the pipe.

A flow simulation was performed using the same geometry as CAF, with an equivalent amount of oil as a single-phase flow. According to the simulation results, the upstream pressure gradient of single phase oil was approximately 23% greater than the value predicted by the formula proposed by (Dosunmu et al., 2015).

5.4   Qualitative Evaluation of Energy Savings

As stated in Chapter IV, it is possible to evaluate the efficacy of the lubricated flow through the CAF-1 and DI-2-8 systems qualitatively using the contours describing the flow pattern occurred along the pipe length. As depicted in Fig. 29(a) and 29(c), it is evident that the flow of oil (represented in red) occurs consistently in the central region of the pipe, with water (represented in blue) surrounding it, from the point of inlet to the intersection, for both geometries. However, this flow trend ceased to occur as the oil made contact with the pipe wall prior to dividing into downstream regions. The oil core of DI-2-8 was effectively recovered through the implementation of additional water insertion. When oil did not constantly make touch with the pipe wall (as shown in Fig. 29(c)), pressure drop and energy loss were reduced. The energy savings derived from the use of CAF technique are primarily attributed to the reduction in friction between heavy oil and pipe wall. Despite the initial prediction that CAF simulation via T50-50 would result in lower energy loss compared to single phase oil transportation, the modified geometry of T50-50 (DI-2-8) was found to offer greater energy savings potential compared to the geometry without additional water. In terms of energy consumption, the CAF structure observed throughout the majority of the pipe length during the DI-2-8 simulation run may be defined as a means of conserving energy when compared to the initial T50-50 design. In the CAF condition or when

water was primarily attached to the pipe wall (Fig. 41(a) to 41(c)), the wall shear stress value was very low (almost zero), whereas the larger wall shear stress was revealed in the previous condition without additional water with some areas of the inner pipe wall being wetted by oil (Fig. 41(d) to 41(f)). The significant variation in wall shear stress observed between the two aforementioned flow conditions can be attributed to the substantial discrepancy in viscosity ratio between water and heavy oil. An increase in the viscosity of oil results in a corresponding increase in the magnitude of wall shear stress, which in turn influences the value of the friction factor. The friction factor is defined as the ratio of wall shear stress to flow inertial force. As a result, it can be observed that, under equivalent conditions of fluid velocity, pipe length, and diameter, the pressure gradient associated with CAF is significantly lower compared to that of single-phase oil flow or instances where oil fouling has taken place.

T50-50 without additional water

(a) isometric view   (b) top view

(c) back view

Modified T50-50 with additional water (DI-2-8)

(d) isometric view   (e) top view

(f) back view
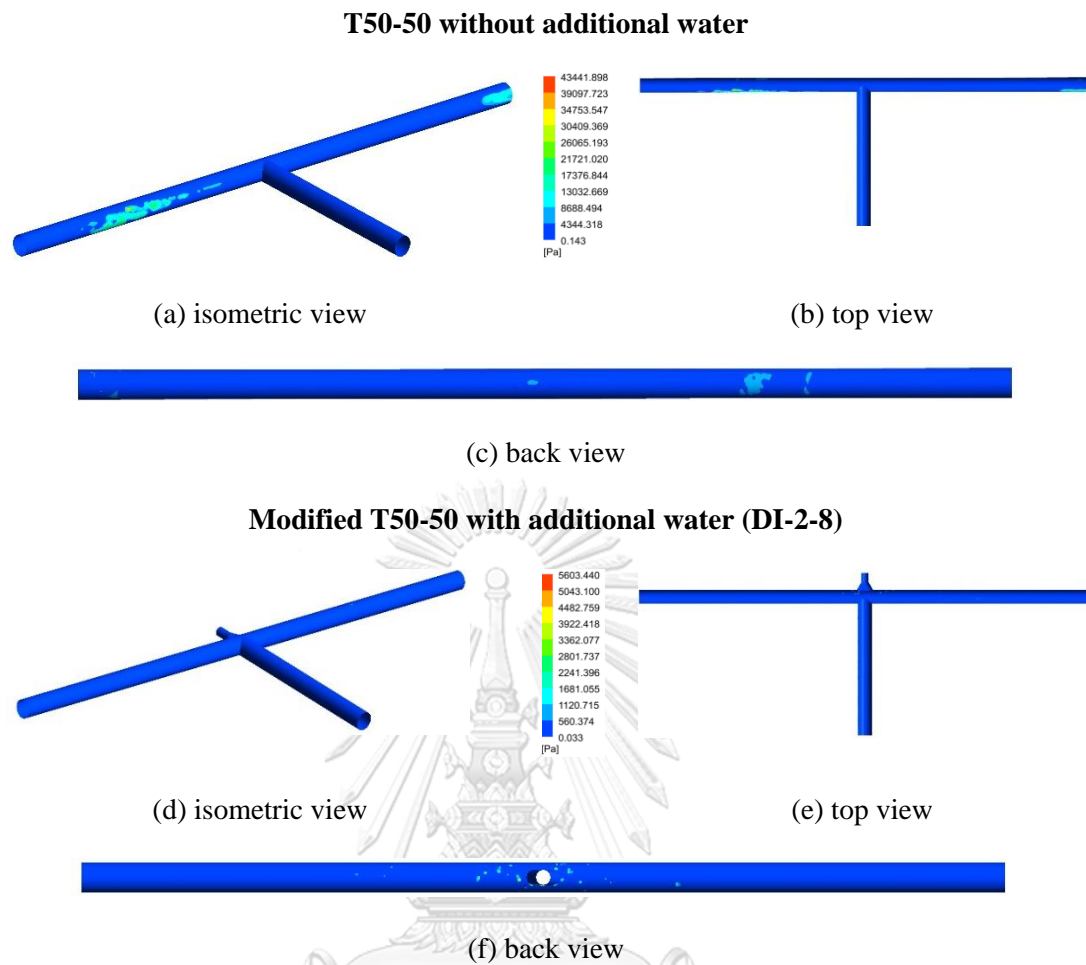
Fig. 38 − Wall shear stress contour on the pipe wall of T50-50 without additional water insertion (a to c) and with DI-2-8 additional water insertion (d to f)

5.5   Quantitative Evaluation of Energy Savings

The quantification of energy savings is achieved through the utilization of parameters such as power consumption and pressure drop. Prior research has employed the power consumption reduction factor (f_ψ), the reduction in pressure gradient (ΔP^*), and the reduction factor in pressure drop ($f_{\Delta P}$) as indicators for assessing the energy efficiency of the CAF system (Coelho et al., 2020; Peysson et al., 2007; Silva et al., 2020; J. Sun et al., 2022). The present study utilized identical energy savings indicators to assess the energy usage of the proposed DI-2-8 model. The indicators were primarily

derived through a comparison of power consumption and pressure drop between biphasic oil-water transport systems (DI-2-8 and the original T50-50 design without additional water injection) and a single-phase flow system that conveyed the same quantity and type of oil. The formulas of those energy savings indicators are referred to Eq. 2.8 – 2.10 as explained in Section 2.8.

In this calculation, the biphasic oil-water system included both oil and water that were injected into the intake in the upstream region. Additional water that was injected at the intersection was part of the biphasic flow system for the DI-2-8 suggested model.

Table 13 − Results of power reduction factor, pressure drop reduction, and pressure gradient reduction factor from current study

Case	Phase	$u_{o,inlet}$ or $u_{w,inlet}$ (m/s)	$\dot{m}_{inlet}$ (kg/s)	ΔP (kPa)	f_ψ	ΔP^* (%)	$f_{\Delta P}$
Single oil	oil	1.62	2.763	1511	-		
T50-50	water	4.36	6.382	76.16	5.9	94	17
	oil	6.35	2.763	103.84			
T50-50 with DI-2-8	water-1	4.36	6.382	11.18	30.3	98	54
	water-2	2	0.96	24.53			
	oil	6.35	2.763	20.33			

The findings in Table 11 demonstrate that when transporting heavy oil of identical type and mass flow rate, conventional single-phase oil pipelines create greater energy consumption and cost due to increased pressure drop. The utilization of the CAF in the design of pipes, specifically in the context of T50-50 shaped pipes, was

projected to yield a substantial reduction in both energy consumption and pressure drop. Table 13 demonstrates that the power consumption reduction factor (f_ψ) is greater than 1 for both T50-50 without additional water insertion and the modified geometry of T50-50 with ducting water insertion. The flow system design of T50-50, as presented in Chapter IV, was capable of preserving the CAF structure along the upstream line, as evidenced by the phase configurations depicted in Fig. 29(a). Although the structure of the CAF was deformed upon passing the intersection, the reduction in friction caused by water lubrication along the upstream section facilitated a decrease in the final pressure drop value. The consumption reduction factor (f_ψ) demonstrates that the proposed design maintains consistency in the CAF even after passing the intersection, resulting in noteworthy energy savings when pumping viscous heavy oil compared to the original T50-50 design. The proposed design showed an overall energy savings ratio of 30.3, which translates to a cost reduction of 97% for transporting the same amount of oil and a cost efficiency of around 14% higher than T50-50 lubrication flow without additional water.

The present design proposal takes into account the energy consumed during the pumping of additional water into the flow system, as this factor has a significant impact on the overall energy consumption. However, the magnitude of power necessary to facilitate the pumping of the supplementary water was deemed negligible in relation to the impact of the resultant CAF configuration. The pressure drop resulting from the introduction of additional water was found to be greater than that of the main inlet of the pipe. This can be attributed to the fact that the additional water entered the complex flow at an intersection, from a direction opposite to that of the water insertion. As a result, it had to overcome the presence of oil that obstructed the entrance point of the

additional water. The proposed design exhibited a higher percentage reduction (98%) in overall pressure drop and pressure gradient of the flow system compared to the previous T50-50 design that lacked additional water at the intersection (94%). One of the features that makes CAF attractive is its ability to reduce pressure drop by more than 90%. The findings obtained in this study are comparable to those reported in previous works conducted by Peysson et al. (2007), Silva et al. (2020), and Bensakhria et al. (2004), wherein pressure drop reduction of over 95% was observed as the most favourable outcome.

The proposed design for CAF involved utilizing injected water at the upstream section to generate lubricating forces. In theory, the force of lubrication has a tendency to push the core towards the center of the pipe, while the force of buoyancy has a tendency to elevate the core towards the uppermost portion of the pipe (Bensakhria et al., 2004). However, once the intersection was passed, the pipe geometry affected the flow's stability. The interaction between the two forces was insufficient in achieving complete centralization of the core fluid. Because of this, the oil's position was unpredictable and occasionally touched the pipe wall. The additional injection of water served for increasing the lubrication force, thereby facilitating the displacement of the core fluid towards the central region. Several experimental studies have demonstrated that an increase in water flow rate can result in a greater reduction in pressure drop. Additionally, it has been observed that the use of a small amount of water is more likely to cause oil fouling on the pipe wall (Bensakhria et al., 2004; Coelho et al., 2020; Joseph et al., 1997). It is generally recommended to establish an ideal lubrication rate that corresponds to the least possible consumption of lubricant, which may vary depending on the specific geometry or flow circumstances. Moreover, the issue of dewatering is a

factor to be taken into account when determining the quantity of water utilized as a lubricant.

5.6 Conclusion

Both a qualitative and quantitative assessment of a horizontal T-pipe's energy savings has been conducted. In comparison to the same product and volume of oil without lubrication, the results show that CAF can transport heavy oil more effectively by minimizing the pressure drop to more than 90%. Oil fouling developed after reaching the intersection in the case of lubricated flow through a T-pipe without additional water injection. Nevertheless, a decrease in energy was still observed with this kind of geometry in comparison to the transportation of oil as a single-phase fluid, resulting in a 94% reduction in pressure drop. On the other hand, the suggested method of installing additional water injection at the intersection demonstrated relatively stable CAF formation after passing the intersection. The result of this modified design can repair the CAF after breaking at the intersection while improving energy savings by up to 4% more than the previous original geometry. In addition, the computation of the CAF yielded high power reduction factor values (greater than 1) for both simulated scenarios. The specific value of the CAF was found to be equivalent to over 80% of the transportation costs associated with single-phase oil transportation.

CHAPTER VI CONCLUSION

In the present research study, the computational fluid dynamics (CFD) of oil-water transportation using Core Annular Flow (CAF) technique in horizontal T and Y-pipes was investigated. A series of simulation studies has been completed to answer the main objectives of this work as listed in Section 1.2. To summarize the investigation results, this conclusion section divides into 3 parts:

Part 1 : CFD model of CAF for oil pipeline transportation in horizontal T and Y-junctions and the occurrence of CAF in the studied systems

Part 2 : The strategy for CAF recovery for oil pipeline transportation in horizontal T-junction

Part 3 : Evaluation of CAF energy saving for oil pipeline transportation in horizontal T-junction

6.1 Part 1: CFD Model and Occurrence of CAF for Oil Pipeline Transportation in Horizontal T and Y- Junctions

This part represents the works reported in Chapter III. This study used 3D simulations with volume of fluid (VOF) multiphase model. This work initiated with a grid independence test to obtain the optimum grid size. Different combinations of junction pipe configurations were tested in eight scenarios. Current simulation works divided into 2 different oil properties. First simulation was dedicated for oil as Newtonian fluid and second work was for oil as non-Newtonian Carreau fluid. In every simulation, the CAF occurred along the upstream region, however it was not possible to keep the CAF stable after it passed the junction area until it reached the pipe outlet.

From the analysis of 2^k factorial statistical experimental design, the optimum design of simulated pipe geometries was predicted to be achieved for T-shaped pipe specifically T20-50 (for first simulation work) and T50-50 (for second simulation work). From these two cases, it can be concluded the CAF is strongly affected by the geometry of pipe and the properties of oil. However, more design factors were involved for affecting the flow performance of Non-Newtonian fluid as the effect of share rate in the geometry of the T and Y-pipes.

Part 2: The CAF Recovery Strategy for Oil Pipeline Transportation in Horizontal T-Junction

This part summarizes the work reported in Chapter IV. An additional water tapping point was inserted at the intersection area on the opposite direction of upstream section to clean the attached oil at the intersection inner pipe wall and to increase water fraction to provide sufficient additional force to push the oil to the core. Variations were made for the insertion shape (V-insertion and ducting insertion) and additional water velocity. It was observed that ducting insertion with water velocity of 2 m/s (DI-2-8) was predicted to provide a better performance of CAF referring to the result of cross-sectional phase configuration at downstream region, time-averaged local oil holdup for both sides of downstream region at various pipe axis, and predicted cross-sectional time-average pressure along pipe axis.

Further simulation work dedicated for the second simulation by scaling the T50-50 pipe up to 10 times bigger dimension. The used of Reynolds number as similarity parameter for scaling up did not show the occurrence of CAF even at the upstream. However, the scaled up has been completed using similar fluid velocities to previous

smaller size of pipe. As a result, CAF still occurred at upstream region. For bigger dimension of T50-50, CAF formation is shown at downstream region near junction but then oil fouling is observed near the outlet. For, DI-2-8, CAF still occurred in downstream with more eccentric and thin oil core result.

6.2 Part 3: Evaluation of CAF Energy Saving for Oil Pipeline Transportation in Horizontal T-Junction

The evaluation of attainable energy savings by applying CAF was presented in Chapter V. The results confirm that effectiveness of CAF to transport the heavy oil by reducing the pressure drop to more than 90%. The additional water insertion at the junction or coded as geometry DI-2-8 showed energy savings improvement to 4% higher than the previous original geometry. The CAF application in the T pipe was estimated to reduce the power consumption that can save 80% of transportation costs compared to single-phase oil transportation.

6.3 Research Outcome and Novel Contribution

The research outcome and novel contribution of current study are:

- The 3D model of CAF in horizontal T-pipe with the estimation of scaled-up results to predict the CAF formation tendency that is very useful to be applied in petroleum industry for transporting heavy oil.

- Geometry factors that can affect the CAF formation in horizontal T and Y shaped pipes for preliminary design consideration of oil pipeline.

- A strategy to recover CAF in horizontal T-pipe to obtain maximum advantage of CAF in transporting viscous fluid.

- Energy savings prediction that might be obtained when transporting heavy oil through horizontal T-pipe that can support the feasibility study of liquid-liquid CAF application in T-pipe.

6.4 Recommendations for Future Studies

The implications of various fluid flow directions, surface velocities, heat characteristics, and fluid physical parameters should be considered for future study with CAF inside T and Y-shaped pipes. Since the diameter variables in this study shown significant influence on the flow performance parameter, variation of the diameter ratio was also intriguing to be examined. In addition, as the CAF technique needs water as lubricant, it would be useful to consider the post treatment process in computing overall energy savings as the effect of adding more water to lubricate oil. Furthermore, the further work intended to obtain an optimal lubricate rate would assist to provide reference about the minimal use of the lubrication fluid needed. Further work to scale up the pipe dimension of CAF case is strongly suggested to consider not only Reynolds number but also other dimensionless parameters that able to facilitate the shear and viscosity factors.

REFERENCES

Andrade, T. H. F., Silva, F. N., Neto, S. R. F., & Lima, A. G. B. (2013). Applying CFD in the analysis of heavy oil-water two-phase flow in joints by using core annular flow technique. *International Journal of Multiphysics, 7*(2), 137-151. doi:10.1260/1750-9548.7.2.137

ANSYS. (2018). ANSYS Fluent Tutorial Guide 18. *ANSYS Fluent Tutorial Guide 18, 15317*(April), 727-746.

Anto, R., Deshmukh, S., Sanyal, S., & Bhui, U. K. (2020). Nanoparticles as flow improver of petroleum crudes: Study on temperature-dependent steady-state and dynamic rheological behavior of crude oils. *Fuel, 275*, 117873-117873. doi:https://doi.org/10.1016/j.fuel.2020.117873

Arney, M. S., Bai, R., Guevara, E., Joseph, D. D., & Liu, K. (1993). Friction factor and holdup studies for lubricated pipelining--i. *International Journal Multiphase Flow, 19*(6), 1061-1076.

Arney, M. S., Ribeiro, G. S., Guevara, E., Bai, R., & Joseph, D. D. (1996). Cement-lined pipes for water lubricated transport of heavy oil. *International Journal of Multiphase Flow, 22*(2), 207-221. doi:https://doi.org/10.1016/0301-9322(95)00064-X

Azzopardi, B. J., & Rea, S. (1999). Modelling the Split of Horizontal Annular Flow at a T-Junction. *Chemical Engineering Research and Design, 77*(8), 713-720. doi:10.1205/026387699526854

Azzopardi, B. J., & Whalley, P. B. (1982). The effect of flow patterns on two-phase flow in a T junction. *International Journal of Multiphase Flow, 8*(5), 491-507. doi:https://doi.org/10.1016/0301-9322(82)90020-9

Babakhani Dehkordi, P., Azdarpour, A., & Mohammadian, E. (2018). The hydrodynamic behavior of high viscous oil-water flow through horizontal pipe undergoing sudden expansion—CFD study and experimental validation. *Chemical Engineering Research and Design, 139*, 144-161. doi:10.1016/j.cherd.2018.09.026

Babakhani, P. (2017). PhD Thesis: Experimental and Numerical Analysis of Multiphase Flow within Horizontal Pipeline with Variable Cross-Sectional Area.

Balakhrisna, T., Ghosh, S., Das, G., & Das, P. K. (2010). Oil–water flows through sudden contraction and expansion in a horizontal pipe – Phase distribution and pressure drop. *International Journal of Multiphase Flow, 36*(1), 13-24. doi:10.1016/j.ijmultiphaseflow.2009.08.007

Bannwart, A. C. (2001). Modeling aspects of oil–water core–annular flows. *Journal of Petroleum Science and Engineering, 32*(2), 127-143. doi:https://doi.org/10.1016/S0920-4105(01)00155-3

Bannwart, A. C., Rodriguez, O. M., Carvalho, C., Wang, I., & Vara, R. (2004). Flow Patterns in Heavy Crude Oil-Water Flow. *Journal of Energy Resources Technology-transactions of The Asme - J ENERG RESOUR TECHNOL, 126*. doi:10.1115/1.1789520

Bensakhria, A., Peysson, Y., & Antonini, G. (2004). Experimental Study of the Pipeline Lubrication for Heavy Oil Transport. *Oil & Gas Science and Technology, 59*(5), 523-533. doi:10.2516/ogst:2004037

Bird, R. B., Stewart, W. E., & Lightfoot, E. N. (2002). *Transport Phenomena*: J. Wiley.

Brackbill, J. U., Kothe, D. B., & Zemach, C. (1992). A continuum method for modeling surface tension. *Journal of Computational Physics, 100*(2), 335-354. doi:10.1016/0021-9991(92)90240-Y

Brauner, N. (1991). Two-phase liquid-liquid annular flow. *International Journal of Multiphase Flow, 17*(1), 59-76. doi:10.1016/0301-9322(91)90070-J

Charles, M. E., Govier, G. W., & Hodgson, G. W. (1961). The horizontal pipeline flow of equal density oil-water mixtures. *The Canadian Journal of Chemical Engineering, 39*(1), 27-36. doi:https://doi.org/10.1002/cjce.5450390106

Chen, J.-l., He, L.-m., Luo, X.-m., Bai, H.-t., & Wei, Y.-h. (2012). Simulation of Oil-Water two Phase Flow and Separation Behaviors in Combined T Junctions. *Journal of Hydrodynamics, 24*(6), 848-857. doi:10.1016/s1001-6058(11)60312-0

Cheng, H., Hills, J. H., & Azzorpardi, B. J. (1998). A study of the bubble-to-slug transition in vertical gas-liquid flow in columns of different diameter. *International Journal of Multiphase Flow, 24*(3), 431-452. doi:https://doi.org/10.1016/S0301-9322(97)00067-0

Chhabra, R. P., & Richardson, J. F. (2008). Chapter 1 - Non-Newtonian Fluid Behaviour. In R. P. Chhabra & J. F. Richardson (Eds.), (Second Edi ed., pp. 1-55). Oxford: Butterworth-Heinemann.

Churchill, S. W. (1988). *Viscous flows : the practical use of theory*. Boston: Butterworths.

Coelho, N. M. D. A., Taqueda, M. E. S., Souza, N. M. O., de Paiva, J. L., Santos, A. R., Lia, L. R. B., . . . de Moraes Júnior, D. (2020). Energy savings on heavy oil transportation through core annular flow pattern: An experimental approach. *International Journal of Multiphase Flow, 122*. doi:10.1016/j.ijmultiphaseflow.2019.103127

Colombo, L. P. M., Guilizzoni, M., Sotgia, G. M., & Marzorati, D. (2015). Influence of sudden contractions on in situ volume fractions for oil–water flows in horizontal pipes. *International Journal of Heat and Fluid Flow, 53*, 91-97. doi:10.1016/j.ijheatfluidflow.2015.03.001

Crivelaro, K. C. O., Damacena, Y. T., Andrade, T. H. F., Lima, A. G. B., & Farias Neto, S. R. (2009). *Numerical simulation of heavy oil flows in pipes using the core-annular flow technique*. Paper presented at the Computational Methods in Multiphase Flow V.

Dessimoz, A.-L., Cavin, L., Renken, A., & Kiwi-Minsker, L. (2008). Liquid–liquid two-phase flow patterns and mass transfer characteristics in rectangular glass microreactors. *Chemical Engineering Science, 63*(16), 4035-4044. doi:10.1016/j.ces.2008.05.005

Dianita, C., Piemjaiswang, R., & Chalermsinsuwan, B. (2021). CFD simulation and statistical experimental design analysis of core annular flow in T-junction and Y-junction for oil-water system. *Chemical Engineering Research and Design, 176*, 279-295. doi:10.1016/j.cherd.2021.10.011

Dianita, C., Piemjaiswang, R., & Chalermsinsuwan, B. (2022). Effect of T- and Y-Pipes on Core Annular Flow of Newtonian/Non-Newtonian Carreau Fluid Using Computational Fluid Dynamics and Statistical Experimental Design Analysis. *Iranian Journal of Science and Technology, Transactions of Mechanical Engineering*. doi:10.1007/s40997-022-00568-z

Dosunmu, I. T., & Shah, S. N. (2015). Pressure drop predictions for laminar pipe flow of carreau and modified power law fluids. *The Canadian Journal of Chemical Engineering, 93*(5), 929-934. doi:10.1002/cjce.22170

Ejaz, F., Pao, W., Shakir Nasif, M., Saieed, A., Memon, Z. Q., & Nuruzzaman, M. (2021). A review: Evolution of branching T-junction geometry in terms of diameter ratio, to improve phase separation. *Engineering Science and Technology, an International Journal, 24*(5), 1211-1223. doi:10.1016/j.jestch.2021.02.003

Garmroodi, M. R. D., & Ahmadpour, A. (2020). A numerical study on two-phase core-annular flows of waxy crude oil/water in inclined pipes. *Chemical Engineering Research and Design, 159*, 362-376. doi:10.1016/j.cherd.2020.04.017

Ghosh, S., Das, G., & Das, P. K. (2011). Simulation of core annular in return bends—A comprehensive CFD study. *Chemical Engineering Research and Design, 89*(11), 2244-2253. doi:10.1016/j.cherd.2011.03.015

Ghosh, S., Mandal, T. K., Das, G., & Das, P. K. (2009). Review of oil water core annular flow. *Renewable and Sustainable Energy Reviews, 13*(8), 1957-1965. doi:10.1016/j.rser.2008.09.034

Goldstein, A., Ullmann, A., & Brauner, N. (2017). Exact solutions of core-annular laminar inclined flows. *International Journal of Multiphase Flow, 93*, 178-204. doi:10.1016/j.ijmultiphaseflow.2017.01.010

Grassi, B., Strazza, D., & Poesio, P. (2008). Experimental validation of theoretical models in two-phase high-viscosity ratio liquid-liquid flows in horizontal and slightly inclined pipes. *International Journal of Multiphase Flow, 34*(10), 950-965. doi:10.1016/j.ijmultiphaseflow.2008.03.006

Guangbin, D., Zongming, L., Guangli, C., Shougen, H., & Jun, Z. (2010). Experimental investigation of gas–solid two-phase flow in Y-shaped pipeline. *Advanced Powder Technology, 21*(4), 468-476. doi:10.1016/j.apt.2010.01.009

Hart, A. (2014). A review of technologies for transporting heavy crude oil and bitumen via pipelines. *Journal of Petroleum Exploration and Production Technology, 4*(3), 327-336. doi:10.1007/s13202-013-0086-6

Hu, H., Jing, J., Tan, J., & Yeoh, G. H. (2019). Flow patterns and pressure gradient correlation for oil–water core–annular flow in horizontal pipes. *Experimental and Computational Multiphase Flow, 2*(2), 99-108. doi:10.1007/s42757-019-0041-y

Hughmark, G. A., & Pressburg, B. S. (1961). Holdup and pressure drop with gas-liquid flow in a vertical pipe. *AIChE Journal, 7*(4), 677-682. doi:10.1002/aic.690070429

Hwang, C. Y. J., & Pal, R. (1997). Flow of two-phase oil/water mixtures through sudden expansions and contractions. *Chemical Engineering Journal, 68*(2-3), 157-163. doi:10.1016/S1385-8947(97)00094-6

Ibraheem, A. (2021). Evaluating the Efficiency of Polyhedral Mesh Elements in Solving the Problem of the Flow around Ship's Rudder. *International Journal of Engineering and Management Sciences (IJEMS), 6*(2), 241-256. doi:10.21791/IJEMS.2021.2.21.difficult

Ingen Housz, E. M. R. M., Ooms, G., Henkes, R. A. W. M., Pourquie, M. J. B. M., Kidess, A., & Radhakrishnan, R. (2017). A comparison between numerical predictions and experimental results for horizontal core-annular flow with a

turbulent annulus. *International Journal of Multiphase Flow, 95*, 271-282. doi:10.1016/j.ijmultiphaseflow.2017.01.020

Ismail, A. Shamsul I., Ismail, I., Zoveidavianpoor, M., Mohsin, R., Piroozian, A., Misnan, M. S., & Sariman, M. Z. (2015). Review of oil–water through pipes. *Flow Measurement and Instrumentation, 45*, 357-374. doi:10.1016/j.flowmeasinst.2015.07.015

Jamshed, S. (2015). Chapter 1 - Introduction to CFD. In S. Jamshed (Ed.), (pp. 1-20). Oxford: Academic Press.

Jiang, F., Chang, J., Huang, H., & Huang, J. (2022). A Study of the Interface Fluctuation and Energy Saving of Oil–Water Annular Flow. *Energies, 15*(6). doi:10.3390/en15062123

Jiang, F., Li, H., Pourquié, M., Ooms, G., & Henkes, R. (2021). Simulation of the hydrodynamics in the onset of fouling for oil-water core-annular flow in a horizontal pipe. *Journal of Petroleum Science and Engineering, 207*. doi:10.1016/j.petrol.2021.109084

Jiang, F., Long, Y., Wang, Y., Liu, Z., & Chen, C. (2016). NUMERICAL SIMULATION OF NON-NEWTONIAN CORE ANNULAR FLOW THROUGH RECTANGLE RETURN BENDS. *Journal of Applied Fluid Mechanics, 9*, 431-441.

Jiang, F., Wang, K., Skote, M., Wong, T. N., & Duan, F. (2018). Simulation of non-Newtonian oil-water core annular flow through return bends. *Heat and Mass Transfer/Waerme- und Stoffuebertragung, 54*(1), 37-48. doi:10.1007/s00231-017-2093-5

Jing, J., Yin, X., Mastobaev, B. N., Valeev, A. R., Sun, J., Wang, S., . . . Zhuang, L. (2021). Experimental study on highly viscous oil-water annular flow in a horizontal pipe with 90° elbow. *International Journal of Multiphase Flow, 135*. doi:10.1016/j.ijmultiphaseflow.2020.103499

Joseph, D. D., Bai, R., Chen, K. P., & Renardy, Y. Y. (1997). Core-Annular Flows. *Annual Review of Fluid Mechanics, 29*(1), 65-90. doi:10.1146/annurev.fluid.29.1.65

Kaushik, V. V. R., Ghosh, S., Das, G., & Das, P. K. (2012). CFD simulation of core annular flow through sudden contraction and expansion. *Journal of Petroleum Science and Engineering, 86-87*, 153-164. doi:10.1016/j.petrol.2012.03.003

Khalili-Garakani, A., Mostoufi, N., Sadeghi, F., Hosseinzadeh, M., Fatoorehchi, H., Sarrafzadeh, M., & Mehrnia, M. (2011). Comparison between different models for rheological characterization of activated sludge. *Iranian Journal of Environmental Health Science & Engineering, 8*, 255-264.

Kiernan, D. (2021). *Natural Resources Biometrics*.

Li, X., & Wang, S. (2013). Flow field and pressure loss analysis of junction and its structure optimization of aircraft hydraulic pipe system. *Chinese Journal of Aeronautics, 26*(4), 1080-1092. doi:10.1016/j.cja.2013.04.004

Lintermann, A. (2021). Computational Meshing for CFD Simulations. In K. Inthavong, N. Singh, E. Wong, & J. Tu (Eds.), (pp. 85-115). Singapore: Springer Singapore.

Livinus, A., Yeung, H., & Lao, L. (2017). Restart time correlation for core annular flow in pipeline lubrication of high-viscous oil. *Journal of Petroleum Exploration and Production Technology, 7*(1), 293-302. doi:10.1007/s13202-016-0241-y

Loh, W. L., & Premanadhan, V. K. (2016). Experimental investigation of viscous oil-water flows in pipeline. *Journal of Petroleum Science and Engineering, 147*, 87-97. doi:10.1016/j.petrol.2016.05.010

Lu, P., Zhao, L., Deng, S., Zhang, J., Wen, J., & Zhao, Q. (2018). Simulation of two-phase refrigerant separation in horizontal T-junction. *Applied Thermal Engineering, 134*, 333-340. doi:https://doi.org/10.1016/j.applthermaleng.2018.01.087

Macías-Hernández, M. J., Dávila-Maldonado, O., Guzmán-Vargas, A., Sotelo-Boyás, R., & Zarazua-Villalobos, L. (2016). CFD simulation of interfacial instability from the nozzle in the formation of viscous core-annular flow. *The Canadian Journal of Chemical Engineering, 94*(10), 2004-2012. doi:https://doi.org/10.1002/cjce.22580

Marappa Gounder, R. (2019). Introductory Chapter: Heavy Crude Oil Processing - An Overview. In.

Martínez-Palou, R., De, M., Mosqueira, L., Zapata-Rendón, B., Mar-Juárez, E., Bernal-Huicochea, C., . . . Aburto, J. (2010). Transportation of heavy and extra-heavy crude oil by pipeline: A review. doi:10.1016/j.petrol.2010.11.020

McKibben, M., Gillies, R., & Shook, C. (2000). A laboratory investigation of horizontal well heavy oil—water flows. *The Canadian Journal of Chemical Engineering, 78*, 743-751.

Memon, Z. Q., Pao, W., Hashim, F. M., & Ali, H. M. (2020). Experimental investigation of two-phase separation in T-Junction with combined diameter ratio. *Journal of Natural Gas Science and Engineering, 73*. doi:10.1016/j.jngse.2019.103048

Montes, D., Cortés, F. B., & Franco, C. A. (2018). Reduction of heavy oil viscosity through ultrasound cavitation assisted by NiO nanocrystals-functionalized SiO2 nanoparticles. *Dyna, 85*(207), 153-160. doi:10.15446/dyna.v85n207.71804

Montes, D., Taborda, E. A., Minale, M., Cortés, F. B., & Franco, C. A. (2019). Effect of the NiO/SiO2 Nanoparticles-Assisted Ultrasound Cavitation Process on the Rheological Properties of Heavy Crude Oil: Steady State Rheometry and Oscillatory Tests. *Energy & Fuels, 33*(10), 9671-9680. doi:10.1021/acs.energyfuels.9b02288

Montgomery, D. C. (2012). *Design and Analysis of Experiments, 8th Edition*: John Wiley \& Sons, Incorporated.

Moukalled, F., Mangani, L., & Darwish, M. (2016). The Finite Volume Method. In (pp. 103-135). Cham: Springer International Publishing.

Myers, R. H., Montgomery, D. C., & Anderson-Cook, C. M. (2011). *Response Surface Methodology: Process and Product Optimization Using Designed Experiments*: Wiley.

Oja, M. (2023). *Behavioral Statistics*

Oliemans, R. V. A., Ooms, G., Wu, H. L., & Duijvestijn, A. (1987). Core-annular oil/water flow: the turbulent-lubricating-film model and measurements in a 5 cm pipe loop. *International Journal of Multiphase Flow, 13*(1), 23-31. doi:10.1016/0301-9322(87)90004-8

Ooms, G., & Poesio, P. (2003). Stationary core-annular flow through a horizontal pipe. *Phys Rev E Stat Nonlin Soft Matter Phys, 68*(6 Pt 2), 066301. doi:10.1103/PhysRevE.68.066301

Ooms, G., Vuik, C., & Poesio, P. (2007). Core-annular flow through a horizontal pipe: Hydrodynamic counterbalancing of buoyancy force on core. *Physics of Fluids, 19*(9). doi:10.1063/1.2775521

Osundare, O., Falcone, G., Lao, L., & Elliott, A. (2020). Liquid-Liquid Flow Pattern Prediction Using Relevant Dimensionless Parameter Groups. *Energies, 13*, 4355. doi:10.3390/en13174355

Paszkiewicz, L. (2012). Extra heavy oils in the world energy supply. (June).

Peysson, Y., Bensakhria, A., Antonini, G., & Argillier, J. F. (2007). Pipeline lubrication of heavy oil: Experimental investigation of flow and restart problems. *SPE Production and Operations, 22*(1), 135-140. doi:10.2118/97764-pa

Picchi, D., & Poesio, P. (2016). Stability of multiple solutions in inclined gas/shear-thinning fluid stratified pipe flow. *International Journal of Multiphase Flow, 84*. doi:10.1016/j.ijmultiphaseflow.2016.03.002

Picchi, D., Ullmann, A., & Brauner, N. (2018). Modeling of core-annular and plug flows of Newtonian/non-Newtonian shear-thinning fluids in pipes and capillary tubes. *International Journal of Multiphase Flow, 103*, 43-60. doi:10.1016/j.ijmultiphaseflow.2018.01.023

Puspitasari, D., Indarto, Purnomo, & Khasani. (2014). Kerosene-Water Flow Pattern in T-Junction Vertical Diameter Ratio 0.5 (Variation of Inclination Branch). *Applied Mechanics and Materials, 493*, 306-312. doi:10.4028/www.scientific.net/AMM.493.306

Rodriguez, O. M. H., & Bannwart, A. C. (2006). Experimental study on interfacial waves in vertical core flow. In (Vol. 54, pp. 140-148): Elsevier.

Saieed, A., Pao, W., Hewakandamby, B., Azzopardi, B. J., Wood, D. A., & Ali, H. M. (2018). Experimental investigation on the effect of diameter ratio on two-phase slug flow separation in a T-Junction. *Journal of Petroleum Science and Engineering, 170*, 139-150. doi:10.1016/j.petrol.2018.06.033

Salager, J.-L., Briceno, M., & Bracho, C. L. (2001). Heavy hydrocarbon emulsions. Making use of the state of the art in formulation engineering. *Encyclopedic Handbook of Emulsion Technology*, 455-495.

Salim, S. M., & Cheah, S. C. (2009, 2009). *Wall y+ Strategy for Dealing with Wall-bounded Turbulent Flows*.

Saniere, A., Hénaut, I., & Argillier, J. F. (2004). Pipeline transportation of heavy oils, a strategic, economic and technological challenge. *Oil and Gas Science and Technology, 59*(5), 455-466. doi:10.2516/ogst:2004031

Santos, R. G., & Lo. (2014). Brazilian Journal of Chemical Engineering - An overview of heavy oil properties and its recovery and transportation methods. *Brazilian Journal of Chemical Engineering, 31*(03), 571-590.

Shi, J., Gourma, M., & Yeung, H. (2017). CFD simulation of horizontal oil-water flow with matched density and medium viscosity ratio in different flow regimes. *Journal of Petroleum Science and Engineering, 151*, 373-383. doi:10.1016/j.petrol.2017.01.022

Shi, J., Gourma, M., & Yeung, H. (2021). A CFD study on horizontal oil-water flow with high viscosity ratio. *Chemical Engineering Science, 229*. doi:10.1016/j.ces.2020.116097

Shih, T. H., Liou, W. W., Shabbir, A., Yang, Z., & Zhu, J. (1995). A new k-ε eddy viscosity model for high reynolds number turbulent flows. *Computers and Fluids, 24*(3), 227-238. doi:10.1016/0045-7930(94)00032-T

Silva, B. F., Magalhães, H. L. F., Gomez, R. S., Cabral, E. d. M., Batista, F. A., Pereira, A. B. d. C., . . . Lima, A. G. B. d. (2020). Isothermal Transport (Core-Flow Type) of Heavy and Ultraviscous Oil in Curved Pipes: A Transient Study by CFD. *Open Journal of Fluid Dynamics, 10*(02), 122-134. doi:10.4236/ojfd.2020.102008

Simpson, J. L. (1963). Pipeline transportation of wax-laden crude oil as water suspension. In.

Sotgia, G., Tartarini, P., & Stalio, E. (2008). Experimental analysis of flow regimes and pressure drop reduction in oil–water mixtures. *International Journal of Multiphase Flow, 34*(12), 1161-1174. doi:10.1016/j.ijmultiphaseflow.2008.06.001

Souas, F., Safri, A., Benmounah, A., Boumediene, H., Ezzouar, B., & Alger, A. (2020). A review on the rheology of heavy crude oil for pipeline transportation. doi:10.1016/j.ptlrs.2020.11.001

Strazza, D., Grassi, B., Demori, M., Ferrari, V., & Poesio, P. (2011). Core-annular flow in horizontal and slightly inclined pipes: Existence, pressure drops, and hold-up. *Chemical Engineering Science, 66*(12), 2853-2863. doi:10.1016/j.ces.2011.03.053

Strazza, D., & Poesio, P. (2012). Experimental study on the restart of core-annular flow. *Chemical Engineering Research and Design, 90*(11), 1711-1718. doi:10.1016/j.cherd.2012.03.011

Sun, J., Guo, L., Fu, J., Jing, J., Yin, X., Lu, Y., . . . Brauner, N. (2022). A new model for viscous oil-water eccentric core annular flow in horizontal pipes. *International Journal of Multiphase Flow, 147*. doi:10.1016/j.ijmultiphaseflow.2021.103892

Sun, X., Peng, J., & Zhu, K. (2010). Stability of core-annular flow of power-law fluids in the presence of interfacial surfactant. *Science China Physics, Mechanics and Astronomy, 53*(5), 933-943. doi:10.1007/s11433-010-0171-5

Sun, X. W., Peng, J., & Zhu, K. Q. (2012). The axisymmetric long-wave interfacial stability of core-annular flow of power-law fluid with surfactant. *Acta Mechanica Sinica/Lixue Xuebao, 28*(1), 24-33. doi:10.1007/s10409-012-0016-8

Taborda, E. A., Franco, C. A., Lopera, S. H., Alvarado, V., & Cortés, F. B. (2016). Effect of nanoparticles/nanofluids on the rheology of heavy crude oil and its mobility on porous media at reservoir conditions. *Fuel, 184*, 222-232. doi:10.1016/j.fuel.2016.07.013

Tripathi, S., Bhattacharya, A., Singh, R., & Tabor, R. F. (2015). Lubricated Transport of Highly Viscous Non-newtonian Fluid as Core-annular Flow: A CFD Study. *Procedia IUTAM, 15*, 278-285. doi:10.1016/j.piutam.2015.04.038

van Duin, E., Henkes, R., & Ooms, G. (2019). Influence of oil viscosity on oil-water core-annular flow through a horizontal pipe. *Petroleum, 5*(2), 199-205. doi:10.1016/j.petlm.2018.01.003

Wang, W., Cao, Y., & Okaze, T. (2021). Comparison of hexahedral, tetrahedral and polyhedral cells for reproducing the wind field around an isolated building by LES. *Building and Environment, 195*, 107717-107717. doi:https://doi.org/10.1016/j.buildenv.2021.107717

Woodbury, A., Shepherd, J., Staten, M., & Benzley, S. (2011). Localized Coarsening of Conforming All-Hexahedral Meshes. *Eng. Comput. (Lond.), 27*, 95-104. doi:10.1007/978-3-540-87921-3_36

Wu, J., Jiang, W., Liu, Y., He, Y., Chen, J., Qiao, L., & Wang, T. (2020). Study on hydrodynamic characteristics of oil-water annular flow in 90° elbow. *Chemical Engineering Research and Design, 153*, 443-451. doi:10.1016/j.cherd.2019.11.013

Yang, B., Su, W., Deng, S., Zhao, L., & Lu, P. (2019). State-of-art of branching T-junction: Experiments, modeling, developing prospects and applications. *Experimental Thermal and Fluid Science, 109*, 109895-109895. doi:https://doi.org/10.1016/j.expthermflusci.2019.109895

Yang, B., Su, W., Deng, S., Zhao, L., & Lu, P. (2020). State-of-art of impacting T-junction : Phase separation, constituent separation and applications. *International Journal of Heat and Mass Transfer, 148*, 119067-119067. doi:https://doi.org/10.1016/j.ijheatmasstransfer.2019.119067

Yang, L., Wang, J., Jiang, Y., & Zou, L. (2020). Oil–water flow splitting in eccentric annular T-junction tubes—Experimental and CFD analysis. *Chemical Engineering Science, 228*, 116000-116000. doi:10.1016/J.CES.2020.116000

VITA

NAME	Cindy Dianita
DATE OF BIRTH	11 August 1986
PLACE OF BIRTH	Palembang (Indonesia)
INSTITUTIONS ATTENDED	Dept. of Chemical Engineering, Faculty of Engineering, Universitas Indonesia 2005-2009 Dept. of Oil and Gas Transportation and Storage, Faculty of Pipeline Engineering, Ufa State Petroleum Technological University (Russia) 2012-2014
HOME ADDRESS	Department of Chemical Engineering – Faculty of Engineering, Universitas Indonesia, Kampus Baru UI Depok – Jawa Barat (West Java) – Indonesia
PUBLICATION	1. CFD simulation and statistical experimental design analysis of core annular flow in T-junction and Y-junction for oil-water system (Chemical Engineering Research and Design, Vol. 176, 2021) 2. Effect of T- and Y-Pipes on Core Annular Flow of Newtonian/ Non-Newtonian Carreau Fluid Using Computational Fluid Dynamics and Statistical Experimental Design Analysis (Iranian Journal of Science and Technology - Transactions of Mechanical Engineering, 2022) 3. Computational fluid dynamics approach for energy savings evaluation in core annular flow of a horizontal T-pipe (Energy Reports, Vol.9, 2023)